Thesis for a Ph. D. Degree

Predictions of seasonal to near-future tropical cyclone activities over the western North Pacific and the North Atlantic

북서태평양과 북대서양의 계절 및 가까운 미래 태풍 활동 예측

Woosuk Choi

August 2017

School of Earth and Environmental Sciences
Graduate School
Seoul National University

Predictions of seasonal to near-future tropical cyclone activities over the western North Pacific and the North Atlantic

By
Woosuk Choi

Dissertation Submitted to the Faculty of the Graduate School of the Seoul National University in Partial Fulfillment of the Requirement for the Degree of Doctor of Philosophy

Degree Awarded:
August 2017

Advisory committee:

Professor	Kwang-Yul Kim, Chair
Professor	Chang-Hoi Ho, Advisor
Doctor	Hee-Dong Yoo
Professor	Seok-Woo Son
Doctor	Joo-Hong Kim

이학박사학위논문

Predictions of seasonal to near-future tropical cyclone activities over the western North Pacific and the North Atlantic

북서태평양과 북대서양의 계절 및 가까운 미래 태풍 활동 예측

2017년 8월

서울대학교 대학원

지구환경과학부

최 우 석

Abstract

Every summertime, tropical cyclone (TC) activity over the worldwide tropical ocean has been receiving large attention due to its destructive impacts on heavily populated countries. To reduce and prepare the potential damages from the TC approach/landfall, development of skillful TC prediction model has been one of the most essential missions for meteorological agency. In this dissertation, the detailed physical relationships between TC activity and environmental fields are investigated. On the basis of these understandings, a track-pattern-based model is developed to predict seasonal to near-future TC activity over the western North Pacific (WNP) and the North Atlantic (NA) basins. This model employs a hybrid statistical–dynamical method and is the first approach to predicts spatial distribution of TC track density covering the entire basin. Thus, it would be a milestone for the prediction of long-term TC track distribution without simulating the climate model.

There are three major steps to operate the track-pattern-based model. First, climatological basin-wide TC tracks during the TC season are identified into several patterns using the fuzzy *c*-means method. Second, the TC counts for each cluster are predicted by using a hybrid statistical–dynamical method. The hybrid prediction for each pattern is based on the statistical relationships (interannual correlation in this thesis) between the seasonal TC frequency of the pattern and the seasonal-mean key predictors dynamically forecast by the

National Centers for Environmental Prediction (NCEP) Climate Forecast System version 2 (CFSv2). Third, the final forecast map of track density is constructed by merging the spatial probabilities of the all clusters and applying necessary bias corrections.

The leave-one-out cross validation shows good skill of the WNP TC prediction model, with the correlation coefficients between the hindcasts and the observations ranging from 0.71 to 0.81. The hindcasts of the WNP seasonal TC track density exhibit significant predictability in reproducing the observed pattern. As a real forecast, this model fairly forecast the anomalous spatial distribution of WNP TC track density for the 2010 typhoon season, representing the lowest count since 1951. A higher-than-normal track density was successfully forecast near the East China Sea, Korea, and Japan. The total seasonal TC genesis frequency integrated over the seven patterns is well below normal (about 16.4) close to the observations. The skillful performance in 2010 using the seasonal TC prediction model is attributed to the skillful forecast of the ENSO transition by the NCEP CFS, cooperated with the validity of the prediction model itself.

In addition to the WNP basin, a seasonal prediction model of the NA TC activities for the period August–October has been developed on the basis of representative TC track patterns. Using the fuzzy *c*-means method, a total of 432 TCs are categorized into the following four groups: 1) TCs off the East Coast of the United States, 2) TCs over the Gulf of Mexico, 3) TCs that

recurve into the open oceans of the central NA, and 4) TCs that move westward in the southern NA. The model is applied to predict the four TC groups separately in conjunction with global climate forecasts from the NCEP CFSv2. By adding the distributions of the four TC track patterns with pre-calculated TC genesis frequencies, this seasonal TC forecast model provides the spatial distribution of TC activities over the entire NA basin. Multiple forecasts initialized in six consecutive months from February to July are generated at monthly intervals to examine the applicability of this model in operational TC forecasting. Cross-validations of individual forecasts show that the model can reasonably predict the observed TC frequencies over NA at the 99% confidence level. The model shows a stable spatial prediction skill, proving its advantage for forecasting regional TC activities several months in advance. In particular, the model can generate reliable information on regional TC counts in the near-coastal regions as well as in entire NA basin.

Among the TC activity, intense TCs accompanying torrential rain and powerful wind gusts often cause substantial socio-economic losses in the regions around their landfall than weak TCs. Thus, we develop the prediction model targeting only intense TCs in the WNP and the NA basins. Different intensity criteria are used to define intense TCs for these two basins, category 3 and above for WNP and category 1 and above for NA, because the number of TCs in the NA basin is much smaller than that in the WNP basin. Using a fuzzy clustering method, intense TC tracks in the WNP and the NA basins are

classified into three and two representative patterns, respectively. On the basis of the clustering results, a track-pattern-based model is then developed for forecasting the seasonal activities of intense TCs in the two basins. Generally, the WNP intense TC patterns have predictors of dynamical factor (vertical wind shear or low-level relative vorticity) because of thermally mature state over the WNP to develop the TC whereas the NA intense TCs have thermodynamical factor (sea surface temperature) to the predictor due to the thermally insufficient condition to generate TC over the NA. Cross-validation of the model skill for entire training period as well as verification of a forecast for the 2014 TC season suggest that our intense TC model is applicable to operational uses.

Although many studies have attempted to predict TC activities on various time scales, very few focused on near-future predictions. Here we show a decrease in seasonal TC activity over the NA for 2016–2030 using the track-pattern-based TC prediction model. The prediction model is forced by long-term coupled simulations, CFSv2 free runs, initialized using reanalysis data. Unfavorable conditions for TC development including strengthened vertical wind shear, enhanced low-level anticyclonic flow, and cooled sea surface temperature over the tropical NA are found in the simulations. Most of the environmental changes are attributable to cooling of the NA basin-wide sea surface temperature (NASST) and more frequent El Niño episodes in the near future. Consistent NASST warming trend in the Coupled Model

Intercomparison Project phase 5 projections suggests that natural variability is still dominant than anthropogenic forcing over the NA in the near-future period.

Keywords: tropical cyclone, intense tropical cyclone, track-pattern-based, hybrid statistical–dynamical, Climate Forecast System, seasonal, near future, western North Pacific, North Atlantic, spatial distribution, natural variability

Student number: 2010–20354

Table of Contents

List of Tables

List of Figures

1. Introduction

Summertime tropical cyclone (TC) activities over the western North Pacific (WNP) and the North Atlantic (NA) are the most severe weather phenomenon for people dwelling in coastal region. Generally, TC accompanies hazardous disasters such as strong wind gust, wild wave, and heavy rainfall causing a large economic loss and many injured persons. For every boreal summer-to-autumn season, approximately 20 and 10 TCs occur in the WNP and NA ocean basins, respectively (Gray 1968). About half of them strike countries in the coastal regions of two basins bringing torrential rainfall and strong wind gusts to the land (Kim et al. 2005a, 2006; Pielke et al. 2008; Zhang et al. 2009; Fengjin and Ziniu 2010; Smith and Katz 2013; Park et al. 2015).

Smith and Katz (2013) reported that the total estimated damage caused by TCs in the United States (US) was about $418 billion during the period of 1980–2011, about 47% of the total losses from natural disasters. Hurricane Sandy, a category 3 storm, made landfall on the east coast of the US in 2012, claimed nearly 100 human lives and caused 65 billion US dollars in economic losses. In 2013, typhoon Haiyan reached category 5 level and resulted in approximately 6,000 deaths and 13 billion US dollars of property losses in the Philippines. The seriousness of TC-induced catastrophes has been acting as the catalyst for accelerating TC activity studies and developing a skillful

seasonal prediction of TC activities.

To minimize or preclude the societal-economic damages from the TC activity, it has become necessary to develop a TC prediction system ensuring high predictability. Above all, seasonal prediction of TC activity is attempted because tourism and insurance companies are affected by these seasonal forecasts in their policy decisions. A number of empirical models have been developed for the seasonal predictions of TC activities based on their time-lagged relationships with precursory environmental conditions. Since the first attempts in the early 1980s by Neville Nicholls (1979) for the Australian region, William Gray (1984a, 1984b) for the NA region and Chan et al. (1998, 2001) in the WNP basin had been developed seasonal TC prediction model. Some of these models have shown statistically significant skill and have been employed in operational TC prediction system. However, the statistical relationships are at times difficult to interpret physically because of their time-lagged properties. This lagged relationship may eventually result in poor forecasting skill in operational TC predictions.

In addition to statistical forecasts, dynamic simulations of TC using the high-resolution models have also been used for seasonal prediction by incorporating the TC detection algorithm based on key characteristics of TCs (e.g., Knutson et al. 2007; Camargo and Barnston 2009; Zhao et al. 2010; Chen and Lin 2011). Despite demanding substantial computational resources, operational dynamic TC forecasts in seasonal time scale are experimentally

attempted in various modeling agencies (LaRow et al. 2010; Vecchi et al. 2014; Camp et al. 2015). Recently, the performances of dynamic models have been improved significantly from just a few years ago (Camargo et al. 2007a). However, the dynamical prediction of regional TC activity or TC landfall is still challenging because the simulation of TC tracks is quite unreliable in climate models with their own TC detecting criteria (Camargo et al., 2006). So far, these two approaches have been widely applied to existing prediction models of seasonal TC activity.

As an alternative to these statistical or dynamical TC forecasts, several recent studies have introduced hybrid statistical–dynamical approaches for TC prediction over key ocean basins (e.g., Wang et al. 2009; Kim and Webster 2010; Vecchi et al. 2011; H.-S. Kim et al. 2012; Li et al. 2013). These hybrid methods utilize the simultaneous relationship between TC activities (i.e. predictand) and large-scale environmental conditions (i.e. predictors) forecasted by dynamical models to improve upon the traditional pure statistical forecasts. It is known that the hybrid forecast can overcome the weaknesses inherent in the statistical methods and also preserve the physical and direct connections between summertime TCs and the environmental conditions (H.-S. Kim et al. 2012). Furthermore, these approaches have operational advantages because TC predictions can be updated by real-time according to forecasted atmospheric and oceanic conditions from coupled atmosphere-ocean climate models.

Most seasonal TC prediction approaches target the total number of TCs over the entire basin. However, the impact of TCs on human society are mainly associated with their landfalls rather than the total basin-wide TC counts (Pielke and Landsea 1998; Pielke et al. 2008; Weinkle et al. 2012). Recognizing the practical importance of TC pathways, several recent studies attempted to predict the TC track density by track-oriented-pattern categorization approach. Chu et al. (2010) and Chu and Zhao (2011) introduced this concept. They argued that this approach can eventually, in principle, lead to better performance via more detailed physical links with individual TC track patterns.

As a hybrid statistical-dynamical type model, Kim et al. (2012) developed a track-pattern-based model that predicts summertime (June through October, JJASO hereafter) TC activity over the WNP. The key idea of this model is to individually predict seasonal TC counts for a several number of track patterns, and build up a final forecast map of TCs track density by combining all track clusters over the entire basin. Thus, the track-pattern-based model has unique merit in providing predictions for the spatial TC track density anomaly in the WNP. The prediction is operationally made in early-May using the dynamically forecasted atmospheric/oceanic fields by the National Centers for Environmental Prediction (NCEP) Climate Forecast System version 1 (CFSv1), which is a fully coupled ocean-land-atmosphere seasonal prediction system (Saha et al. 2006). However, the operational data

of NCEP CFSv1 is no longer released from April 2011. Thus it is further necessary to reintroduce the model, because several revisions were made for the input data from the NCEP CFSv1 forecasts and the method of incorporating the predictors into the statistical model, which differ from the earlier version described in H.-S. Kim et al. (2012).

This track-pattern-based approach can be applied not only to TC track classification and prediction in WNP, but also to NA basin. The classifications and predictions of the TC track patterns over the NA as well as their frequencies have been reported in several studies (Hall and Jewson 2007, 2008; Kossin et al. 2010; Kozar et al. 2012). A number of previous studies have applied clustering techniques to TC tracks; such studies have shown that clustering analysis can be used to divide the overlapped effects of climate systems into individual categories of TC track patterns (Elsner 2003; Kossin et al. 2010). Based on these properties, we have developed statistical prediction models for each track pattern, and merged the predictions for individual track patterns into a seasonal TC track density forecast for the entire basin. Therefore, one of the objectives of this thesis is to develop a skillful seasonal TC prediction model for the NA basin. Moreover, skill examination of this hybrid statistical–dynamical model is performed in terms of the entire basin aspect. By comparing the model results to observations, we can evaluate the model's forecast skill for the entire NA basin and sub-basins. Specifically, this thesis targets the prediction of TCs that affect the

East Coast of the US, the Gulf of Mexico, and the Caribbean Sea, all of which are severely affected by landfalling TCs.

In addition, we aim to develop models for forecasting intense TCs at seasonal time scales for the WNP and NA basins using a hybrid statistical–dynamical method as well as to understand the distinctions between intense and weak TCs. The track-pattern-based hybrid forecasting method is modified to forecast the intense TC activities in the two basins by using their observations for the 32-year period of 1982–2013. Because these hybrid models showed comparable or higher skills in forecasting seasonal TC activities than numerical modeling approaches thus far, the model is then applied to the real 2014 TC season to examine its performance for the NA and WNP basins.

As well as the seasonal TC prediction, near-future (i.e., the next one or two decades) climate prediction is challenging because of the limitations in our understanding of climate variability, uncertainties in climate models, and the lack of long-term observational data. Climate variability on decadal time scales results from both internal variability (i.e., time-evolving natural oscillation) and external forcings (i.e., greenhouse gas effects) so that near-future prediction is a marginal time scale with application of initial values and forced boundary conditions. As such, it has been referred to as a *predictability desert* between short-range forecasting and long-term future projections (Meehl et al. 2009; 2014). At the same time, the impacts of near-future climate

change have become a serious concern because of their substantial socio-economic costs and environmental risks that directly affect human kinds. Thus, studies on near-future climate are emerging and would help to formulate the long-term plans for mitigating the damages due to extreme weather phenomena, including TCs, under near-future climate conditions.

The changes of TC activities in the next several decades are among the most imminent concerns due to their potential for huge damages in coastal regions. There has been a growing demand to explore the near-future changes in TC activities such as the location and frequency of TC genesis, intensity, and track patterns. Most previous studies on projecting future TC activities focused on the genesis frequency and maximum intensity in the late 21st century (Bengtsson et al. 2007; Stowasser et al. 2007; Emanuel et al. 2008; Knutson et al. 2010, 2015; Murakami et al. 2012; Emanuel 2013). There have been only a few studies predicting TC tracks in the far-future (Park et al. 2017) although tracks are the most crucial factor for determining TC disasters as they are related to landfall locations. Near-future changes in TC track patterns have therefore become necessary to address TC disasters in advance, but little has been known yet.

Previous studies have shown enhanced TC activities in the NA in recent years due to basin-wide sea surface temperature (SST) warming and weakened vertical wind shear (VWS) over the tropical NA (Goldenberg et al. 2001; Saunders and Lea 2005; Elsner and Jagger 2006; Holland and Webster

2007; Klotzbach 2007). Among the large-scale climate variabilities, the Atlantic Multidecadal Oscillation (AMO) and El Niño–Southern Oscillation (ENSO) are known to strongly affect TC activities by modulating the SSTs and VWS over the tropical NA (Gray 1984a; Goldenberg and Shapiro 1996; Xie et al. 2005; Vimont and Kossin 2007; Colbert and Soden 2012; Davis et al. 2015; Krishnamurthy et al. 2016). The recent positive phase of AMO since the late 1990s is responsible for the higher basin-wide SSTs over the NA, which has been attributed to the recent enhancements in TC activities there. In El Niño (La Niña) episodes, fewer (more) TCs have occurred in the NA due to stronger (weaker) VWS and greater (weaker) atmospheric stability over the Caribbean and the tropical Atlantic basin. Thus, if climatological changes in the NASST and ENSO occur in the near future, the NA TC activity will also change in response to the altered environmental conditions (Vimont and Kossin 2007; Davis et al. 2015; Krishnamurthy et al. 2016).

Another objective of this thesis is to predict the NA TC activity in the near-future period 2016–2030 and to explain the mechanisms related to the near-future climate condition, especially in relation to NASST and ENSO variations. To accomplish these objectives, we use a track-pattern-based hybrid prediction model (Choi et al. 2016a). This model has been shown to be capable of simulating realistic seasonal NA TC activity such as track density and genesis frequency. Although this model was originally developed to predict seasonal NA TC activity, it is also applicable for near-future

predictions because the present-day empirical relationships used in the model are likely to be valid for the next 15 years. Finally, the impacts of anthropogenic forcing and natural variability on near-future climate in the NA are discussed by investigating near-future SST predictions from multi-model products.

This thesis is organized as follows. Data and method are described in section 2. Section 3 presents the understanding of seasonal TC activity and development of prediction model in both of the WNP and NA basins. The near-future TC prediction is shown in the section 4 and section 5 provides future study regarding TC prediction. Finally, section 6 gives the concluding remarks including summary and discussions of this thesis.

2. Data and Method

2.1 Data

2.1.1 Tropical cyclone

The best track datasets of WNP TC information are obtained from the Regional Specialized Meteorological Center (RSMC) Tokyo–Typhoon Center and the Joint Typhoon Warning Center (JTWC). Both of the datasets include TC center position (latitude and longitude), the maximum sustained wind speed, and the minimum sea level pressure at least for each 6-h interval. The main difference is that the RSMC TC data includes 10-min averaged maximum sustained wind speed whereas the JTWC provides the 1-min averaged maximum sustained wind speed to apply the Saffir-Simpson hurricane wind scale in the below. A TC in this thesis is selected if its maximum wind speed stronger than tropical storm intensity ($v_{max} \geq 17$ m s^{-1}). Although release period ranges from 1950s to present, we exclude pre-satellite period (before the 1965). The analysis and prediction are focused on the typhoon season (June through October; JJASO) when about 80% of the annual WNP TCs are formed climatologically.

The data for TC activities over the NA basin during 1965–2015 are obtained from the hurricane database (HURDAT) at the National Hurricane Center, National Oceanic and Atmospheric Administration (NOAA), which

posts the location and intensity of all NA TCs at 6-h intervals (McAdie et al. 2009). The HURDAT best track data are available from 1851, however this study has analyzed only the TCs from 1965 when satellite observations became available, to 2015 (Chu 2002). We focus on the TC activities from August through October (ASO) because the number of NA TCs in this three-month period is relevant to about 80% of climatological mean annual NA TC counts. Only the cyclones with maximum sustained wind speeds greater than 17 m s^{-1} are defined as TCs as the WNP TC.

2.1.2 Large-scale environmental fields

To investigate the effects of the large-scale environment on WNP TC activity, atmospheric circulation data is obtained from the NCEP Reanalysis-2 dataset (R-2; Kanamitsu et al. 2002), which has a horizontal resolution of 2.5° × 2.5° in latitude and longitude. We analyzed the VWS defined as the zonal wind difference between 200 hPa and 850 hPa in addition to the zonal wind at 200 hPa and 850 hPa, relative vorticity at the 850 hPa level (U200, U850, and VOR850, respectively), and geopotential height at 500 hPa (Z500). The monthly SST data is obtained from the NOAA Extended Reconstructed SST version 3 (ERSST v3; Smith et al. 2008). ERSST v3 data has a 2° × 2° resolution in latitude and longitude. The reanalysis data and SST during 1982–2015 are used for consistency with the dynamic seasonal forecast described below.

To develop the hybrid prediction models, we investigate empirical relationships between the large-scale environments and TC activity using atmospheric–oceanic circulation data from the NCEP CFSR (Saha et al. 2010). This product is a fully coupled global reanalysis with a spatial resolution of 0.5° × 0.5° in latitude and longitude. We analyzed SST, U200, U850, VWS, and VOR850. The ASO-averaged fields from the CFSR data recorded during 1982–2015 are used for consistency with the NA TC datasets.

For the dynamical component of this hybrid statistical–dynamical model, we adopt the NCEP CFS version 2 (CFSv2), a fully coupled global atmosphere–ocean–land modeling system. NCEP CFSv2 was updated in March 2011 from the earlier CFSv1 model and has since been used for operational seasonal climate forecasting (Saha et al. 2014). In this thesis, the monthly NCEP CFSv2 retrospective forecasts at a 1° × 1° resolution in latitude and longitude for the period 1982–2015 are used. The retrospective data is reforecasted with the CFS Reanalysis as an initial condition, which is utilized to construct a simultaneous statistical relationship between TC activities and environmental fields for each TC cluster. The CFSv2 generates nine-month forecasts consisting of four ensembles per day with different initial conditions at 00, 06, 12, and 18 UTC. The retrospective data includes nine-month forecasts issued every five days, beginning from January 1 of every year; thus, 24 ensemble members are generally included for each month except November, which has 28 members.

In addition, the real-time operational forecasts of CFSv2 are used for model application to real forecast. The real-time operational CFSv2 data are released daily for the four aforementioned reference times. To forecast the TC activity during the TC season, we use 12 ensemble members of NCEP CFSv2 forecasts representing the number of ensembles for half a month. The ensemble average should be needed to avoid the dependence of the forecasts on the initial conditions. These ensemble members are issued on three consecutive days including two five-day periods, 10 and 5 days prior to the forecast in addition to the original forecast day for our TC prediction model (e.g., June 25 and 30 and July 5 for the case of a July 5 TC forecast). Additionally, we verified the model performance against observations every month by changing the forecast day in preceding winter to early summer.

The long-term free runs of CFSv2 in CMIP simulations up to the year 2030 are used for the near-future prediction (Saha et al. 2014). Three ensemble members starting from January 1 of 1988, 1996, and 2002, are used for the CFSv2 CMIP simulations. Although the CFSv2 CMIP simulations are initialized with actual conditions (i.e., CFSR), errors would still arise from long numerical simulation of more than several years. A previous study reported that the system is stable with no drifting caused by technical problems (Saha et al. 2014). Thus, we investigate the changes in the TC activities by averaging all three ensemble members for the present period of 2002–2015 (P1) and for the near-future period of 2016–2030 (P2), which are

the overlap periods of the three ensembles. In addition, the use of CFSv2 to predict near-future TC frequency is advantageous to us because the model itself was used for developing the seasonal prediction, and it reasonably simulates the behavior of climate variations (Saha et al. 2014; Choi et al. 2016a). The CFSv2 in CMIP simulations have the same settings as those used for CFSv2 seasonal hindcast simulations. For the future CO_2 concentration, it is extrapolated to increase by two parts per million in volume per year based on the current seasonal observations.

For comparison with the near-future SST prediction of CFSv2 CMIP simulations, we use 24 CMIP5 models including ACCESS1-0, BCC-CSM1.1, BNU-ESM, CanESM2, CCSM4, CESM1-BGC, CMCC-CM, CMCC-CMS, CNRM-CM5, CSIRO-Mk-3-6-0, FIO-ESM, GFDL-CM3, GFDL-ESM2G, GFDL-ESM2M, GISS-E2-H, GISS-E2-R, HadGEM2-CC, HadGEM2-ES, INM-CM4, IPSL-CM5A-LR, IPSL-CM5B-LR, MPI-ESM-LR, MPI-ESM-MR, and NorESM1-M (see http://cmip-pcmdi.llnl.gov/cmip5/availability.html). The historical simulations, prescribed with observed atmospheric composition and time-evolving land cover changes, and mid-range mitigation simulations (representative concentration pathway 4.5, RCP4.5) corresponding to radiative forcing values of 4.5 W m^{-2} up to the year 2100 are investigated in this study (Taylor et al. 2012). Because 24 CMIP5 models have different horizontal resolutions, they are interpolated into 2.5° × 2.5° grids for consistent analysis. We analyze

the historical and RCP4.5 scenario datasets for the periods 2002–2005 and 2006–2030, respectively.

2.2 Method

2.2.1 Fuzzy clustering algorithm

In this thesis, we first have identified typical TC track patterns in the WNP and NA using the fuzzy *c*-mean method (FCM; Bezdek 1981), one of the most widely used methods in clustering analysis. A previous study of Kim et al. (2011) which examined various clustering techniques found that the FCM can yield reliable classification of TC tracks that have intricate geographical features for defining boundaries separating different clusters. Once these climatological TC patterns are set, it is not necessary to repeat this process due to its quasi-stationary feature and also the basis of our prediction model is prepared. Because all TC datasets must be of equal length for performing FCM, each TC track is interpolated into 20 segments following Kim et al. (2011) who showed that 20 segments are sufficient for representing the characteristics of TC tracks. The FCM is performed by minimizing the *c*-means functional (*J*) defined as

$$J = \sum_{i=1}^{C} \sum_{k=1}^{K} (\mu_{ik})^m \, \|\boldsymbol{x}_k - \boldsymbol{c}_i\|^2, \qquad (1)$$

where

$$\mu_{ik} = \left[\sum_{j=1}^{C} \left(\frac{\|\boldsymbol{x}_k - \boldsymbol{c}_i\|^2}{\|\boldsymbol{x}_k - \boldsymbol{c}_j\|^2} \right)^{\frac{2}{m-1}} \right]^{-1},$$

and

$$\boldsymbol{c}_i = \frac{\sum_{k=1}^{K} (\mu_{ik})^m \boldsymbol{x}_k}{\sum_{k=1}^{K} (\mu_{ik})^m}.$$

C is the number of clusters, *K* is the number of TCs, μ_{ik} is the membership coefficient of the *k*th TC to the *i*th cluster, *m* is the fuzziness coefficient, $\boldsymbol{x}_k$ is the *k*th TC position, $\boldsymbol{c}_i$ is the center of the *i*th cluster, and the symbol $\| \ \|$ represents the Euclidean norm. The membership coefficient, a special measurement of the FCM, indicates the distance of the *k*th TC with respect to the *i*th cluster center as a probability concept. Each TC has membership coefficients with values between zero and one for all clusters. After the membership coefficients and cluster centers are calculated by minimizing the *c*-means functional in Eq. (1), individual TCs are assigned to a specific cluster for which its membership coefficient is largest, allowing for probabilistic characteristics of their tracks. This procedure makes newly-updated TC track data with additional observations to be assigned to one of the track patterns based on the historical data. Finally, TC track densities for each cluster are constructed in a 5° × 5° latitude and longitude grid nest by sorting TC tracks.

The clustering results must be carefully examined as they vary according to the number of clusters (Camargo et al. 2007b; Kim et al. 2011) and will eventually affect the entire model development. To objectively determine the

optimal number of clusters in FCM, we examined the sensitivity of the four scalar indices, the partition coefficient (Bezdek 1981), the partition index (Bensaid et al. 1996), the separation index (Xie and Beni 1991), and the alternative Dunn index (Dunn 1973), to the number of clusters. The definitions and properties of these indices are described in Dunn (1973), Bezdek (1981), Xie and Beni (1991), Bensaid et al. (1996), and Kim et al. (2011). Larger (smaller) values of partition coefficient (partition index, separation index, and alternative Dunn index) indicate that corresponding cluster number is more optimal in FCM (Kim et al. 2011). The comprehensive optimum cluster number detection process using these four indices showed that seven (four) TC track patterns can adequately represent the WNP (NA) TC track properties during the TC season (figures not shown). In same manner, three (two) intense TC track patterns are determined in the WNP (NA) basin.

2.2.2 Track-pattern-based model

The track-pattern-based model was originally developed to predict seasonal TC activity in the WNP as a hybrid statistical-dynamical type (Kim et al. 2012). Process of the model mainly consists of three steps. Step 1 is the process to obtain the seven TC track patterns by the clustering analysis. This step has been done already by clustering 855 TC tracks during the typhoon seasons (i.e., JJASO) of 1965–2006 into the seven representative patterns (Kim et al. 2011). These seven gridded TC track patterns (P_{C_i}), which is the

basis of this seasonal TC track density forecast model, are defined as

$$P_{C_i}(lat, lon) = \frac{N_{within\ 5° \times 5°\ grid\ box}(lat, lon)}{N_{C_i}}, \quad (2)$$

where i is the cluster number, and N_{Ci} indicates the number of TCs in cluster i. These seven patterns are known to be climatologically static parameter. Accordingly, step 1 has been fixed for the time being and the seven patterns are utilized as the basis of this model.

Next step is the actual prediction module of this model. Step 2 is to predict TC frequencies of each track pattern with the NCEP CFSv1 dynamic seasonal forecasts and the statistical Poisson regression models (i.e., a hybrid statistical-dynamical type). As a predictor for this model, the critical large-scale environments (e.g., the typhoon-seasonal mean SST, U200, VWS, U850, Z500, and VOR850) from the NCEP CFSv1 retrospective forecasts have similar interannual relationships with their counterparts from the NCEP R-2 data, indicating that the NCEP CFSv1 has a skill to predict the large-scale environments related to the seasonal TC count of each pattern. In the statistical part, the model prediction of the TC frequency for each track pattern is developed by incorporating the corresponding predictors into the Poisson regression. The Poisson regression is known to show better skill for the case where the predictand consists of non-negative integer data such as TC frequency (Elsner and Schmertmann 1993; Chu and Zhao 2007, 2011; Chu et al. 2010; Kim et al. 2012). A Poisson regression assumed that the expected

occurrence rate is the exponential function of the linear combinations of the predictors. Detailed formula is defined as

$$\tilde{y} = \exp\left(\sum_{j=1}^{k} \beta_j x_j + \beta_0\right), \quad (3)$$

where $\tilde{y}$ is the expected value of occurrence of the event (i.e. predictand) which is equal to Poisson intensity parameter, k is the number of predictors, β_j is the coefficient of the jth predictor (x_j), and β_0 is the constant. In our hybrid statistical–dynamical model, the predictors (x_j) are obtained from the seasonal forecasts of CFSv2. The regression parameters are estimated by maximizing the likelihood of the Poisson distribution using iteration during the training period.

The step 3 is to assemble the forecasts of TC counts with basis track densities of the seven patterns (obtained a priori from the climatology) so that one basin-wide map of TC track density in the WNP can be constructed. If the track-pattern-based forecasts are made, the basin-wide map of TC track density can be constructed by summing the climatological each track pattern density weighted by the forecasted TC count over all patterns divided by the total TC count forecasted. In other words, all of the predicted results are multiplied to the basis of this model (i.e. seven gridded TC track patterns) and combined together to construct the final forecasts (P_l) of TC occurrence for each grid over entire WNP basin. The formula is expressed as

$$P_l = \sum_{i=1}^{7} N_{C_i,l} \times P_{C_i}(lat, lon). \quad (4)$$

In Eq (4), l is the target year, and $N_{Ci,l}$ the predicted number of TCs in cluster i for the year l. The forecasted TC track density represents the probability of TC tracks at each grid point in the entire basin. The final forecast maps (i.e., the total and anomalous track density maps) are issued after biases in the mean and standard deviation are corrected using the modeled and observed climatological track densities.

For validation, we used the leave-one-out cross-validation technique to evaluate the performance of the forecast model. This method has been widely used for estimating forecast models' accuracy in practice (Gray et al. 1992; Elsner and Schmertmann 1993, 1994; Wilks 2006; Chu et al. 2007; Kim et al. 2012; Ho et al. 2013; Choi et al. 2016a, b). Specifically, when predictions are performed for the training period, the model is iteratively adjusted for all available retrospective forecasts data except the target year. Because annual TC activities can be regarded as independent events, the condition for using cross-validation is satisfied (Gray et al. 1992). If we select a certain year for re-forecasting, this technique optimizes our model parameters to make the best fitting on the basis of the remaining years. We repeatedly performed this re-forecast process several times to cover the entire training period.

2.2.3 Upgrade the dynamic part of model from CFSv1 to CFSv2

This model uses NCEP CFS datasets as the dynamic component to develop the hybrid statistical–dynamical process. As mentioned above, the earlier CFSv1 was recently replaced to CFSv2 in March 2011. Following this upgrade, the track-pattern-based model, which was originally developed using CFSv1, was re-built based on the CFSv2 data (Fig. 2.1). In the revised module based on the NCEP CFSv2, the model training period for the statistical prediction is extended to the year 2010 (i.e., 1982–2010). These changes in the dynamic forecast data and training period have a substantial influence on the selected predictors and their critical regions, and hindcast skills for all clusters.

First of all, we can look into the predictor sets for using to the prediction of each track pattern. The selection of appropriate predictors is a crucial factor in yielding better prediction performance of the track-pattern-based model. In this model, the predictors are selected by the following four rules.

1) The predictor candidates are SST, U200, VWS, and VOR850 as previous version. These environmental parameters are known to affect the TC genesis and tracks (e.g., Gray, 1968; Wang and Chan, 2002; Kim et al., 2005b).

2) Critical regions are determined for each predictor and each cluster by considering significant correlation patterns between the observed TC counts and the large-scale environments during JJASO. Correlation analysis is performed for the 12-member (early-May) ensemble mean of NCEP CFSv2

reforecasts as well as the observed environments of the NCEP-R2 data. We can identify statistically significant and physically reasonable regions for candidate predictors of each cluster by comparing the two correlation patterns cluster (figures not shown. See Figs. 6 and 7 in Ho et al., 2013). If there are multiple significant regions in a cluster, the cross-validation tests are performed by changing the critical region, by which the set of critical regions showing the better hindcast skill is determined.

3) Once the critical regions are selected, final predictors are obtained with respect to each member of the NCEP CFSv2 ensemble forecasts. For each ensemble member, the spatial average of candidate predictor variables within their individual critical regions is calculated using only the grid points for which the correlation coefficient is significant at the 95% confidence level, and where the sign of the correlation is the same as that determined from the correlation patterns for the ensemble mean. It is noted that the significant grid points used to construct final predictors are all different between the 12 ensemble members

4) The cross-validation tests are also performed to find the optimal combination of predictors showing the better hindcast skill. In addition, a variance inflation factor (VIF) (Davis et al., 1986) is examined for each ensemble predictor set to avoid multicollinearity among the predictors. If a predictor has a VIF greater than 10, the predictor is dropped from the final

predictor set in order to ensure the stability of the regression-based forecast model (e.g., Davis et al., 1986; Villarini et al., 2011).

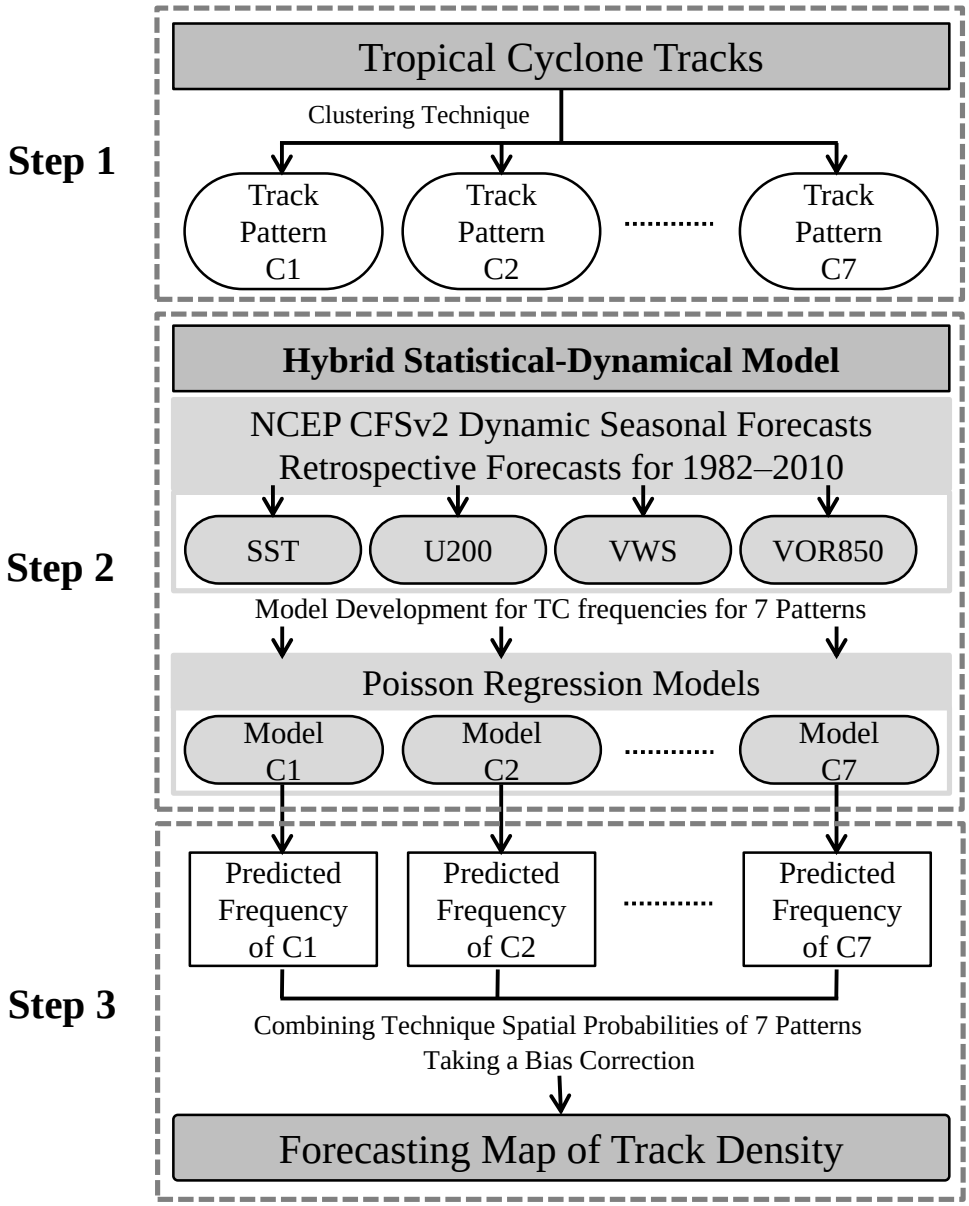

Figure 2.1. Schematic flow diagram of seasonal WNP TC prediction model after the modification.

The final predictor sets are obtained from each ensemble member of the NCEP CFSv2 forecasts, although the critical regions are selected using their ensemble means. Therefore, the grid points used for the final predictor can vary depending on the correlation maps for the individual CFSv2 ensemble members, whereas the critical regions are invariant. As the NCEP CFSv2 reforecasts provide four ensembles every fifth day, the same ensemble members are obtained for the final predictor sets from the NCEP CFSv2 reforecasts as well as operational forecasts. Using these ensemble predictor sets, the hybrid prediction module can provide ensemble predictions. The ensemble prediction of the hybrid statistical–dynamical prediction module yields more accurate forecasts than the use of single predictions (Kim et al., 2012).

We calculated scalar quantities such as the correlation coefficient (COR), root–mean–square errors (RMSEs) and mean square skill score (MSSS) by cross-validation analysis (Table 2.1). These measures are generally used to verify the reliability of the forecast (Wilks, 2006). The formulas of RMSE and MSSS are

$$\mathrm{RMSE} = \ [\mathrm{MSE}]^{\frac{1}{2}} = \ \left[\frac{1}{\mathrm{n}}\sum_{\mathrm{t}=1}^{\mathrm{n}}\left(\mathrm{y}_{\mathrm{obs,t}} - \widetilde{y_t}\right)^2\right]^{\frac{1}{2}}, \tag{5}$$

$$\mathrm{MSSS} = 1 - \ \frac{MSE_{model}}{MSE_{obs}} = 1 - \ \frac{\frac{1}{n}\sum_{t=1}^{n}\left(\mathrm{y}_{\mathrm{obs,t}} - \widetilde{y_t}\right)^2}{\frac{1}{n}\sum_{t=1}^{n}\left(\mathrm{y}_{\mathrm{obs,t}} - \overline{y_{obs}}\right)^2}, \tag{6}$$

where n is the number of the training years (i.e., 32 in this study), $y_{obs,t}$ is the observed TC frequency for the *t*th year, $\tilde{y}_t$ is the ensemble average of the hindcasts of TC frequency for year *t*, and $\overline{y_{obs}}$ is the mean of the observed TC numbers. The accuracy of reconstructed TC counts (i.e., the correlation between the observed and predicted TC counts) for each cluster is slightly improved in the updated version; that is, the statistics (e.g., COR, RMSE, and MSSS) that can be used to measure the reliability of the model forecast (Wilks, 2006) are generally better in the majority of the patterns.

Table 2.1. Correlation coefficients (COR), root–mean–square errors (RMSEs), mean square skill scores (MSSS) between the observed TC frequencies and the ensemble mean of NCEP CFSv1 and CFSv2 hindcasts for the 1982–2010 period.

Pattern	COR		RMSE		MSSS	
	CFSv1	CFSv2	CFSv1	CFSv2	CFSv1	CFSv2
C1	0.75	0.81	1.30	1.31	0.54	0.53
C2	0.74	0.85	1.44	1.12	0.53	0.72
C3	0.72	0.77	1.21	1.17	0.51	0.58
C4	0.81	0.83	0.85	1.02	0.63	0.64
C5	0.74	0.84	0.96	0.87	0.51	0.61
C6	0.77	0.77	1.28	1.26	0.50	0.53
C7	0.71	0.78	1.11	0.96	0.49	0.59

3. Seasonal prediction of tropical cyclone activity

In this section, we describe the seasonal TC prediction. We show a brief introduction of substitution for the new dynamical general circulation model (GCM) as an input data to operate quasi-real time prediction, predictability assessment for the abnormal 2010 case. In addition, the development of track-pattern-based prediction models for TC and intense TC activities over the WNP and NA basins are presented. For the validation, we assess the predictability of models by each track pattern and regional perspective.

3.1 Application of the track-pattern-based model in the WNP

As we mentioned above, there are seven representative TC track patterns over the WNP basin (Kim et al. 2011). The seven patterns include three recurvers (C1–C3) mostly affecting East Asian regions (e.g., East/Southeast China, Taiwan, Korea, Japan, and Luzon Island), two more recurvers over the open ocean (C4 and C5) traveling inshore east ocean and offshore east ocean of Japan, one irregular type confined in the South China Sea (C6), and the west-northwestward moving straight-movers traversing the Philippines (C7). Most of them have physically interpretable potential predictors, which enabled us to constitute this track-pattern-based model. For instance, C1–C3 are known to reflect the influences of ENSO, C4 is a unique cluster which has

an exceptional connection to the phase of the stratospheric quasi-biennial oscillation (QBO), and the rest have their own local or broad-scale potential predictors.

3.1.1 Assessment of the 2010 TC season

a. Observational feature of the 2010 typhoon season

From a climatological aspect, most TCs during 1981–2010 were observed during the typhoon season (JJASO) with an annual total of 25.6 TCs that developed in the WNP (Table 3.1). Fourteen named TCs formed in the WNP basin in 2010 representing the lowest count since 1951, even lower than the previous record of 16 named TCs in 1998. In addition, as far as the typhoon season is concerned, development of 13 named TCs is much lower than the climatological mean of 19.6 TCs during the typhoon season. Although not included in the prediction, the pre- (January–May) and post-typhoon seasons (November–December) were also very quiescent and much calmer than the typhoon season in terms of their number ratio to the climatology (Table 3.1). It is found that all seasons constructively contributed to the record-breaking event that occurred in 2010.

Table 3.1. TC frequencies for pre-typhoon, typhoon, post-typhoon seasons averaged over 1981–2010 (climatology), and those in 2010. The interannual variability is presented in parentheses as a standard deviation.

Season	Pre-typhoon Season	Typhoon Season					Post-typhoon Season	Total
Month	Jan–May	Jun	Jul	Aug	Sep	Oct	Nov–Dec	
Climatology	2.5 (1.5)	1.7 (1.2)	3.6 (1.5)	5.9 (1.5)	4.8 (1.4)	3.6 (1.6)	3.5 (1.7)	25.6 (4.6)
		19.6 (4.1)						
2010	1	0	2	5	4	2	0	14
		13						

The spatial distributions of TC activity parameters (e.g., genesis frequency and track density) are displayed with respect to the typhoon season in Fig. 3.1. Figure 3.1a and 3.1b show the climatology of genesis and track density, binned in a 1° latitude and longitude grid box with a 5° radius circular window, respectively. Here, track density is defined as the TC occurrence count in each grid box divided by the basin-wide seasonal total count, which is then converted to the percentage concept [%]. The gridded genesis frequency and track density for the year 2010 are presented in the middle panels (Fig. 3.1c and 3.1d), including actual genesis points and corresponding tracks. In addition, anomalies from the climatology are shown in the bottom panels to distinguish the characteristic features of 2010 effectively (Figs. 3.1e and 3.1f).

Compared to the climatological distribution, TC genesis locations were concentrated west of 150°E (Fig. 3.1c), which represents a typical pattern during La Niña events (Wang and Chan 2002; Kim et al. 2010). Positive anomalies are confined to the area around Taiwan, with negative anomalies spread over the Philippine Sea (Fig. 3.1e). In harmony with the concentric genesis locations near the continent, TC track density also shows a high density around near-coastal regions in East Asia (Fig. 3.1d). The corresponding anomaly pattern further renders the large increase near the landmass more salient and also recovers the decreased activity to its southeast (Fig. 3.1f). Ten of the 14 named TCs that formed in 2010 made landfall.

Considering the overall quiescent genesis, the landfall probability (i.e., the ratio of TC landfalls to total TC genesis frequency) was extremely high in 2010.

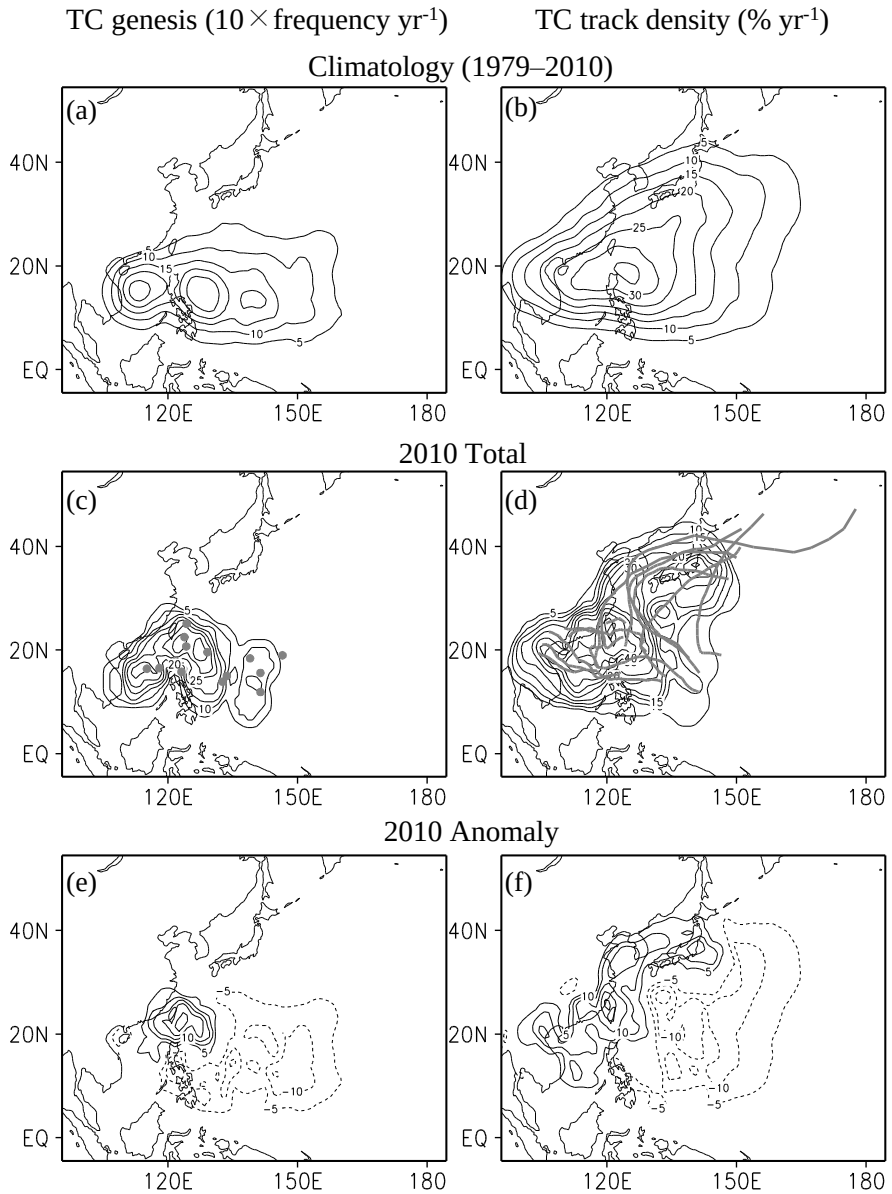

Figure 3.1 TC genesis (left panels; unit: 10 × frequency yr^{-1}) and TC track density (right panels; unit: % yr^{-1}) binned into a 1° × 1° grid box. The value of each grid is counted by the summation of detected TCs within 5° radius from the grid center. Their 1981–2010 climatologies (a and b), totals (c and d) and anomalies (e and f) in 2010 are displayed. Also shown in (c) and (d) are the genesis locations and tracks of TCs, respectively.

The 2010 typhoon season was extraordinary due to the influence of a strong ENSO phase transition from El Niño to La Niña. The observed large-scale environments relevant to TC activity are presented in Fig. 3.2 including the anomalies of (a) SST, (b) VOR850 and 850 hPa horizontal wind, (c) VWS, and (d) steering flow. In Fig. 3.2d, the 5880 gpm lines for the climatology and year 2010 are overlapped to show the typical periphery of the western North Pacific subtropical high (WNPSH) (Tu et al. 2009). Note that the predictors for the track-pattern-based model include SST, U200, VWS, and VOR850.

The tropical Pacific SST anomalies present the general pattern of the La Niña episode characterized by an increased zonal SST gradient along the equator, and warming along the Kuroshio extension (Fig. 3.2a). Corresponding to the anomalous tropical SST distribution, the anomalous 850 hPa horizontal winds show notable easterlies along the near-equatorial zone, forming the meridional shear-induced negative VOR850 anomalies to the north where the main development region of TCs is located (Figs. 3.2b and 3.1a). Such low-level large-scale conditions in the tropical WNP are unfavorable for TC development as both the seasonal-mean convection (Wang and Chan 2002) and the northwestward propagating tropical intraseasonal oscillation are suppressed (Teng and Wang 2003). Further, the VWS anomalies show large negative (positive) values west (east) of 150°E, which correlates well with the westward shift of genesis locations (Figs. 3.2c and 3.1c). Here we demonstrate that the seasonal-mean VOR850 and VWS,

which are necessary conditions for TC development (Gray 1968), disfavored TC genesis in the 2010 typhoon season.

Finally, the large-scale circulation parameters relevant to TC tracks are shown in Fig. 3.2d. Considering the overall genesis locations in 2010 (Fig. 3.1c), a majority of TCs headed toward the Asian continent due to (a) the anomalous steering flows in the genesis locations and inshore seas, and (b) the large expansion of the 5880 gpm line (Figs. 3.2d and 3.1d). In 2010, the 5880 gpm line characterizes the westward expansion of the WNPSH and its northward expansion is physically consistent with warmer SSTs and weaker VWS in the mid-latitudes. The warmer SSTs in the mid-latitudes are highly likely to be a response to more incoming shortwave radiation as the anomalous barotropic anticyclone is centered above that region (Figs. 3.2b and 3.2d).

The west- and southwestward WNPSH expansion can be understood in several ways. First, it can be driven by an eastward-propagating warm tropospheric equatorial Kelvin wave from the warm Indian Ocean (Xie et al. 2009), and/or local negative SST forcing in the tropical Philippine Sea (Wu et al. 2010). Although Wu et al. (2010) showed, through composite analysis, that both are typically observed during an El Niño decaying summer, the SST anomalies in the Philippine Sea during the 2010 season were predominantly positive throughout the season indicating that the latter was not the case in 2010. Second, it can originate from the anomalous easterly Walker circulation

responding to negative heating near the dateline associated with cooling of the tropical central/eastern Pacific (e.g., Sui et al. 2007); that is, the development of La Niña in summer and autumn is a representative case of phenomena favoring this mechanism. As the typhoon season spans boreal summer and autumn, these proposed mechanisms may serve to collaboratively explain the west- and southwestward intrusion of the WNPSH (i.e., weakening of the monsoon trough). Furthermore, it can be induced by the anomalous descent region of the local Hadley circulation in the WNP due to convective heating in the maritime continent (e.g., Sui et al. 2007; Chung et al. 2011). Each of these mechanisms are often referenced to explain the interannual variation of TC genesis frequency in the WNP (e.g., Zhou and Cui, 2008; Du et al. 2011; Zhan et al. 2011; among others), and are applicable to the 2010 typhoon season as well.

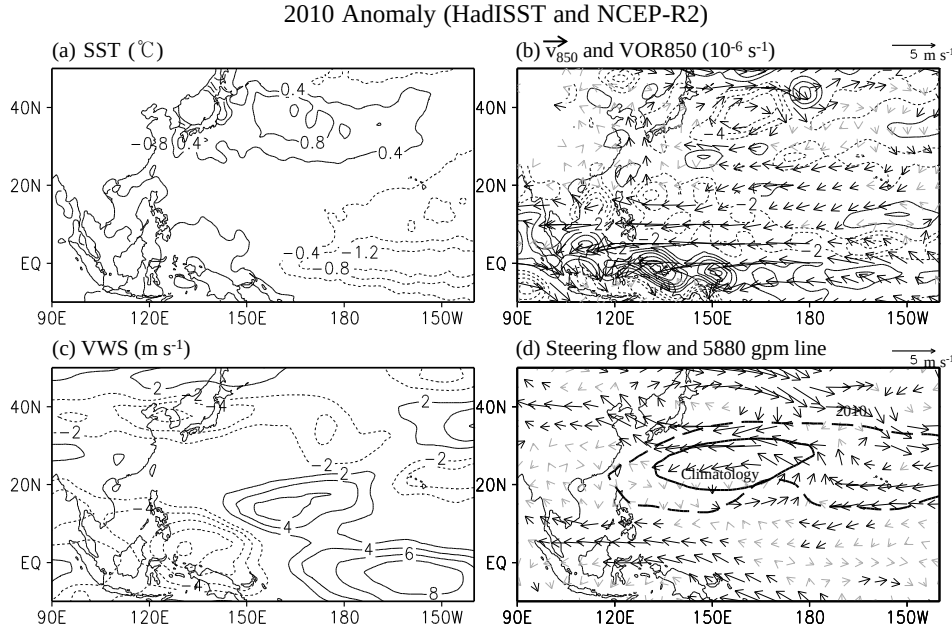

Figure 3.2. Observed anomalies in (a) SSTs, (b) 850 hPa horizontal winds and VOR850, (c) VWS and (d) steering flows. The 5880 gpm lines at 500 hPa in the climatology (dashed line) and 2010 typhoon season (solid line) are overlapped in (d). Wind vectors less than 1 m s^{-1} are shown in grey color.

b. Seasonal prediction of large-scale environments

A direct comparison with the observed large-scale environments (Fig. 3.2) is a simple and effective way to evaluate the NCEP CFSv1 ensemble-mean seasonal forecast. Identical variables are obtained from the NCEP CFSv1 twenty members ensemble forecasts and their ensemble-mean anomalies are illustrated in Fig. 3.3. The 200 hPa horizontal wind is displayed instead of the steering flow in the forecasted large-scale environments as it consists of one of the four potential predictors, i.e., U200. A skillful seasonal forecast of TC activity by the track-pattern-based model largely depends on the predictability of the ensemble forecasts of the NCEP CFSv1. In Fig. 3.3, the statistical significance is calculated by the independent one sample t-test. The test statistic used is $t = \frac{\overline{x} - \mu_0}{s/\sqrt{n}}$, where $\overline{x}$ and s are the mean and standard deviation of twenty ensemble members in 2010, respectively, n is the number of ensemble members, and μ_0 is the climatology of the ensemble-mean during the period of 1981–2010.

The forecasted ensemble-mean SST anomalies display the La Niña pattern in the tropical Pacific (Fig. 3.3a). Despite some discrepancies with observed SST (narrow scale warming in the mid-latitudes and South China Sea), the anomalous forecasted SST pattern is clear enough to say the La Niña episode (Fig. 3.2a). Successful forecast of developing La Niña in one or two antecedent seasons indicates that the NCEP CFSv1 is demonstrative of a

positive performance for the 2010 ENSO prediction. In concert with SST anomalies, the forecast ensemble-mean VOR850 and 850 hPa horizontal wind anomalies also remarkably resemble those in the observation, particularly over the tropics where TCs primarily develop (Fig. 3.3b vs. Fig. 3.2b). From this low-level circulation information, we may expect that the model would predict a substantial decrease in TC activity in the WNP by the same possible mechanisms, as explained above. Moreover, the forecast ensemble-mean VWS anomalies show an unfavorable environment (i.e., an increase in the wind shear magnitude) for TC development across the main development region (Fig. 3.3c). Compared to the observation (Fig. 3.2c), the VWS is over-predicted toward the positive value in the west of the Philippine Sea (west of 150°E) and mid-latitude East Asia, while it is slightly under-predicted in the equatorial central Pacific. In the forecast, the upper-tropospheric westerlies intensify slightly along 40°N in concert with a negligible northward intrusion of the WNPSH. Accordingly, weakly positive VWS anomalies are not unexpected in the mid-latitudes (Fig. 3.3c). Further, mid-latitude storm tracks do not significantly migrate northward resulting in weaker seasonal-mean anticyclonic anomalies along the Kurishio extension region in the forecast (Figs. 3.3b and 3.3d). Naturally, less positive SST anomalies than those in the observation are expected, as shown in Fig. 3.3a. Positively over-predicted VWS anomalies around 20°N west of 150°E, where weak VWS anomalies were detected in the observation (Fig. 3.2c), are

attributed to the anomalous northerlies and easterlies at 200 hPa and 850 hPa (Figs. 3.3b and 3.3d), respectively, both of which act to reinforce climatological flows therein (not shown), i.e., northwesterlies at 200 hPa and easterlies at 850 hPa. Westward expansion of the WNPSH is further reflected by the upper-tropospheric anomalies that are related to the anomalous anticyclone centered in the East China Sea (Fig. 3.3d).

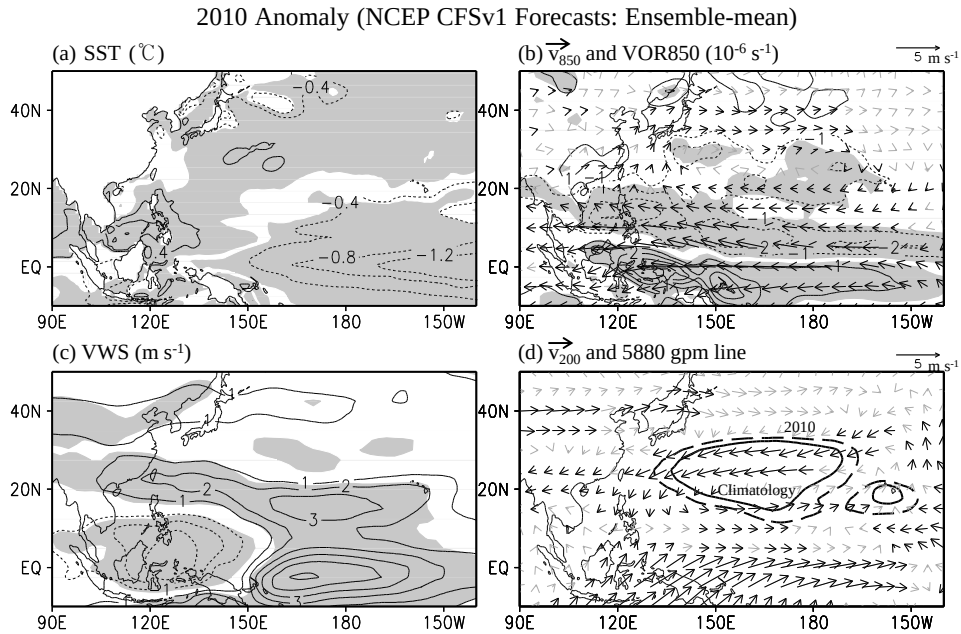

Figure 3.3. NCEP CFSv1 operational ensemble-mean forecasted anomalies in (a) SSTs, (b) 850 hPa horizontal winds and VOR850, (c) VWS and (d) U200. The 5880 gpm lines at 500 hPa in the climatology (dashed line) and 2010 typhoon season (solid line) are overlapped in (d). The shadings and black vectors denote the statistically significant regions at the 99 % confidence levels.

c. Seasonal forecast by the TC prediction model

As described in method section, the track-pattern-based model forecast utilized a total of twenty ensemble members during five consecutive days from 29th April through 3rd May 2010 to forecast the TC activity in the 2010 typhoon season. Thus, the forecasted values hereafter are all from the ensemble-mean of them. First, the forecasted frequencies of the seven track patterns are obtained by step 2 of the track-pattern-based model and listed in Table 3.2. In Table 3.2, the 30-yr climatologies of predicted TC frequencies for the seven patterns and total and their respective standard deviations are also shown in parentheses using the available period of the NCEP CFSv1 retrospective forecasts (1981–2009) and operational forecast in 2010. In addition, the same statistics in the 2010 typhoon season and the climatology are presented based on the 1981–2010 RSMC best track dataset as well. It is again noted that the seven clustered patterns, which were obtained in Kim et al. (2011) using a total of 855 typhoon-seasonal TCs during the period of 1965–2006, are used here based on the empirical fact that the patterns are almost static (e.g., Chu et al. 2010; Kim et al. 2011). The track-pattern-based model has a climatological-mean count very close to the observation as indicated by low mean biases (i.e., forecast minus observation) for each pattern and total (Table 3.2). This is attributed to the advantageous property of the ensemble forecast using the hybrid statistical-dynamical model, i.e., an average of multiple fittings with best predictors. By the way, the interannual

standard deviations (σ) of forecasted TC counts are all smaller than those computed from the observed counts (Table 3.2), let alone the inter-pattern σ (i.e., standard deviation between patterns) for the 2010 forecast (i.e., 0.74 vs. 1.57). These definitely come from the larger number of realizations in the model forecast, which generally reduces year-to-year fluctuation (Table 3.2). Although the extremes are not satisfactorily forecasted by the track-pattern-based model, the signs of anomalies for all patterns are correctly forecasted for the 2010 typhoon season and the summation of them (i.e., 16.4) is well below normal ($< -1\sigma$) (Table 3.1). This indicates the feasibility of the track-pattern-based model using the NCEP CFSv1 operational ensemble forecasts for forecasting the seasonal total TC genesis frequency, though this model did not aim at forecasting this parameter (Kim et al. 2011). With these forecasted TC counts for the seven patterns, the basin-wide map of TC track density can be constructed by step 3.

Using this track-pattern-based model, predicted TC genesis number during the 2010 TC season (i.e., 16.4) is more reliable than those predicted by other agencies. For example, the Tropical Storm Risk predicted in May that 24.1 TCs would occur in 2010. Likewise, the city university of Hong Kong presented in April that 24 TCs will be developed for whole year. At June, the Central Weather Bureau in Taiwan predicted 20–23 TCs would form in 2010. Considering the total genesis frequency of the WNP TC in 2010 year is 14, all of the meteorological agencies showed significant overestimations

of the number of WNP TC.

Thus far, the forecasts of the track-pattern-based model in 2010 have been summarized. In the following subsection, the forecast verifications will be given in detail, which will help to understand the characteristic of the track-pattern-based model.

d. Forecast verification

After step 3 process, applying bias correction process for both mean and variation (Kim et al., 2012), final forecast map is constructed (Fig. 3.4a) showing the total (contour) and anomalous (shading) track densities in comparison with the observation (Fig. 3.4b). These result is derived from each cluster prediction (Table 3.2). We can find that the anomaly forecast for each pattern generally followed the observed anomaly in terms of its sign. Although the model slightly under-predicted the absolute TC count of C1 compared with the observed count, it over-predicted the absolute TC counts for C2, C4, and C5. In contrast, C3, C6, and C7 are nearly perfectly reproduced in terms of the TC count similarity with their observed counterparts (Table 3.2). However, it does not assure that the model prediction success the anomalous track density in the northern South China Sea and Taiwan, despite a near perfect forecast for C3, C6, and C7, i.e., the effective patterns for those regions. Thus, it is apparent that a good forecast of absolute TC counts for the effective patterns of a region does not necessarily guarantee

good regional probability. This implies that bad forecasts in other patterns deteriorate the regional predictability where TCs of the patterns do not directly traverse.

The reason is that this model prediction result is based on relative percentage concept which has a property that all patterns influence the predictability one another as fuzzy idea. Although the absolute counts for C3, C6, and C7 (3, 3, and 2, respectively) are all lower than their respective climatological values (3.5, 4, and 2.5), their relative percentages (23.1%, 23.1%, and 15.4%) are all higher than the climatology percentages (18.3%, 20.4%, and 13.0%). This explains why there was an increase in the anomalous track density around the northern South China Sea and Taiwan in the observation (Fig. 3.4b). Conversely, the anomalous track density is constructed to have negative values therein, which is contrary to the observation (Fig. 3.4a vs. Fig. 3.4b), despite near-perfect forecasts of the decreases in absolute TC counts for those three patterns by step 2 of the model. This occurs as their relative percentages do not increase but in some cases decrease as compared with the climatological percentages (e.g., C3 and C6), with negligible anomalies resulting therein. Further, the final forecast map does not capture the negative anomalies offshore to the east of Japan. In the observation, the effective patterns for that region (i.e., C2, C4, and C5) all largely decreased, leading to clear negative anomalies. Conversely, all effective patterns for that region were over-predicted in the forecast and did

not undergo a significant decrease in their relative percentages compared with their climatological percentages, resulting in negligible anomalies. In contrast to the aforementioned regions, the anomalous track densities followed their observed counterparts and are well above, and below, normal near Korea and Japan, and the subtropical Philippine Sea, respectively. Enhanced predictability for those regions is better explained by the relative percentages than by absolute TC counts.

Table 3.2. TC counts (*N*) and relative percentages of forecasted and observed in each pattern for the 2010 typhoon season. Presented in parentheses are their respective climatology.

Pattern	TC frequency (N)		Relative percentage (%)	
	Forecast	Observation	Forecast	Observation
C1	3.4 (3.3)	4 (3.0)	20.9% (16.5%)	30.8% (16.2%)
C2	1.9 (3.1)	0 (2.8)	11.6% (15.0%)	0.0% (13.4%)
C3	2.7 (3.6)	3 (3.5)	16.2% (17.4%)	23.1% (18.3%)
C4	1.8 (2.1)	1 (2.1)	10.8% (10.2%)	7.7% (10.3%)
C5	1.4 (1.8)	0 (1.8)	8.7% (8.9%)	0.0% (8.5%)
C6	3.1 (4.0)	3 (4.0)	19.0% (19.9%)	23.1% (20.4%)
C7	2.1 (2.4)	2 (2.5)	12.7% (12.0%)	15.4% (13.0%)
Total	16.4 (20.3)	13 (19.6)	100% (100%)	100% (100%)

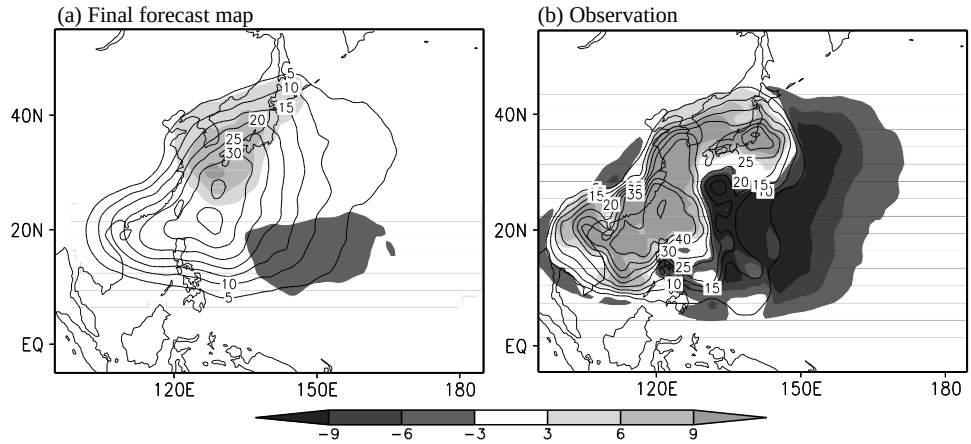

Figure 3.4. (a) Total (contour) and anomaly (shading) of the final forecast map of TC track density and (b) their observed counterparts.

3.1.2 Quasi-real-time operational forecast

The track-pattern-based model was implemented at the National Typhoon Center (NTC) of the Korean Meteorological Administration, and its first experimental forecast for the TC season of 2010 was found to be successful (see aforementioned section). Subsequently, there has been continuous demand to provide technical guidelines for the track-pattern-based model. Separately from such requests, it is further necessary to reintroduce the model via this technical note, because several revisions were made for the input data from the NCEP CFS forecasts and the method of incorporating the predictors into the statistical model, which differ from the earlier version described in Kim et al. (2012). In addition, this thesis permits the model to operate automatically in quasi-real-time. To efficiently operate this seasonal TC forecast system, it is essential for users (e.g. TC forecasters) to have knowledge of the model structure and the capability to handle the model code or process autonomously. As such, this thesis will assist TC forecasters who wish to run and modify the model.

3.2 Prediction of the NA seasonal TC activity

It is notable that this NA prediction model is developed for providing the deterministic predictions for TC occurrence, whereas previous models for the WNP TCs (Kim et al. 2012, Ho et al. 2013) were developed to provide probabilistic information of TC density. Because, after clustering, the number of seasonal TCs in the NA is insufficient for constructing the probabilistic distribution over the vast NA basin, our model targeting the NA basin prediction shows higher predictability in the TC occurrence than probabilistic TC density (figure not shown). Moreover, our model can realistically predict TC occurrence without requiring the bias correction process used for WNP TC prediction.

3.2.1. Pattern classification of the NA TC tracks

Figure 3.5 displays the four TC track patterns and the entire 432 TC tracks over the NA during ASO from 1965 to 2012. The TCs of cluster 1 (C1-pattern) generally originate off the North American East Coast (sub-tropical western NA) and propagate northeastward along the US East Coast (Fig. 3.5a). These TCs often affect and make a landfall in the eastern US region. The C2-pattern is characterized by tracks entering the Gulf of Mexico and the Caribbean Sea (Fig. 3.5b). These TCs generally form near Cuba and Haiti and move northwestward to the Gulf of Mexico. The devastating hurricane Katrina in 2005 belongs to this cluster. The TCs in the C3-pattern originate over the vast

open ocean of the NA and move to mid- and high-latitude regions with recurving tracks (Fig. 3.5c). Although this type of TC has the longest life span and the strongest intensity, its damages are usually small because its track remains mostly over the ocean. The C4-pattern TCs are generated near the tropical region of the NA and move westward affecting maritime islands (Fig. 3.5d). All together, the total TC track density of the NA clearly depicts two major paths of TCs. The first is a straight northwestward ridge to the Gulf of Mexico in the tropical regions (C2, C4), and the second is a northeastward recurving ridge at mid-latitude (Fig. 3.5e). The numbers (percentages) of C1, C2, C3, and C4 TCs are 112 (25.9%), 123 (28.5%), 98 (22.7%), and 99 (22.9%) of the total 432 (100%) TCs, respectively.

Our classification of the NA TC track patterns is highly consistent with previous studies. Kossin et al. (2010) and Kozar et al. (2012) suggested that the climatological TC tracks in the NA basin can be classified into four groups. Although the method and the period in their study are different from those in this study, their results are similar to those in the present study. Nakamura et al. (2009) clustered the TC tracks into six groups by using the *k*-means method with mass moments. In that study, TCs recurving to mid-latitude were classified into four clusters. In the present study, however, such TCs were grouped in two clusters (i.e., C1- and C3-pattern). Classification of the TC tracks into more groups may be helpful for identifying the separated linkage with diverse climate variability. Nevertheless, more clusters lead to smaller

numbers of TCs assigned to each cluster, which in turn makes it difficult to construct reliable statistical forecast models. Given the objective of this study, seasonal prediction of NA TC activities, we sorted the NA TC tracks as four patterns as well as aforementioned result of optimum cluster number detection process.

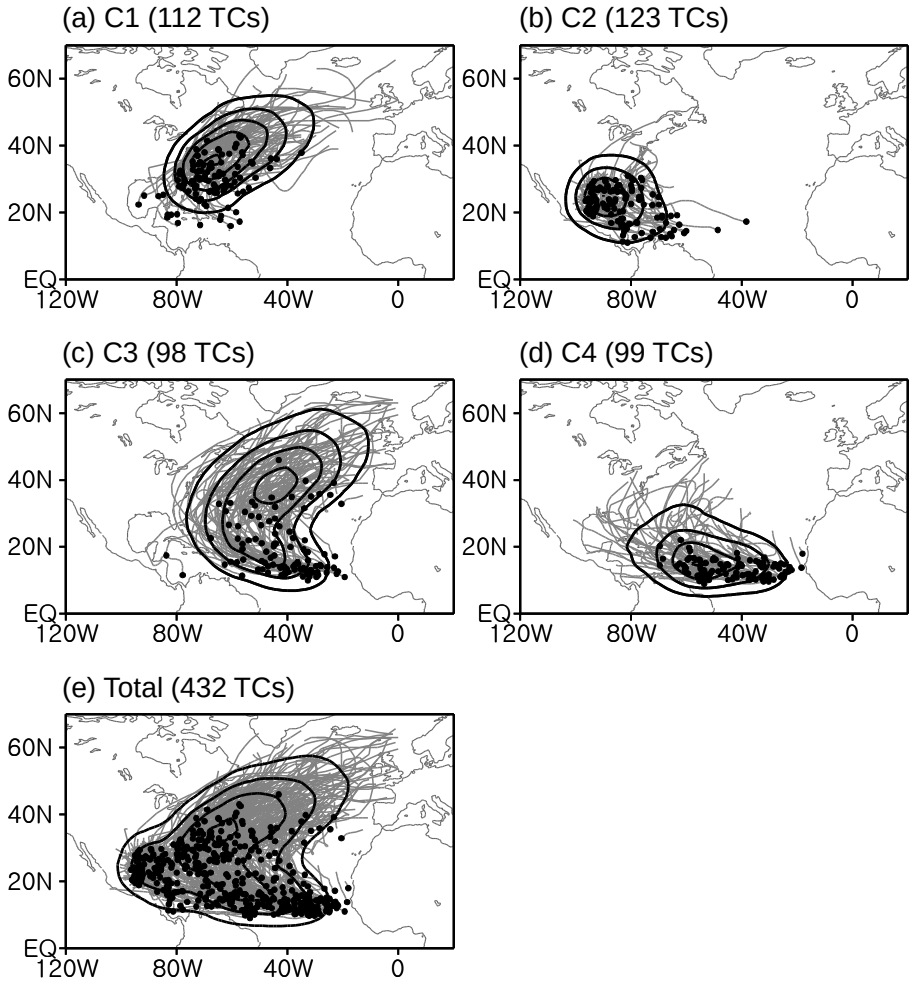

Figure 3.5. (a)–(d) Four track patterns of NA TCs during the period 1965–2012 TC season and (e) total tracks. Contours represent climatological track densities; the interval is 10 except in (e), which is 5. Black circles indicate the genesis position of each TC, and gray lines show individual TC tracks. The number of TCs for each pattern is shown in parenthesis.

3.2.2. Simultaneous relationships and predictors

As we mentioned in the above section, construction of the hybrid statistical–dynamical TC prediction model for each track pattern is a core step in this development. Prior to developing the model, we first examined the empirical relationships between TC activity and large-scale environmental fields for each track pattern. Candidate variables in constructing the model are decided as ASO-averaged SST, VWS, VOR850, and U850, all of which are well-known large-scale factors that influence the NA TC activities (Gray et al. 1992; Blake and Gray 2004; Saunders and Lea 2005; Klotzbach 2007). Other factors such as moist stability and mid-level relative humidity also affect TC activity (Gray 1998); however, these are not regarded as suitable for predictors because of the lack of reliability in today's climate model simulations (John and Soden 2007; Saha et al. 2014).

Figure 3.6 shows the temporal correlations between the TC frequency and the selected atmospheric and oceanic variables for each cluster based on the ensemble mean of the NCEP CFSv2 retrospective issued on July 5. The critical domains (rectangular boxes in Fig. 3.6) are identified as that when both correlations of the NCEP R-2 (figure not shown) and CFSv2 retrospective data with TC activity equal or exceed the 90% confidence level. The NCEP CFSv2 closely reproduces the observed relationships between TC frequency and large-scale atmospheric and oceanic forcings with high statistical significance in the critical domains. It is also required that the

selected domains with variables should be physically related to the corresponding TC track patterns. Predictors are computed by obtaining the area averages of grid point values in the critical domains that meet the threshold of statistical significance at the 90% confidence level. The relative importance of individual predictors and their combinations for each track pattern can then be determined in sensitivity tests. As long as the NCEP CFSv2 effectively simulates the TC-environmental fields relationships, we can anticipate that the hybrid-type model will in principle provide credible predictions.

The VWS is negatively correlated with the C1 TC frequency in the mid-latitude region (Fig. 3.6a). It is noted that small VWS (i.e. weak baroclinity) is a key for TC formation as well as for maintaining TC activities. Based on this, VWS is included as a predictor as it is expected to affect TCs especially in the mid-latitudes where strong westerlies in the upper troposphere can negatively affect TCs. Some regions like the equatorial eastern Pacific show positive correlations between TCs and VWS, which can be recognized as well-known anti-correlation of the NA TC activity and eastern Pacific VWS (Frank and Young 2007). However, this significant anti-correlation pattern is not well shown in the correlation map of the CFSv2 retrospectives because the number of grid points showing significant correlation with the C1-pattern TCs is too small (Fig. 3.6a). Thus, we exclude such regions. The C1-pattern TCs are also positively correlated with local VOR850 over the eastern US

coastal region, where this type of TC is dominant (Fig. 3.6b).

If a TC season is in a La Niña phase in the equatorial Pacific or if positive SST anomalies appear over low-latitude regions of the NA, C2-pattern TCs (i.e. TCs in the Gulf of Mexico) are found to be more active (Goldenberg et al. 2001; Holland and Webster 2007; Kossin and Vimont 2007; Vecchi and Soden 2007). Both of the remote influence of the negative anomalous SST values in the eastern Pacific and the local positive SST effect in the NA induce a rising motion over the Gulf of Mexico. Because negatively correlated SST regions with statistically significant at the 90% level are not reached in the CFSv2 correlation map, only positively correlated SST patterns in the low-latitude regions of the NA are used as a predictor (Fig. 3.6c). This physical mechanism also results in triggering positive vorticity anomalies and creates favorable conditions for TC genesis in the off-equatorial region (Fig. 3.6d). The U850 shows a significant positive relationship with C2-pattern TCs over the tropics; thus U850 is selected as a predictor (Fig. 3.6e). Equatorial low-level zonal wind is related to Madden–Julian Oscillation (MJO), which has been shown to modulate TC activity in the Gulf of Mexico and northwestern Caribbean Sea (Klotzbach 2010). In fact, MJO itself may not be suitable for seasonal prediction because its time scale is subseasonal (i.e. about 30–60 days). Nevertheless, the dynamical mechanism of U850 for affecting C2 TC activity analogous to the MJO effect is still valid even in a seasonal time scale.

The prediction model of C3-pattern TCs uses SST, VOR850, and U850 as predictors. C3-pattern TCs activities show positive correlations with basin-wide SST in the NA (Fig. 3.6f), which is a pattern similar to the Atlantic Multidecadal Oscillation. Along with that, C3-pattern TC frequency is positively correlated with VOR850 (Fig. 3.6g). Both create well-known favorable conditions for TC development and were thus selected as predictors. The U850 over the tropical NA also positively correlates to C3-pattern TCs (Fig. 3.6h). When the strong eastward zonal wind is dominant over the tropical NA, TCs (here, C3-pattern TCs) may be steered to recurve without making a landfall on the North American coast. For C4, we invite the positive relationships of mid-latitude VWS as a predictor (Fig. 3.6i). Because the strengthening of mid-latitude VWS can weaken TC activity, TCs usually have tracks that are active only in low-latitude regions (i.e. C4-pattern TCs). Moreover, the anomalous positive vorticity in the tropics apparently can contribute to C4 TC genesis (Fig. 3.6j), similar to that in the other cases. These results imply that if favorable conditions of low-level vorticity are presented during the ASO season, the NA TCs are more likely to develop.

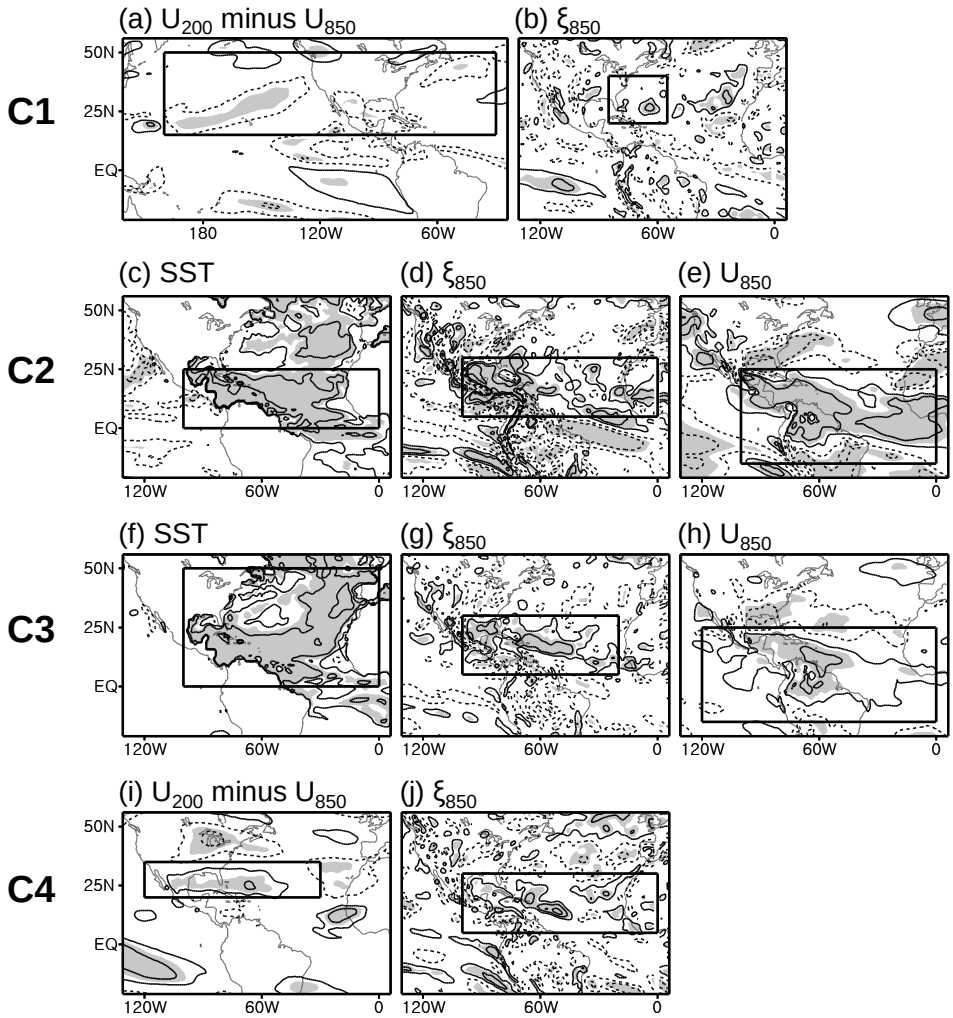

Figure 3.6. Distribution of correlation coefficients between observed C1–C4 TC frequencies and the ensemble average of CFSv2 retrospectives initialized on July 5 for each predictor. The contour interval is 0.2; the zero contour line is omitted. Shading indicates areas statistically significant at the 90% confidence level. Critical regions are presented as a rectangular box.

3.2.3. Validation

Examination of the model skill employs a leave-one-out cross-validation method which is widely used to assess the performance of statistical prediction. Figure 3.7 shows the ensemble-mean hindcasts for the TC frequency for individual clusters (Figs. 3.7a–d) as well as the total TC numbers (Fig. 3.7e) initialized in early February to early July on a monthly interval. The 12 members of the NCEP CFSv2 retrospective forecasts are used to calculate the ensemble means. Although individual forecasts oscillate with relatively large variances (not shown), the ensemble mean for constructing the final forecast agrees well with observations (black lines in Figs 3.7a–e) regardless of the forecast lead time. These are consistent with those reported by Kwon et al. (2007), who showed that multi-member ensemble means generally outperform individual members in statistical predictions of TC activity. In addition, to objectively evaluate the model performance compared to the reference forecast, reforecasts from the model based on NCEP R-2 instead of CFSv2 retrospectives are overlapped (black dashed lines in Figs. 3.7a–e). In this comparison, the reforecast using the reanalysis data (i.e. NCEP R-2 in this study) can be regarded as the reference forecast. The reforecasts using the NCEP R-2 compare well with observations with no forecast biases. As shown in the hindcasts from the CFSv2 retrospectives and reforecasts using NCEP R-2 data, the overall climatology and variability of TC activities are well represented in the model despite some forecast

uncertainties due to the errors in CFSv2 seasonal forecasts. Thus, we conclude that the ensemble mean hindcasts from CFSv2 are reliable.

It is noteworthy that the hindcast of CFSv2 effectively resolves the interannual variability and most of the observed extreme TC activity seasons (e.g., 2000 in C1, 2005 in C2, and 1995 in C3), suggesting that our model is skillful also in predicting abnormal TC activities. Note that the predicted frequency does not reach the zero TC count because the Poisson regression model cannot generate zero (e.g., 1994 and 1995 in C1, 2008 in C3, and 1985 in C4). One notable forecast error is that the hindcast substantially overestimates the observed TC frequency in 2010, particularly for clusters C2, C3, and C4 (Figs. 3.7b–d). This discrepancy is mainly caused by large-scale positive VOR850 anomalies in the CFSv2 retrospective forecast in 2010. The CFSv2 retrospective shows broad positive VOR850 anomalies over the low-latitude NA region concentrated over the Gulf of Mexico (not shown), which were subsequently adopted as predictors for C2–C4 patterns (Figs. 3.6d, g, j).

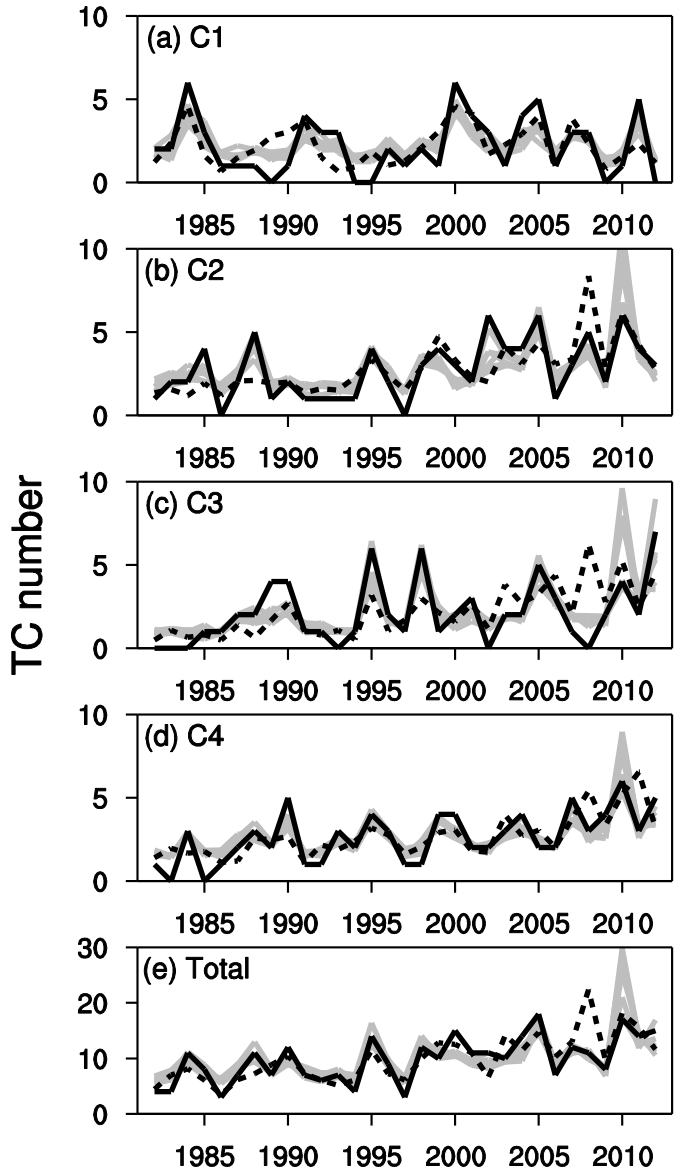

Figure 3.7. Time series of TC frequency from observations (black solid line), from reforecasts using the NCEP R-2 data (black dashed line), and from the ensemble mean of the model hindcast driven by the CFSv2 retrospective run (gray solid line) for the period 1982–2012.

To examine the statistical skill, the COR, RMSEs, and MSSS of ensemble averaged hindcasts using CFSv2 and reforecasts using NCEP R-2 with the observation are analyzed on varying forecast day (Table 3.3). For all clusters, the TC hindcasts show significant relationships with observations at the 99% confidence level with COR values exceeding 0.66. These results indicate that our model can reliably reforecast the interannual variability of the observed TC activities with several months of lead time. The RMSEs of the four TC patterns are approximately one, suggesting that our model error is about one TC for individual track patterns. Likewise, the model error in predicting the total TC number over the NA basin is about two per year. The MSSS is the ratio of the mean-square error of the predictions compared to that of the observation. This measure is applicable only for deterministic forecasts. A large MSSS indicates prediction skill improvement over climatology-based reference forecasts in which the MSSS is equal to zero. MSSS are all significantly larger than zero (Table 3.3), suggesting that our model shows significant forecast skill compared with climatology-based reference prediction. Moreover, all of the CFSv2 ensemble averaged hindcasts show better skill than that using NCEP R-2 data. These statistical measures also advocate again that the effect of uncertainty in model parameters due to errors in CFSv2 seasonal forecasts is a relatively minor factor in model predictability.

Table 3.3. Correlation coefficients (COR), root–mean–square errors (RMSEs), mean square skill scores (MSSS), and Gerrity skill scores (GSS) of ensemble averaged hindcasts from CFSv2 retrospectives in six issue days and the reforecast using the NCEP R-2 with the observation for the period 1982–2012.

	COR / RMSE / MSSS / GSS						
	February 5	March 2	April 1	May 1	June 5	July 5	NCEP R-2 reforecast
C1	0.93 / 1.10 / 0.61 / 0.83	0.89 / 1.08 / 0.62 / 0.69	0.86 / 1.12 / 0.59 / 0.82	0.92 / 1.00 / 0.68 / 0.75	0.91 / 0.99 / 0.68 / 0.66	0.89 / 1.08 / 0.62 / 0.63	0.67 / 1.31 / 0.44 / 0.53
C2	0.89 / 0.82 / 0.77 / 0.70	0.83 / 0.96 / 0.69 / 0.55	0.74 / 1.30 / 0.43 / 0.46	0.71 / 1.25 / 0.47 / 0.58	0.75 / 1.18 / 0.53 / 0.58	0.79 / 1.08 / 0.61 / 0.57	0.65 / 1.37 / 0.37 / 0.55
C3	0.92 / 0.78 / 0.83 / 0.68	0.87 / 0.95 / 0.75 / 0.68	0.80 / 1.15 / 0.63 / 0.66	0.75 / 1.26 / 0.56 / 0.73	0.66 / 1.52 / 0.36 / 0.63	0.74 / 1.30 / 0.53 / 0.66	0.50 / 1.72 / 0.18 / 0.56
C4	0.93 / 0.71 / 0.78 / 0.85	0.92 / 0.67 / 0.80 / 0.85	0.85 / 0.80 / 0.72 / 0.77	0.81 / 0.89 / 0.66 / 0.77	0.76 / 1.00 / 0.56 / 0.65	0.80 / 0.90 / 0.64 / 0.66	0.59 / 1.28 / 0.29 / 0.34
Total	0.91 / 1.80 / 0.80 / 0.76	0.87 / 2.03 / 0.74 / 0.83	0.78 / 2.71 / 0.55 / 0.71	0.78 / 2.68 / 0.55 / 0.66	0.77 / 2.96 / 0.46 / 0.56	0.82 / 2.45 / 0.63 / 0.64	0.71 / 3.11 / 0.40 / 0.49

As well as the TC number prediction, it is also worth to see the forecast results in terms of categories compared to its climatology; below normal (BN), normal (N), and above normal (AN). When the number of TCs are 0.5 standard deviations above (below) the average TC frequency, that year is assigned to AN (BN) category. Understandably, the other years are defined as category N. The categorized results of observation and ensemble averaged hindcasts are shown in contingency tables for each cluster and total TC number (Table 3.4). The diagonal components of each matrix, both observations and predictions are the same category, mean successful prediction. The other components can be interpretable as forecast failures. Table 3.4 shows C1 model correctly predicts the 21 years among the 31 years (1982–2012), which is about 68% success rate. In the similar way, success rate of C2, C3, C4, and total TC models are 65%, 74%, 71%, and 74% respectively.

Table 3.4. Contingency tables between the observed TC activity and hindcast results issued on July 5 for the period 1982–2012.

C1		Observation			
		BN	N	AN	Total
Forecast	BN	8	2	0	10
	N	6	7	1	14
	AN	0	1	6	7
	Total	14	10	7	31
C2		Observation			
		BN	N	AN	Total
Forecast	BN	7	3	0	10
	N	2	7	5	14
	AN	0	1	6	7
	Total	9	11	11	31
C3		Observation			
		BN	N	AN	Total
Forecast	BN	10	1	0	11
	N	4	8	2	14
	AN	0	1	5	6
	Total	14	10	7	31
C4		Observation			
		BN	N	AN	Total
Forecast	BN	7	3	0	10
	N	1	9	3	13
	AN	0	2	6	8
	Total	8	14	9	31
Total		Observation			
		BN	N	AN	Total
Forecast	BN	8	0	0	8
	N	3	9	4	16
	AN	0	1	6	7
	Total	11	10	10	31

To assess quantitatively the predictability as these three categories, we introduce the Gerrity skill score (hereafter GSS; Gerrity, 1992). GSS takes account of equitability for multi-categorical forecasts, so it is an appropriate measure for this purpose. GSS is generally used for verification of the forecast/observation outcome represented by the contingency table (see Table 2 in Kim et al. 2010). GSS is defined as

$$\mathrm{GSS} = \sum_{i=1}^{3} p_{ij} s_{ij} \tag{7}$$

where p_{ij} is the marginal probabilities of each cell and s_{ij} is the scoring weights. The scoring weights are given by

$$s_{ij} = \begin{cases} \dfrac{1}{2}\left(\displaystyle\sum_{r=1}^{i-1} a_r^{-1} + \sum_{r=i}^{2} a_r\right), & i = j \\ \dfrac{1}{2}\left[\displaystyle\sum_{r=1}^{i-1} a_r^{-1} - (j-i) + \sum_{r=j}^{2} a_r\right], & i < j \\ \dfrac{1}{2}\left[\displaystyle\sum_{r=1}^{j-1} a_r^{-1} - (i-j) + \sum_{r=j}^{2} a_r\right], & i > j \end{cases} \tag{8}$$

$$a_r = \frac{1 - \sum_{r=1}^{i} p_r}{\sum_{r=1}^{i} p_r} \tag{9}$$

where *r* is a dummy summation index and p_r is sample probability to the total number. The GSS of one is recognized as perfect prediction, zero is reference skill, and negative value of that represents poor skill than reference. All of the GSSs of multiple forecasts shown in Table 3.4 are much higher than

zero, which means that our model well predicts TC activity with three categories (i.e., BN, N, and AN) than the reference forecast based on climatology.

In summary, our model is skillful with various forecast lead time. Some of the long-lead predictions (e.g., five–six months lead forecast) show slightly better skill than the short lead-time predictions (e.g., one–two months lead), although the predictability of CFSv2 normally decreases as the lead-time increases. This is expected as all prediction models of multiple leads are optimized for their own training period. As mentioned earlier, the hybrid statistical–dynamical model picks statistically significant grids for obtaining predictors. Although the number of significant grids for longer lead-time prediction decrease, the skillful predictors from selected variable sets and grids maintain the high prediction skill of the model. Thus, stable skill with varying forecast lead-time is a unique virtue of the hybrid statistical–dynamical model for predicting ASO TC activities, which differs from that in previous traditional statistical models (e.g., Gray et al. 1992; Elsner and Schmertmann 1993; Hess et al. 1995; Lehmiller et al. 1997; Blake and Gray 2004; Saunders and Lea 2005; Elsner and Jagger 2006; Klotzbach 2007; LaRow et al. 2010).

3.2.4. Regional prediction

Our model is used to predict seasonal TC track patterns for the entire NA

basin. To assess the forecast skill in generating spatial TC distributions during the training period, we analyzed the rank-correlation for each 5° × 5° grid point in the NA basin for different forecast lead months (Fig. 3.8). Because the observed and forecasted TC frequency do not follow a Gaussian distribution at each grid point, we use rank-correlation as a statistical measure for the model skill in order to consider prediction model errors (Vecchi et al. 2014). By using rank-correlation which represents the degree of similarity between two rankings, we can evaluate the significance relationship between them. Strong rank-correlations (> 0.5) for all forecast lead months appeared in regions with high TC frequency, suggesting the model is more skillful in regions with high TC activity. Most of these high predictability grids are located in regions in which the four TC track patterns overlap. Although these results imply that the seasonal prediction results represented as a TC track density distribution may vary with time, the rank-correlation patterns are largely invariant of the forecast lead time.

The direct impact of TCs to human society is closely linked to TC landfall accompanied by strong wind gusts and heavy rainfall; therefore, coastal regions are more vulnerable to TC effects. To examine the model skill for these vulnerable coastal regions, we focused on three major regions particularly vulnerable to TCs (Fig. 3.8a). The first region (R1) includes the US East Coast area, where population and economic activities are heavily concentrated. The second region (R2) covers the Gulf of Mexico, the western

Caribbean Sea, and their neighboring countries. The third region (R3) includes the eastern Caribbean Sea, a main region of TC genesis and their pathways. Spatially, these regions show substantial rank-correlation, indicating high forecast skill (Fig. 3.8). By assessing TC distribution over these three vulnerable regions, we can interpret the results of TC activity prediction microscopically as well as macroscopic view of the entire basin-wide map.

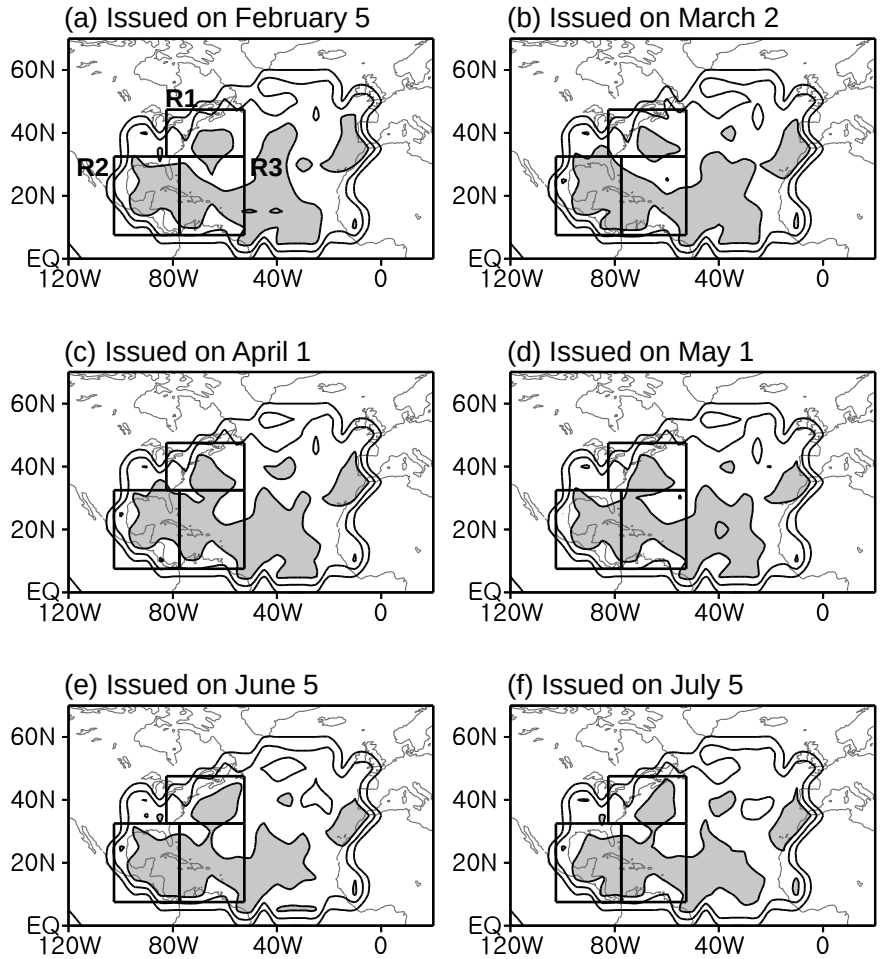

Figure 3.8. Spatial distribution of retrospective rank-correlation between the observed TC passages and ensemble average of hindcasts results in a 5° × 5° grid box. The contour interval is 0.25; shading indicates areas with rank-correlation greater than 0.5. (a)–(f) Multiple forecasts initialized in February 5, March 2, April 1, May 1, June 5, and July 5, respectively. Three vulnerable TC-influenced domains, defined as R1, R2, and R3 regions are also shown.

Figure 3.9 depicts the temporal variations of the observed TC frequency and the ensemble mean hindcast for six different lead times in the three regions. To compare observations and hindcasts consistently, both of parameters are converted into track densities in 5° × 5° grid boxes covering the entire NA basin. The area averages for the three regions are then evaluated. The three time series show no climatological forecast biases for all regions, which is consistent with the aforementioned time series of each cluster. Although there are some forecast failures such as overestimation for R2 in 2010, the correlations of different lead times are all above 0.70 for the three vulnerable regions, which is statistically significant at the 99% confidence level. In addition to the interannual variability of regional TC activities, the model also effectively captured the extreme TC activity years (e.g., 2005 in R2 and 1995 in R3; Fig. 3.9). Therefore, our model is also reliable and skillful for predicting sub-basin coastal TC activity.

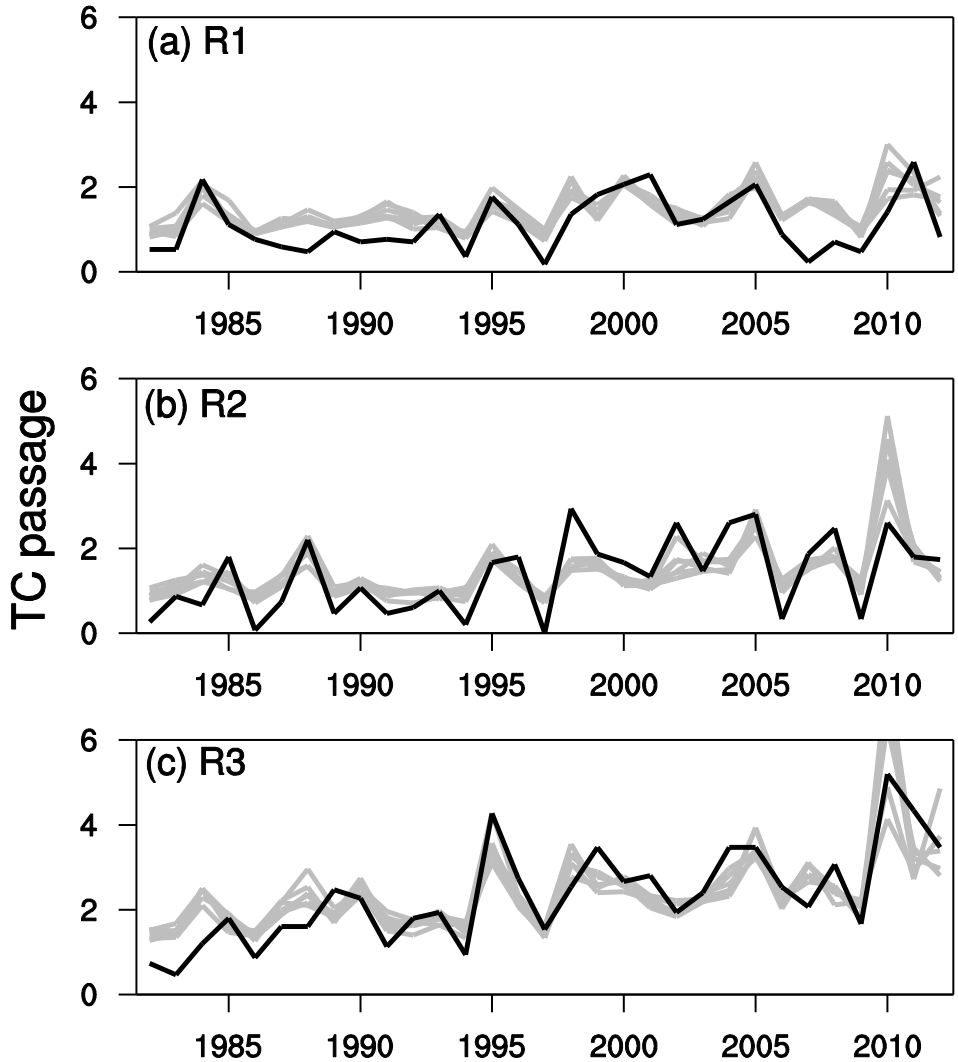

Figure 3.9. Time series of regional averaged TC passages in (a) R1, (b) R2, and (c) R3 regions. The black line indicates observation, and gray lines show ensemble averaged values of CFSv2 retrospectives for six forecast days including February 5, March 2, April 1, May 1, June 5, and July 5 for the period 1982–2012.

3.3. Predictions of intense TC activities in the WNP and NA

3.3.1. Definition of intense TC

Table 3.5 shows the TC frequency and its landfall ratio in the WNP basins according to the Saffir–Simpson scale with the maximum 1-min sustained wind speed from the JTWC datasets. A total of 631 TCs occurred in the WNP basin during the 32 TC seasons of 1982–2013. In the WNP, 214, 122, 54, 74, 106, and 61 TCs reached tropical storm intensity to category 5, and 43%, 65%, 65%, 58%, 63%, and 62% of them landed in coastal regions, respectively. As reported in a number of previous studies (Oouchi et al. 2006; Manganello et al. 2012; Kim et al. 2015), the observed TC frequency does not monotonically decrease with intensity, showing a momentary minimum at category 2. Intense TCs generally maintain their cyclonic structures longer than weaker ones, which in turn, may increase their chances of hitting coastal regions within their lifespans. In the WNP basin, approximately 43% of TCs of tropical storm intensity made landfall, whereas approximately 60% of TCs of categories 1–5 made landfall.

To develop a seasonal forecast model focused only on intense TCs, target intensity criteria should be determined. The intense TC activity, focused on this thesis, should show different climate variation compared to typical TC because that is the main reason for this development of intense TC separately.

Most operational centers consider category 3–5 TCs as intense TCs (Saunders and Lea 2005; Bell et al. 2012) because such storms are responsible for more than 85% of the total damages in the US (Pielke et al. 2008). Despite the current categorization, construction of a robust regression model requires a sufficient number of samples for intense TCs (Wilks 2006). At 241, the total number of TCs of category 3–5 in the WNP is sufficient for this purpose. When we check the variation of TC activity correspondent to intensity from the TS to category 3, there are quite independent between typical and intense TC activity (Fig. 3.10a). Therefore, we define an intense TC in the WNP as category 3 and above.

Table 3.5. The number of TCs and its landfall rate (parenthesis) in the WNP for TC seasons during the period 1982–2013.

Category of storm (wind speeds)	WNP
Tropical storm (34 – 63 knots)	214 (43 %)
Category 1 (64 – 82 knots)	122 (65 %)
Category 2 (83 – 95 knots)	54 (65 %)
Category 3 (96 – 112 knots)	74 (58 %)
Category 4 (113 – 136 knots)	106 (63 %)
Category 5 (≥137 knots)	61 (62 %)

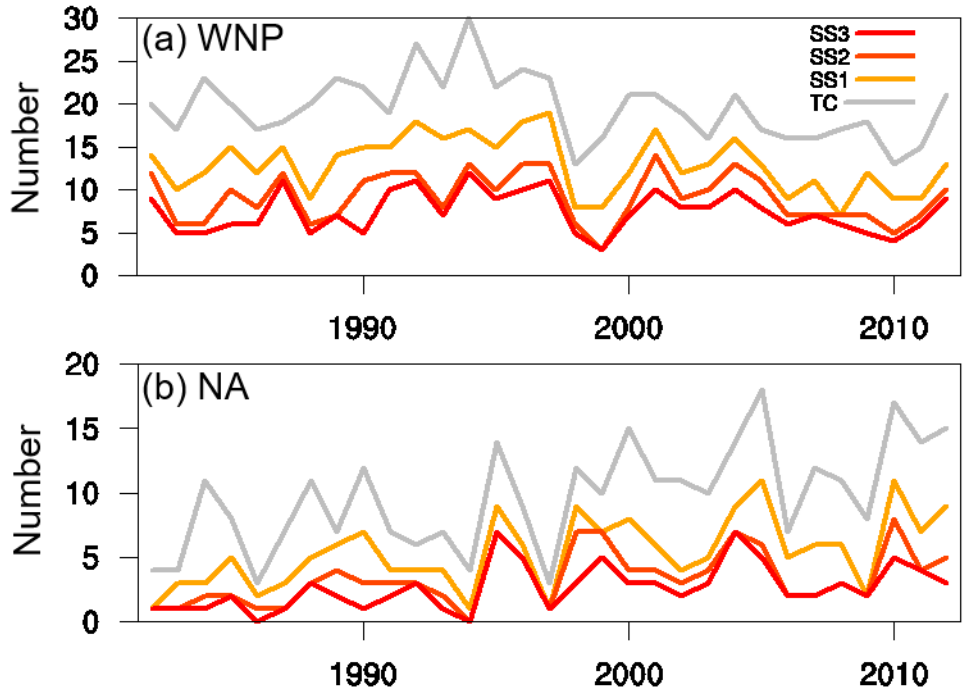

Figure 3.10. Time series of TC frequencies in the WNP and NA basins according to the Saffir-Simpson hurricane wind scales during the period of 1982–2013.

Table 3.6 stratifies the TC frequency and its landfall ratio in the NA basins according to the Saffir–Simpson scale with the maximum 1-min sustained wind speed from the HURDAT datasets. A total of 310 TCs formed in the NA basin during the 1982–2013 TC seasons. In the NA basin, 139 TCs reached tropical storm intensity; 31% of them made landfall. In the same period, 64, 24, 37, 35, and 11 TCs reached maximum intensity at hurricane scale category 1 to 5, respectively, and 47%, 46%, 59%, 60%, and 100% of them made landfall. As we mentioned above, it is interesting to note that the percentage of TC landfalls increases with increasing TC intensities. All of the category 5 hurricanes in the NA basin made landfall during the study period.

However, if we take the definition of intense TC to same one as the WNP basin, only 83 TCs in the NA counted during the 32-year period including 37, 35, and 11 for categories 3, 4, and 5, respectively. At 2.6, the number of TCs per year is too small for constructing a statistically significant forecasting model. The annual numbers of category 3–5 TCs in the NA basin are found to be closely correlated with those of category 1–5, with a correlation coefficient (COR) of 0.79, suggesting that category 1–5 and 3–5 TCs are closely related (Fig. 3.10b). On the basis of this consideration, intense TCs in the NA are defined as those of category 1 and above, bringing the total number of intensive TCs to 171. This measure resulted in a sufficient number of samples.

Table 3.6. Same as Table 3.5 except for NA basin.

Category of storm (wind speeds)	NA
Tropical storm (34 – 63 knots)	139 (31 %)
Category 1 (64 – 82 knots)	64 (47 %)
Category 2 (83 – 95 knots)	24 (46 %)
Category 3 (96 – 112 knots)	37 (59 %)
Category 4 (113 – 136 knots)	35 (60 %)
Category 5 (≥137 knots)	11 (100 %)

3.3.2 Development of hybrid statistical-dynamical model

To prepare the basis of intense TC forecast model for the WNP, the FCM is applied to the WNP intense TC tracks such as those of categories 3–5. Establishing a basis of track pattern is a key step in attempting TC track density prediction without using high-resolution dynamic model simulations that require heavy computational resources (Kim et al. 2012; Ho et al. 2013; Choi et al. 2016). After detecting the optimum number of clusters, intense TC tracks are classified into three clusters (Fig. 3.11). TCs belonging to WNP C1 develop mainly over the southeastern part of the main TC genesis region of the WNP (Fig. 3.11a) and move toward the mid-latitude region including Korea and Japan, passing through the East China Sea. A total 97 intense C1 TCs develop with relatively narrow track density such that their maximum values reach above the 25. Offshore Japan, 59 TCs in C2 show recurving tracks (Fig. 3.11b). Only few of the C2 intense TCs make landfall; most of them dissipate over the ocean without making landfalls. The remaining 85 TCs in cluster 3 (C3) are concentrated over the South China Sea and move westward (Fig. 3.11c). Most of the total 241 intense TCs are generated in the low-latitude broad region of the WNP, and their track density core is located over the Philippines Sea (Fig. 3.11d). The total intense TC track density shows two representative ridges: recurved to mid-latitude and westward straight-moving (Fig. 3.11d). It is noted that although all patterns move toward different areas, they share the main genesis region, which is an important

point in terms of seasonal forecasts.

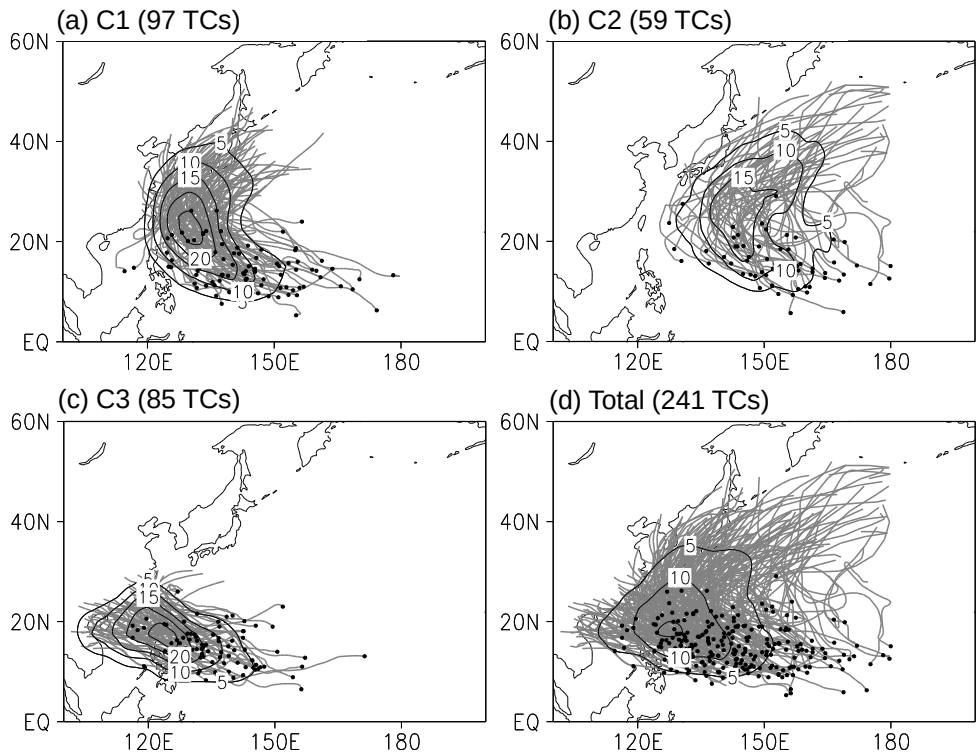

Figure 3.11. Three track patterns and total WNP intense TCs during June through October in the period 1982–2013. Contours represent climatological track densities; the interval is 5. Black circles indicate the genesis position of each TC, and gray lines show individual TC tracks. The number of TCs for each pattern is shown in parenthesis.

Next, we investigated the statistical relationships between WNP intense TC activities during JJASO (i.e. the WNP TC season) and large-scale circulations to determine predictors (Fig. 3.12). We conducted a correlation analysis for reanalysis and retrospective data initialized on May 1. Among the potential predictors, we selected the positive relationship of the east–central Pacific SST, tropical U200, and VOR850 as the WNP C1 predictors after verification of resemblance between two COR maps from reanalysis and retrospective. It is noted that the following characteristics of atmospheric and oceanic conditions are consistently found in both of reanalysis and CFSv2 data. Developments of more intense TCs of the WNP during the El Niño episode are characterized by positive SST anomalies in the east–central tropical Pacific (Figs. 3.12a and 3.12d). On the basis of previous studies on the ENSO effects on WNP TC activity (Wang and Chan 2002; Chan 2007; Kim et al. 2012), we can understand the physical mechanism that relates atmospheric circulation with Pacific SST distribution to move the TC genesis regions relatively southeastward. In a weakened low-level easterly condition caused by a reduced zonal SST gradient over the tropical Pacific (i.e. an El Niño year), the Asian summer monsoon trough extends farther eastward. The energy transfer from the mean flow to synoptic eddies in the extending monsoon trough is crucial for TC development (Sobel and Bretherton 1999; Wu et al. 2012). If the genesis region moves farther from land and TCs remain longer over the ocean, the chance for TCs to intensify increases. Other fields

such as U200 and VOR850 also show systematic features associated with these El Niño episode characteristics (Figs. 3.12b, 3.12c, 3.12e, and 3.12f). The C2 prediction model adopts a negative relationship of SST and Z500 in the mid-latitude Pacific and a positive relationship of U200 in the subtropics (Figs. 3.12g–l). Compared with the SST pattern of C1, considerable positive correlation related to El Niño was noted in the tropical Pacific in addition to a distinguishable mid-latitude negative correlation pattern. This negative relationship with SSTs may be a response to the Z500 associated with the strength of the subtropical high. The weakened Z500 in El Niño years results in enhanced convective activities (i.e., penetration of TCs) and SST cooling therein. Thus, SSTs and Z500s with negative relationships with the C2 TCs are the critical predictors in separating C2 and C1 TCs. A strong U200 in the mid-latitude zonal band can steer the TC track to recurve; thus, it is selected as a predictor. In the C3 prediction model, the negative relationship of the subtropical U200 and influence of the tropical VWS are used as predictors (Figs. 3.12m–p). Negative VWS anomalies in the tropical region can be favorable atmospheric conditions for TC genesis because more instabilities can be frequently developed in an organized convection system such as a TC. All the predictors are verified that they are free multicollinearity problem by checking the VIFs of each predictor.

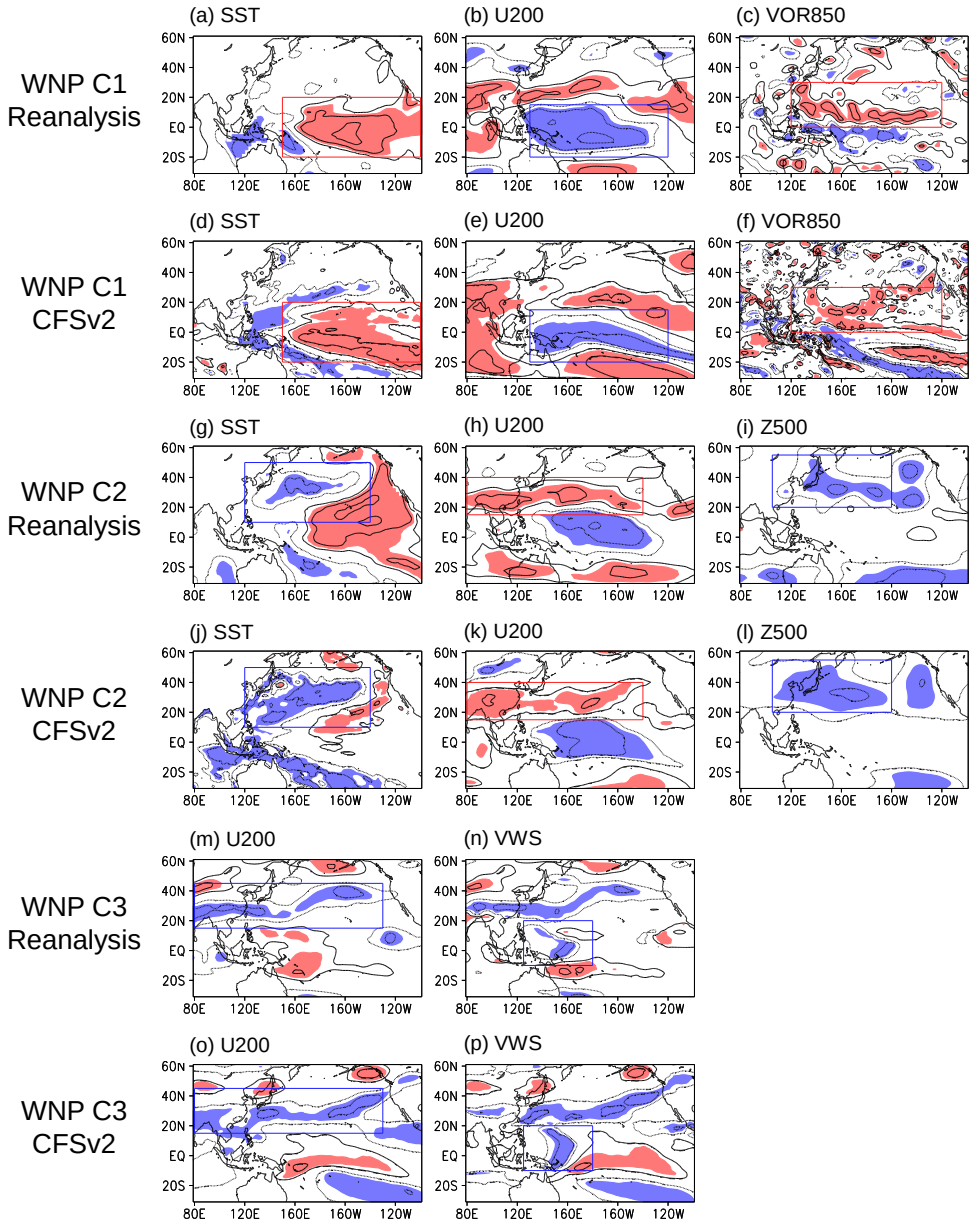

Figure 3.12. Distribution of correlation coefficients between observed C1–C3 intense WNP TC frequencies and the ensemble average of CFSv2 retrospectives initialized on May 1 for each predictor. The contour interval is 0.2; the zero contour line is omitted. Red (blue) shading indicates areas statistically positive (negative) significant at the 90% confidence level. Critical regions are presented as a rectangular colored box.

b. Validation

Assessing predictability of the model is described in this section. We re-forecasted the annual intense TC frequencies for the WNP basin using the present model to evaluate the performance of the forecasting model. We examined the time series of observed intense TC number and forecast results with varying issuance days (Fig. 3.13). Multiple hindcasts effectively reproduce the variability of the observed time series although their amplitudes differed slightly. Further, several observed peaks such as 2002 in C1, 1987 in C2, and 1985 in C3 are partly simulated by the WNP forecast model with no overall forecasting bias. However, limitations remain in simulations of 1992 and 1994 in C1, 1997 in C2, and 2002 in C3. This result may indicate forecasting failure in some of the training period years as an inherent property of the statistical Poisson regression technique or due to NCEP CFSv2 seasonal prediction uncertainty (Kim et al. 2012).

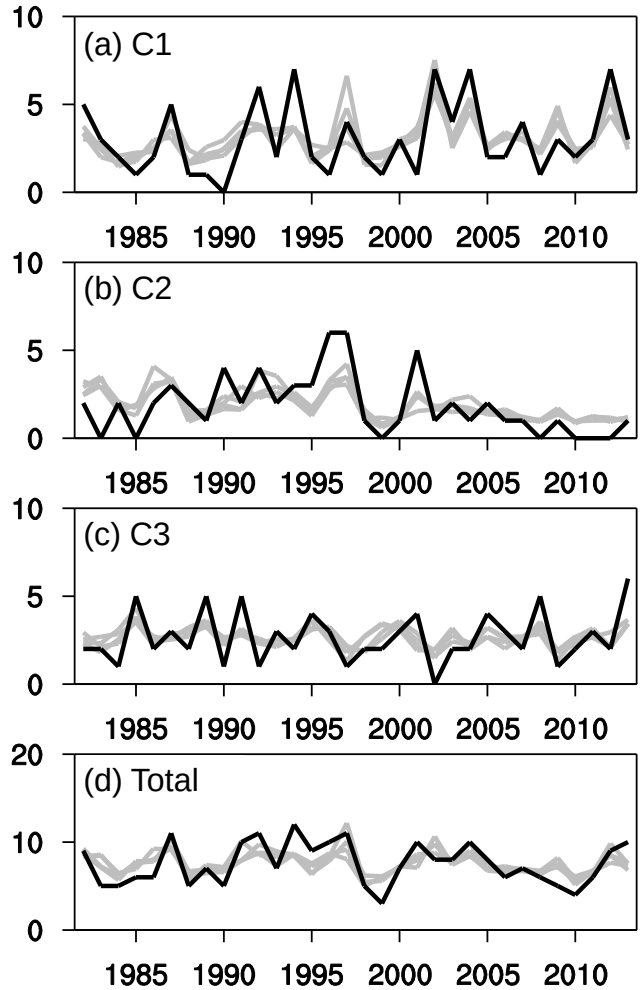

Figure 3.13. Time series of intense TC frequency in WNP from observations (black solid line) and from the ensemble mean of the model hindcasts driven by the four CFSv2 retrospective run (gray solid line) for the period 1982–2013.

We calculated statistics measures such as the COR, RMSEs, and MSSS by cross-validation analysis for multiple forecasting days to concretely investigate the WNP prediction model performance (Table 3.7). The COR values for all clusters and the total intense TCs between observations and each prediction exceed 0.55, implying that our model can provide reliable intense TC variability. In addition, we can expect the standard error of our model with RMSE is in the range of 1.0–1.5 for every cluster, and that for total intense TC is below two. Moreover, all MSSSs exhibit significantly positive values, which means our model skill is improved over the climatology-based reference model. Generally, the WNP C2 model shows the lowest performance scores among the three WNP patterns although we performed various tests of predictor combinations to show best performance. Because the C2 model adopts mid-latitude region predictors, it would be estimated that the relatively inferior skill of CFSv2 over the mid-latitude region (Saha et al. 2014) is responsible for this low performance. Skill restriction of the WNP C2 model eventually leads to lower performance of total intense TC prediction.

Table 3.7. Correlation coefficients (COR), root–mean–square errors (RMSEs), and mean square skill scores (MSSS) of ensemble averaged hindcasts from CFSv2 retrospectives in four issue days for the period 1982–2013 in WNP basin.

	COR / RMSE / MSSS			
	February 5	March 2	April 1	May 1
C1	0.86 / 1.22 / 0.63	0.79 / 1.36 / 0.54	0.74 / 1.40 / 0.52	0.66 / 1.52 / 0.43
C2	0.67 / 1.29 / 0.40	0.65 / 1.30 / 0.39	0.55 / 1.39 / 0.30	0.61 / 1.32 / 0.37
C3	0.77 / 1.09 / 0.42	0.79 / 1.06 / 0.45	0.55 / 1.23 / 0.26	0.64 / 1.13 / 0.37
Total	0.76 / 1.64 / 0.51	0.77 / 1.60 / 0.54	0.59 / 1.91 / 0.34	0.65 / 1.79 / 0.42

The forecast model for the NA basin is developed in the same manner as that for the WNP basin. Through the optimum cluster number detection process, we concluded that the intense NA TC tracks should be classified into two major patterns (Fig. 3.14). The 68 intense TCs in the NA are grouped into cluster 1 (C1), which develop over the broad low-latitude NA basin and propagate northwestward to the Gulf of Mexico and southeast coast of the US (Fig. 3.14a). The reminding 103 intense TCs are grouped into cluster 2 (C2), which move to mid-latitude regions with recurving tracks (Fig. 3.14b). The C2 TCs develop mainly over the western ocean off Sahel and the eastern offshore region of the US; some even affect the east coast of Canada. Because the number of C2 TCs is greater than C1 TCs, the track density of the total 171 intense TCs is slightly biased to C2 (Fig. 3.14c).

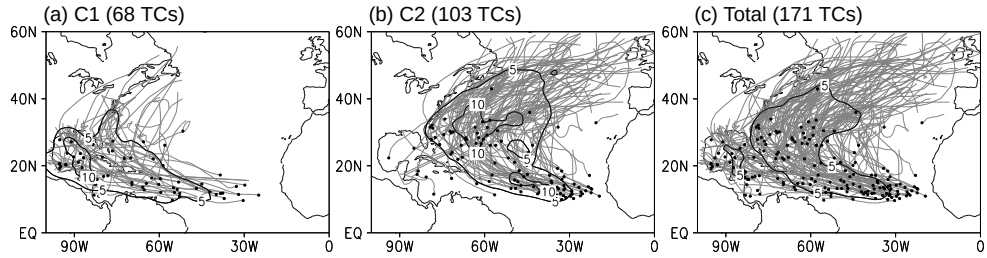

Figure 3.14. Same as Fig. 3.11 except for two patterns during the August through October in NA.

A hybrid statistical–dynamical model for intense TC forecasting in the NA basin is constructed for individual track patterns. First, we have identified empirical relationships between each track pattern and the mean atmospheric/oceanic fields of reanalysis datasets in the NA TC season (ASO). As discussed above, we have analyzed multiple fields such as SST, U200, VWS, VOR850, and U850, which are known as appropriate factors for investigating summertime TC activity. Second, the same correlation analysis is also performed on the basis of the CFSv2 retrospective data. Third, comparing both correlation maps of potential predictor fields from reanalysis and retrospective data, we determined the critical regions that simultaneously show statistical significant correlations in the two maps. Finally, we verified that these relationships with potential predictors are physically relevant to the corresponding TC pattern in the context of providing favorable environmental conditions for TC activity. If all conditions are met, the predictor is obtained by averaging the values over the grids showing significant CORs with ASO TCs. After conducting iterative predictability tests by using different predictor sets, the optimal predictor combinations for providing the best performance are selected for each pattern model.

Figure 3.15 shows the spatial distribution of CORs between the ASO intense TCs in the NA basin and the predictor variables obtained from reanalysis and retrospective data initialized on July 5 for 1982–2013. The maps in the figure show statistically significant regions at the 90% confidence

level as shadings, with positive correlations in red and negative correlations in blue, and critical domains are shown as shaded boxes. The prediction model of C1 in the NA utilizes SST, U200, and VOR850 as predictor variables from the NCEP CFSv2 retrospective datasets. The C1 TCs are positively correlated with SSTs in the tropical NA (Figs. 3.15a and 3.15d). In addition, a negative relationship of U200 in the tropical region (Figs. 3.15b and 3.15e) and a positive relationship of VOR850 over the main C1 active area (Figs. 3.15c and 3.15f) are identified, which implies that more C1 TCs tend to form in weaker U200 condition over the tropics and in the warm Atlantic Meridional Mode phase (Gray 1984; Kossin et al. 2010). All of the above relationships of atmospheric and oceanic variables with Cl cluster activity are consistently found in both of reanalysis and CFSv2 data. Thus, we adopted the local positive influence of SST in the NA, VOR850 in the tropics, and the negative relationship of U200 over the low latitude band as predictors. Selection of these predictors is physically reasonable because warm SST, positive relative vorticity, and weakened vertical wind shear associated with decelerated U200 are all favorable conditions for TC development. Similarly, the predictor sets for C2 intense TCs are appointed (Figs. 3.15g–j). A positive relationship of SST over the entire NA is found (Figs. 3.15g and 3.15i). Because the C2 TCs form in the vast tropical open ocean of the NA and move to the mid-latitude ocean with recurving tracks, the basin-wide SST variability is an obvious predictor. In the case of U850, a positive relationship

is shown over the tropical NA (Figs. 3.15h and 3.15j). This is also regarded as one of the predictors because eastward low-level zonal wind obstructs intense TC track entry toward Gulf of Mexico or Caribbean Sea.

When developing regression model, the multicollinearity problem can be a critical issue. We have checked the VIF which quantifies the multicollinearity for each predictor to ensure the use of the predictor in the model (Davis et al. 1986). As we mentioned above, it is noted that the threshold of variance inflation factor is 10 (Davis et al. 1986; O'Brien 2007; Villarini et al. 2011). When VIF reaches to 10 or larger, the severity of multicollinearity could be strong and the predictor should be rejected. In this NA prediction model, all the maximum values of variance inflation factors are smaller than 10 (not shown), implying that the predictors can be useful to be employed in the model. Using these predictors, a forecast model is developed based on the Poisson regression of individual clusters.

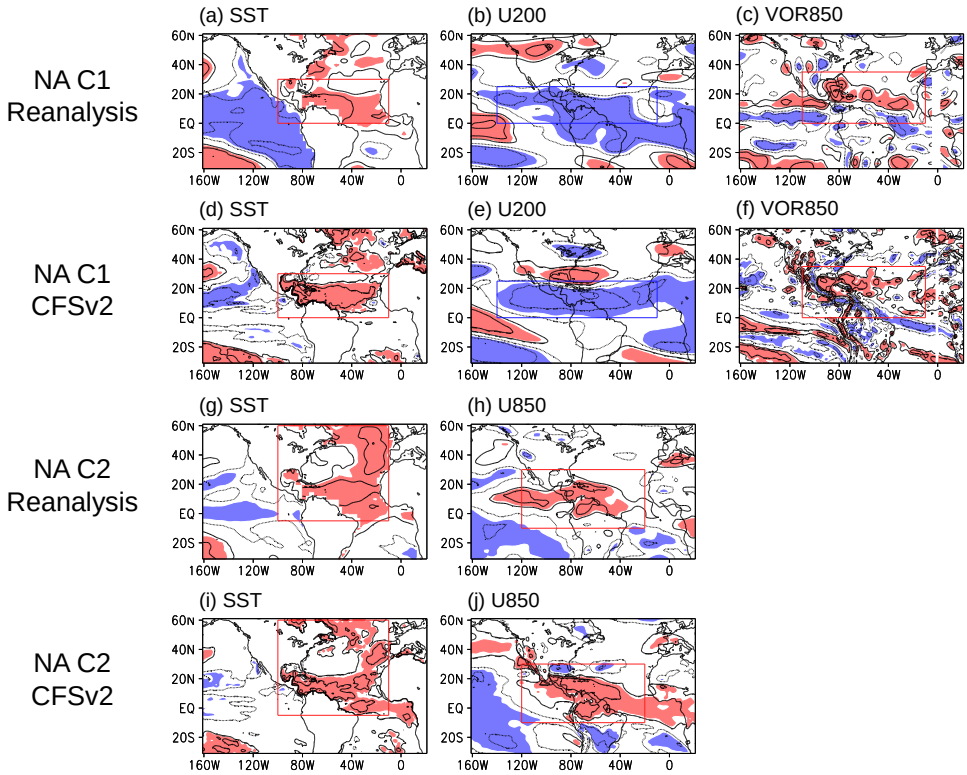

Figure 3.15. Same as Fig. 3.12 except for two patterns in NA initialized on July 5.

Figure 3.16 shows the observation and six hindcasts initialized in February 5 through July 5 from the cross-validation of each pattern model for the number of intense TCs in the NA basin. This figure shows only 12 ensemble mean time series for every hindcast because the final result is provided as the form of ensemble mean. As for the WNP forecast model, variability of the observed intense TC activity (black line) is effectively reproduced by multiple predictions (gray lines) with varying initial times. Although the Poisson regression model does not reach the zero line, the prediction results resolve several explicit peaks. The peaks at 1987, 1995, 2005, and 2007 for C1 (Fig. 3.16a) and 1995, 1998, and 2010 for C2 are reasonably predicted in our model (Fig. 3.16b). The time series of total intense TC prediction obtained from C1 plus C2 shows variability similar to the observation (Fig. 3.16c). It should be noted that although our model is based on the interannual variability, it has simulated the enhanced NA intense TC activities after the 2000s. This strength occurred because the selected predictors from the CFSv2 are determined by a thorough sensitivity test to indicate best performance. Furthermore, no climatological model forecast biases are generally present.

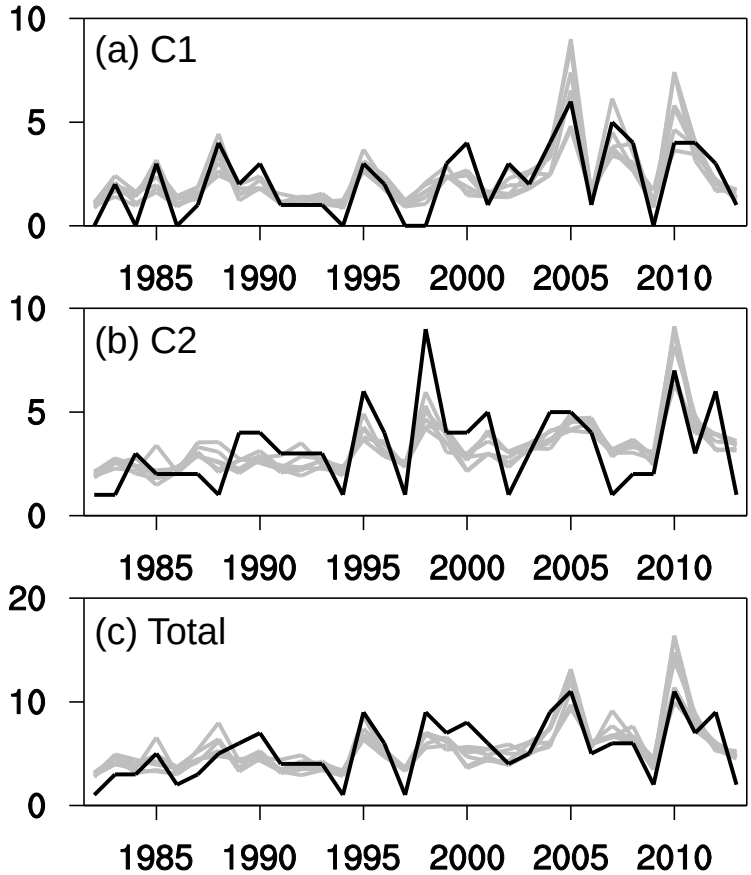

Figure 3.16. Same as Fig. 3.13 except for two patterns hindcasts driven by the six CFSv2 retrospective run in NA.

To objectively assess the prediction performance, we calculated aforementioned statistical measures such as COR, RMSE, and MSSS of multiple hindcasts (Table 3.8). RMSE represents the expected errors for statistical prediction, and MSSS denotes the forecast accuracy of our statistical–dynamical model compared with a climatology-based reference model (World Meteorological Organization 2002; Wilks 2006; Kim et al. 2012). All multiple forecasts represent good skill regarding COR values above the statistical significance at the 99% confidence level. Because of the annual fluctuation of C1 TCs is less than that of C2, the performance of the C1 model appears to be better than that of C2 in terms of variability from the COR analysis. In the case of the total intense TC number, the COR values are between C1 and C2 CORs as a result of their overlapping variabilities. The RMSEs of C1 are approximately one and those of C2 are 1.3–1.6, and the general errors of the total intense TC are 1.6–2.1. The MSSSs of all multiple predictions of C1 and C2 in addition to the total number of intense TCs are larger than zero, which means the present model skill is improved over the reference forecast. The model skill does not appear to increase with time evolution close to the TC season. This is one of the distinctive properties of the model using a simultaneous relationship on the basis of the hybrid approach. Because the model utilizes only the selected grid point values that show skillful variability for calculating the predictor, prediction is optimized and predictability is retained at high levels despite the increasing forecast lead

time (Choi et al. 2016). In summary, our NA prediction model shows stable good performance regardless of the forecast issue date, which is special advantage of using the hybrid method for operational purposes.

Table 3.8. Same as Table 3.7 except for six issue days in NA basin.

	COR / RMSE / MSSS					
	February 5	March 2	April 1	May 1	June 5	July 5
C1	0.85/ 0.90 / 0.71	0.82 / 0.98 / 0.66	0.79 / 1.06 / 0.60	0.72 / 1.16 / 0.51	0.79 / 1.02 / 0.63	0.76 / 1.09 / 0.58
C2	0.77 / 1.35 / 0.53	0.75 / 1.37 / 0.51	0.59 / 1.58 / 0.35	0.61 / 1.56 / 0.37	0.62 / 1.55 / 0.38	0.58 / 1.61 / 0.33
Total	0.79 / 1.72 / 0.62	0.81 / 1.62 / 0.66	0.72 / 2.01 / 0.48	0.70 / 2.08 / 0.44	0.75 / 1.86 / 0.55	0.71 / 2.00 / 0.49

3.3.3 Real prediction in the 2014 TC season

After constructing the forecast model, we evaluated the model in a 2014 real-time forecast of one-month lead time to the TC season for the WNP basin. By presenting validation of actual prediction, we can provide the insight of our model results interpretation as well as discussions of practical purpose. The 2014 prediction of intense TC activity issued on May 1 and its validation were also performed for the WNP basin. Six intense TCs were formed in WNP during the 2014 TC season including Neoguri, Rammasun, Halong, Phanfone, Vongfong, and Nuri. Only typhoon Rammasun entered the South China Sea, whereas the other typhoons moved northward with recurving tracks. In addition, these intense TCs made landfall except for Nuri. As a reflection of these activities, positive anomalies were dominant over the Philippine Sea–East China Sea–Japan train, whereas negative anomalies occurred over the South China Sea and the eastern part of the WNP (Fig. 3.17a). The seasonal forecast of the WNP during JJASO resembled the observational anomalous positive track density over the East China Sea–Japan region (Fig. 3.17b). According to our prediction results, information of seasonally active intense TC occurrence over the East China Sea in 2014 could be successfully documented in advance. The total intense TC frequency from the prediction was approximately 7.2, including 4.08 for C1, 1.51 for C2, and 1.58 for C3; this value is larger than that in observation. Overestimation of WNP C1 mainly contributed to that of the total intense TC frequency. Moreover,

negative anomalous TC activity over the South China Sea was also noted in the prediction, which indicates that lower intense TC activity compared with the climatological average can be expected in that region. Overall, the actual prediction of 2014 intense TCs in the WNP suggested that the present models are satisfactory for use as operational forecast systems specifically focusing on intense TC activity.

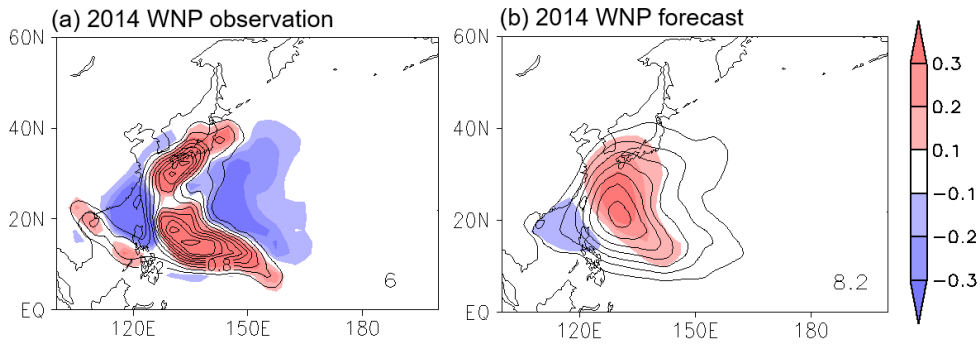

Figure 3.17. Observed TC activity and prediction results from the model for the WNP basin during the 2014 TC season. Contours represent TC occurrence at each grid with an interval of 0.2 in the WNP. Shading denotes anomalies with respect to climatological TC occurrence. The total intense TC number is given in the bottom-right corners.

In the 2014 NA TC season, positive anomalies compared with their climatology appeared adjacent oceans along the east coast of the US, whereas a negative anomaly region occurred over the Gulf of Mexico and the Caribbean Sea (Fig. 3.18a). These results were caused by four intense TCs that developed in the NA basin during the 2014 TC season. Hurricanes Cristobal and Gonzalo developed over the open ocean and moved with recurving paths. In addition, Hurricane Edouard generated over the central NA, and Hurricane Fay intensified into a category 1 storm despite its short lifetime. In the prediction issued on July 5, negative anomalies over the NA basin prevailed, though the positive tendency was not well anticipated (Fig. 18b). The forecasted 2014 NA intense TC frequencies for each cluster are as follows: 0.81 in C1 and 2.08 in C2. Considering that the climatological frequencies of C1 and C2 are 2.1 and 3.2, respectively, our model generally underestimates the 2014 intense TC activity. Therefore, higher activities than the climatology over the adjacent seas from observation were not included in the prediction. The total genesis frequency from the model was approximately 2.9, which is a slightly smaller value within the general error range than the observed genesis number.

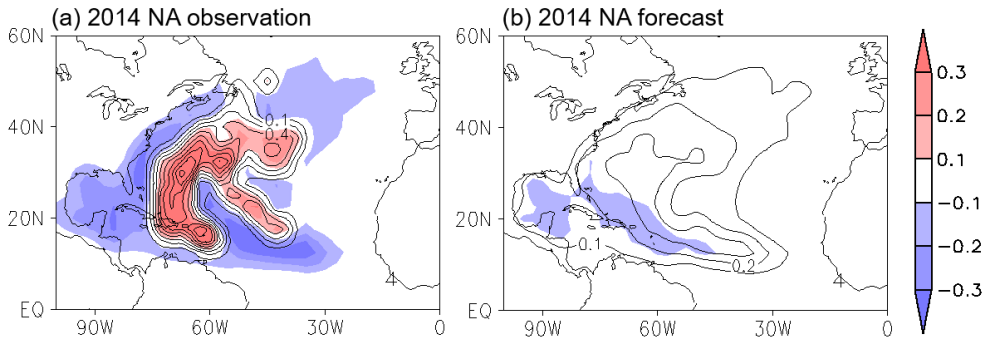

Figure 3.18. Same as Fig. 3.17 except for contour interval of 0.1 in the NA.

4. Near-future prediction of tropical cyclone activi ty

This section shows prediction the NA TC activity in the near-future period 2016–2030 and explanation the mechanisms related to the near-future climate condition, especially in relation to NASST and ENSO variations. To accomplish these objectives, we use a track-pattern-based hybrid prediction model developed in a previous study (Choi et al. 2016a). This model has been shown to be capable of simulating realistic seasonal NA TC activities such as track density and genesis frequency. Although this model was originally developed to predict seasonal NA TC activities, it is also applicable for near-future predictions because the present-day empirical relationships used in the model are likely to be valid for the next few decades. Finally, the impacts of anthropogenic forcing and natural variability on near-future climate in the NA are discussed by investigating near-future SST predictions from multi-model products.

4.1 Strategy for the near-future TC prediction

4.1.1 Application of seasonal TC prediction model

To predict near-future TC activities over the NA basin, we use the track-

pattern-based model developed in a previous study (Choi et al. 2016a), which divided the climatological TC tracks into four representative patterns and predicted each pattern using the simultaneous empirical relationships with large-scale environments derived from the seasonal climate forecasts. Then, the prediction results of all track patterns were combined to produce the TC forecasts over the NA basin.

The original version in the previous study used the NCEP CFSv2 seasonal reforecasts during the period 1982–2012 and quasi-real-time CFSv2 operational forecasts. In this study, the track-pattern-based TC prediction model is developed using the NCEP CFSR datasets. We modify the statistical training period to 1982–2015 to include very recent climate variability. However, the overall structure for this model and its logical flow are the same as those in the original version.

Figure 4.1 shows the four representative patterns of NA TC tracks (TC1–TC4) and the associated interannual correlation maps between TC track patterns and climate predictors. We identify climatological NA TC track patterns by using the fuzzy *c*-means method (Choi et al. 2016a). Then, the hybrid prediction model is developed for each track pattern. The candidate variables for the predictor are SST, VWS, VOR850, and U850, which are well-known climate factors strongly related to TC activity. If the characteristics of the predictors are empirically explainable for TC activity and the corresponding relations are statistically significant, we employ their

relations as predictors. The positive relationships with SST and VOR850 are used for calculating predictors; other connections of VWS and U850 are also utilized. Because significant relations are still retained despite the inclusion of recent years, the detailed domain for the predictor region and combinations of predictors are the same as those used in the original version of the model.

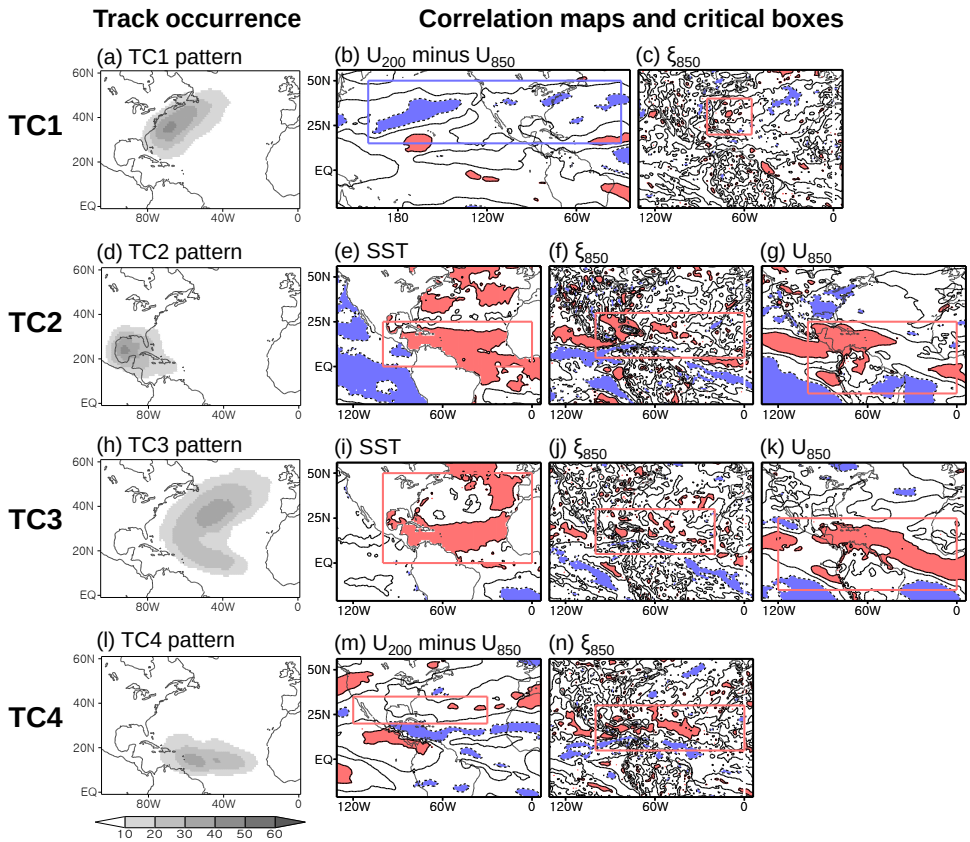

Figure 4.1. (a), (d), (h), (l) Gridded TC occurrences of the four track patterns for hurricane seasons (August–October) of 1965–2015 over the North Atlantic. (b)–(c), (e)–(g), (i)–(k), and (m)–(n) Spatial correlation coefficients between observed TC frequencies and predictor variables from CFSR during 1982–2015 for each track pattern. Red (blue) shadings indicate areas with statistically significant positive (negative) correlations at the 90% confidence level. The predictor regions are presented as a colored box.

To reforecast TC frequencies of the four track patterns, we use a leave-one-out cross-validation method. This method has been mainly used to evaluate the skill of statistical model employing the independent predictors on different years (Kim et al. 2012; Ho et al. 2013; Choi et al. 2016a, b). When we select a certain target year for prediction, the model is optimized to produce the best fitting result by using the remaining years. This process is iteratively performed to reforecast predictand (i.e., TC) for the whole training period. Statistical measures of hindcasts verify the performance of this model even with the inclusion of recent years in the training period (Table 4.1). All correlation coefficients between reforecasted TC and observed TC are statistically significant at the 95% confidence level. Moreover, we investigate the root–mean–square errors (RMSE) and mean–square skill scores (MSSS) to objectively assess the predictability. The RMSE value is the mean error of the forecasting model; a lower RMSE value indicates better performance. The MSSS value is a measure of improvement in performance over the reference prediction: A positive (negative) MSSS value implies that the model is better (worse) than the reference prediction. The MSSS value in the case of best prediction is 1. The expected errors (i.e., RMSE) for all track patterns are less than 1.59, and all of the MSSS values are positive. Therefore, the RMSE and MSSS of all TC track patterns demonstrate the skillful performance of our model.

Table 4.1. Correlation coefficients (CORR), root–mean–square errors

(RMSEs), and mean–square skill scores (MSSS) of hindcasts using the CFSR compared with best-track observations for the period 1982–2015.

Cluster	CORR	RMSE	MSSS
TC1	0.75	1.07	0.56
TC2	0.63	1.59	0.22
TC3	0.65	1.48	0.38
TC4	0.66	1.38	0.41

4.1.2. Multivariate linear regression model using the NASST and Niño 3.4 indices

To examine the role of NASST and ENSO effects on changes in the NA TC activities, we set up the multivariate linear regression model using the NASST and Niño 3.4 indices. The empirical orthogonal function (EOF) analysis is applied to define the NASST index. The NASST index is calculated by projecting the ASO-averaged NASST (0°–70°N) anomalies onto the leading EOF mode of CFSR SST (1982–2015), which would be known as the spatial pattern of AMO (not shown). We use NASST as an index for regression instead of AMO because there is not enough available SST data length to define AMO index as other previous studies. The Niño 3.4 index is the area-averaged SST anomalies over the region of 5°S–5°N, 170°W–120°W. The indices of NASST and Niño 3.4 are mutually independent, with an insignificant correlation coefficient value of r = 0.06 for the period 1982–2015, which therefore satisfies the statistical assumptions for the multivariate linear regression model. All time-evolving two-dimensional fields (y) such as SST, U200, U850, VWS, and VOR850 are decomposed into NASST-regressed fields (y_{AMO}), Niño 3.4-regressed fields (y_{ENSO}), and their residuals (y_{Res}). The formulas of each field are written as

$$y_p = \alpha_0 + \alpha_{NASST} x_{NASST} + \alpha_{ENSO} x_{ENSO}$$

$$y_{NASST} = \alpha_0 + \alpha_{NASST} x_{NASST}$$

$$y_{ENSO} = \alpha_0 + \alpha_{ENSO} x_{ENSO}$$

$$y_{Res} = y - y_p + y_{Clim},$$

where y_p is the predicted field, y_{Clim} is the climatological average, α_0 is the regression constant, α_{NASST} is the regression coefficient of NASST, x_{NASST} is the NASST index, α_{ENSO} is the regression coefficient of ENSO (i.e., Niño 3.4), and x_{ENSO} is the Niño 3.4 index. By investigating the predictions with these different fields, we can determine the responsible mechanisms for regional TC activity changes in the near future.

4.2 Near-future prediction of the NA TC activity

4.2.1. Observational responses of the NA TC to NASST and ENSO

Before performing TC predictions, it is necessary to examine the sensitivities of the TC prediction model to the changes in NASST and ENSO phases, and whether these sensitivities are physically explainable. Although the predictors of track-pattern-based models are strongly linked to NASST and ENSO variabilities, high predictability of the TC activity responses to the phases of NASST and ENSO is not guaranteed because the model uses the area-averaged climate variables as predictors. Thus, we need to identify the responses of NA TC activity from the model with observation during the statistical training period of this model (i.e., 1982–2015).

Figure 4.2 presents the differences in the gridded TC occurrences between

the positive and negative phase of NASST and ENSO. It is well known that more (fewer) NA TCs form during a NASST warming (cooling) period associated with the positive (negative) phase of AMO years (Fig. 4.2a). Some regions in the tropical NA have experienced 1.5 more TC occurrences in the NASST positive years than negative years, which means that almost 50% more (less) TCs occur in the positive (negative) NASST years compared to the climatological TC numbers. Weakened TC activities of up to one less TC occurrence in the El Niño years compared to the La Niña years are noted over the Gulf of Mexico and the East Coast of North America (Fig. 4.2b) due to sinking motion over the Gulf of Mexico and the Caribbean Sea induced by the upward motion in the eastern Pacific (Frank and Young, 2007). The core regions of TC occurrence differences between positive and negative phases of NASST and ENSO are significant at the 95% confidence level.

The hindcasts of TC activity from the model using Climate Forecast System Reanalysis (CFSR) can reasonably reproduce the observed responses of TC occurrences associated with the NASST and ENSO phases despite some overestimations (underestimations) in the mid-latitude NA offshore (Gulf of Mexico) for the NASST (ENSO) case (Figs. 4.2c and 4.2d). In addition, the model responses are significant in most parts of the NA basin. In general, this model realistically simulates the overall TC activity changes associated with NASST and ENSO variations. To verify the origin of performance, we prescribe NASST- and Niño 3.4-regressed fields to the TC

prediction model. Figures 4.2e and 4.2f show TC activity responses of the model to the phase differences of NASST and ENSO with their regressed fields used as input data. They are nearly identical to the reconstructions using the original CFSR fields (Figs. 4.2c and 4.2d). This result implies that most of the predicted TC activity responses originate from their regressed fields (i.e., NASST and ENSO); thus, the performance source of the reforecast is from its own variability. For the TC activity response to NASST (ENSO), the effect of Niño 3.4- (NASST)-regressed fields is negligible (not shown). Thus, this model can reasonably predict TC activities based on independent links with NASST and ENSO.

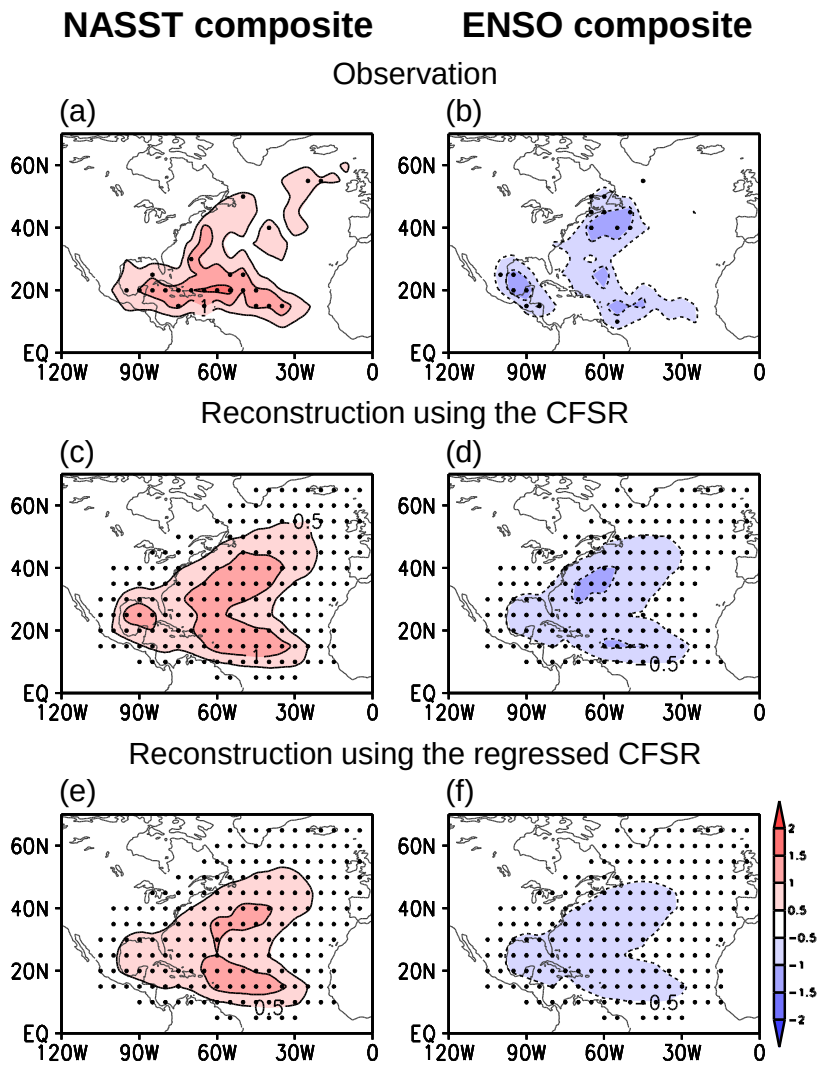

Figure 4.2. Composite differences in seasonal TC occurrence for positive minus negative phase years of the North Atlantic basin-wide SST (NASST) and El Niño–Southern Oscillation (ENSO) during the period 1982–2015. (a),(b) The best-track observations, (c),(d) CFSR reconstructions, (e) reconstruction using the NASST-regressed CFSR, (f) reconstruction using the Niño 3.4-regressed CFSR. Black dots indicate that the differences are statistically significant at the 95% confidence level in each 5° × 5° latitude–longitude grid area.

4.2.2. Prediction results and contributions of the NASST and ENSO

This good validation of the model performance lends credence to our predictions of the changes in TC activities for the near-future period. Here, we investigate the differences in the gridded TC occurrences between present decades (2002–2015, P1) and near-future decades (2016–2030, P2). Table 4.2 shows the changes for the four clusters (TC1–TC4, Fig. 4.1) and their summation of seasonal TC frequencies for each ensemble during the two periods. All clusters and their summation of TC frequencies are expected to decrease in the near future except for TC2 in Climate Forecast System version 2 (CFSv2) initialized in 1996 (CFS1996). Frequencies in TC2 in CFSv2 initialized in 1988 (CFS1988), TC1 in CFS1996, TC3 and TC4 in CFSv2 initialized in 2002 (CFS2002) are expected to decrease significantly in P2 compared with that in P1. For the averages of the three ensembles, the number of TC1 through TC4 during the August to October (ASO) of P2 will decrease by 0.15, 0.32, 0.53, and 0.53, respectively, which correspond to 5–20% reduction. The total number of seasonal TCs is reduced by 1.53 (about 12% decrease, 11.25 in P2 and 12.78 in P1).

Table 4.2. Seasonal TC genesis frequencies of each track pattern and their summation by the track-pattern-based model for periods 2002–2015 (P1), 2016–2030 (P2), and the difference between the two periods. Asterisks represent statistical significance level for each ensemble member at the 95% (***), 90% (**), and 80% (*) levels.

Ensemble	Period	TC1	TC2	TC3	TC4	Sum
CFS1988	P1	1.02	5.63	2.16	3.61	12.42
	P2	0.80	4.74	1.78	3.25	10.57
	P2 minus P1	–0.22	–0.89*	–0.39	–0.36	–1.86*
CFS1996	P1	0.93	5.23	1.95	3.53	11.65
	P2	0.74	5.58	1.93	3.17	11.42
	P2 minus P1	–0.19*	0.34	–0.02	–0.36	–0.23
CFS2002	P1	1.00	5.92	3.17	4.17	14.26
	P2	0.97	5.50	1.98	3.31	11.75
	P2 minus P1	–0.03	–0.42	–1.20***	–0.86**	–2.51***
Average	P1	0.99	5.59	2.43	3.77	12.78
	P2	0.84	5.27	1.89	3.24	11.25
	P2 minus P1	–0.15	–0.32	–0.53	–0.53	–1.53

According to these changes, the TC activity is predicted to weaken over the entire NA basin in the near-future period (Fig. 4.3a). In particular, seasonal TC occurrences over the region of 10°N–20°N, 60°W–30°W and in the open ocean of the NA basin will decrease by up to 0.4. It means that about four less TCs per decade are anticipated over the core region of reduced TC activities. All three ensembles based on the CFSv2 Coupled Model Intercomparison Project (CMIP) consistently show reduced TC activities except for the Caribbean Sea and the Gulf of Mexico. The large decrease in NA TCs is concentrated mainly in the open ocean with a maximum seasonal decrease of 0.2 (i.e., two less TCs per decade) in the 50°N region.

The weakened TC activities over the NA can be explained by the effects of the phase transitions in NASST and ENSO during the near-future period. The decrease in the TC activity over the open ocean is attributed mainly to the effects of NASST (Fig. 4.3b). The prediction using the NASST-regressed fields explains a large portion of the reduced TC occurrences offshore. However, no region shows the same sign in all three CFSv2 CMIP ensembles. For the ENSO effects, the overall decrease in the basin-wide NA TC activities is caused by changes in the ENSO effects during P2 (Fig. 4.3c). In particular, the remote effects of ENSO can reduce TC activities over the Caribbean Sea, the Gulf of Mexico, and the East Coast of the United States. Unlike NASST, the changes in the ENSO phase show the same TC change tendencies in the entire NA basin. Although residual fields from NASST and ENSO can lead

to decreases in TC activities over the tropical region, its variation shows relatively small amplitudes compared to the TC reductions by the changes in NASST and ENSO (Fig. 4.3d). Summation of these three decomposed changes presented nearly the same amplitude and spatial distribution of the total TC activity decrease (not shown).

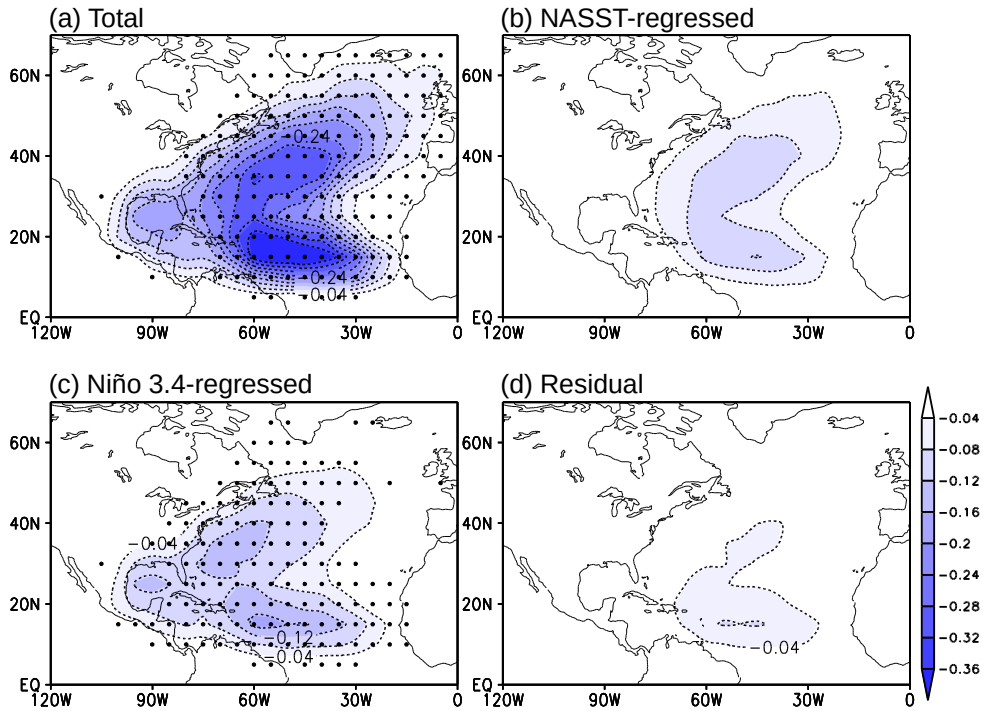

Figure 4.3. Ensemble-averaged differences for seasonal TC occurrence between the two periods (2016–2030 minus 2002–2015) by using the (a) total fields, (b) North Atlantic basin-wide SST (NASST)-regressed fields, (c) Niño 3.4-regressed fields, and (d) residual fields. Black dots indicate regions in which all three ensembles of reconstruction show the same sign in each 5° × 5° latitude–longitude grid area.

We have analyzed near-future TC changes by considering the NASST and ENSO impacts. Here, we investigate how the changes in NASST and ENSO are simulated in the CFSv2 CMIP runs, and we examine their relationship to the predicted TCs changes. Table 4.3 presents a comparison of the event frequency per decade for NASST and ENSO phases between P1 and P2 for each ensemble member and their averages. Calculations of the long-term NASST and ENSO events over several decades are not available because the analysis period is limited to 2002–2030, the common period for all three ensembles. However, we were able to assess the climatological phase transitions of NASST and ENSO, and their changes in event frequency between P1 and P2. All ensembles predict more frequent NASST neutral phase and less frequent positive phase. For ENSO, all three ensembles show more frequent El Niño events in the near-future period. Thus, more frequent El Niño episodes, fewer neutral and La Niña phases are expected to occur in P2. These changes in the climate variability will become unfavorable for the TC genesis and development over the NA in the near-future period.

Table 4.3. Event frequencies per decade for positive, neutral, and negative phases of the North Atlantic basin-wide SST (NASST) and El Niño–Southern Oscillation (ENSO) for periods 2002–2015 (P1) and 2016–2030 (P2) and their difference.

Ensemble	Period	NASST			ENSO		
		Positive	Neutral	Negative	El Niño	Neutral	La Niña
CFS1988	P1	4.29	2.86	2.86	3.57	2.86	3.57
	P2	1.33	4.67	4.00	4.00	6.00	0.00
	P2 minus P1	–2.96	1.81	1.14	0.43	3.14	–3.57
CFS1996	P1	1.43	4.29	4.29	1.43	4.29	4.29
	P2	1.33	5.33	3.33	4.67	2.67	2.67
	P2 minus P1	–0.10	1.04	–0.96	3.24	–1.62	–1.62
CFS2002	P1	4.29	3.57	2.14	2.86	4.29	2.86
	P2	2.00	4.67	3.33	4.67	2.00	3.33
	P2 minus P1	–2.29	1.10	1.19	1.81	–2.29	0.47
Average	P1	3.34	3.57	3.10	2.62	3.81	3.57
	P2	1.55	4.89	3.55	4.45	3.56	2.00
	P2 minus P1	–1.79	1.32	0.45	1.83	–0.25	–1.57

Combinations of the NASST and ENSO phase transitions result in large-scale environmental changes in P2. Figure 4.4 shows the ensemble-averaged changes for seasonal environmental fields such as SST, zonal wind at the 200 hPa (U200) and 850 hPa levels (U850), VWS, and relative vorticity at 850 hPa (VOR850), which are predictor variables for the TC prediction model (Fig. 4.1). Although the near-future changes in these three ensemble averages reveal that the SST warming will occur in the mid-latitude central NA, other tropical and subpolar gyre regions in the NA show SST cooling in P2 (Fig. 4.4a). In addition, notable SST warming regions appear in the central to eastern Pacific. These results imply that the NASST phase slowdown from the positive to neutral phase in conjunction with more frequent El Niño events are anticipated in P2 compared with that in P1 as discussed earlier. All atmospheric circulations are systematically organized with these SST change patterns (Figs. 4.4b–e). The difference between the easterlies at 850 hPa and the westerlies at 200 hPa over the tropical NA causes the VWS to increase in P2. Both the strengthened VWS and weakened VOR850 over the tropical NA, shown in ensemble-averaged CFSv2 CMIP simulations, lead to unfavorable conditions for TC developments.

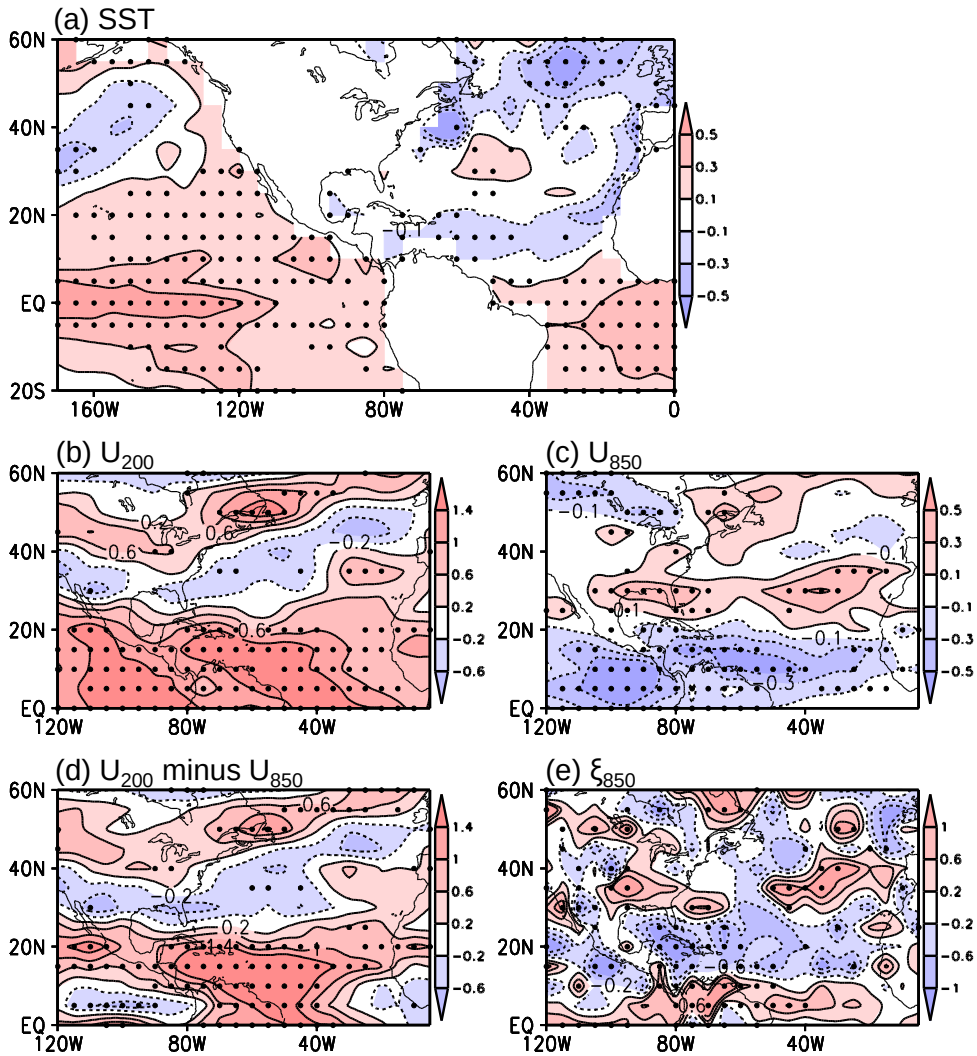

Figure 4.4. Ensemble-averaged seasonal differences in (a) sea surface temperature (SST; ℃), (b) zonal wind at 200 hPa (m s^{-1}), (c) zonal wind at 850 hPa (m s^{-1}), (d) vertical wind shear (m s^{-1}), and (e) relative vorticity at 850 hPa (10^{-6} s^{-1}) between the two periods (2016–2030 minus 2002–2015). Black dots indicate regions in which all three ensembles of CFSv2 CMIP runs show the same sign.

These SST changes in the NA and eastern Pacific can be understood with their own regressed fields. The SST decreases in the tropical NA and subpolar gyre occur in the changes of NASST-regressed SST (Fig. 4.5a). The decadal SST variability in the NA subpolar gyre is known to be closely related to AMO (Hermanson et al. 2014). Because the variability of NASST is closely related to AMO, the subpolar gyre heat convergence induces SST cooling and the NASST phase change. The upper and lower tropospheric wind fields changes related to the NASST variability lead to an increase in VWS in the tropical Atlantic region and a decrease in VOR850 in the subtropical NA region (Figs. 4.5b–e). All of these variations induce decreased TC activities in the NA offshore in near-future period. The SST warming in the eastern Pacific is also found in Niño 3.4-regressed fields (Fig. 4.6). Enhanced VWS in tropical and mid-latitude region of NA as well as weakened the VOR850 in inshore (Caribbean and Gulf of Mexico) associated with the ENSO variation would cause reduction of overall TC activity in the entire basin (Figs. 4.6b–e).

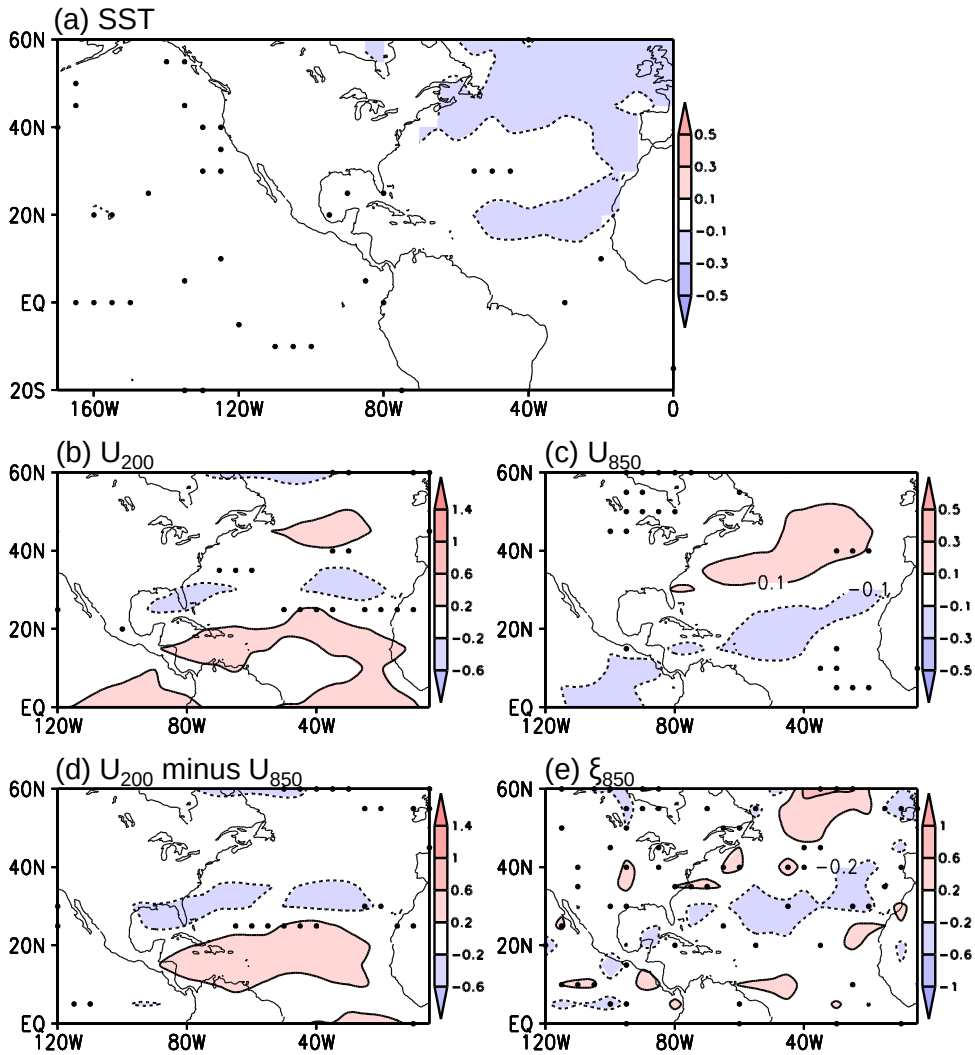

Figure 4.5. Same as Fig. 4.4 except for the North Atlantic basin-wide SST-regressed fields.

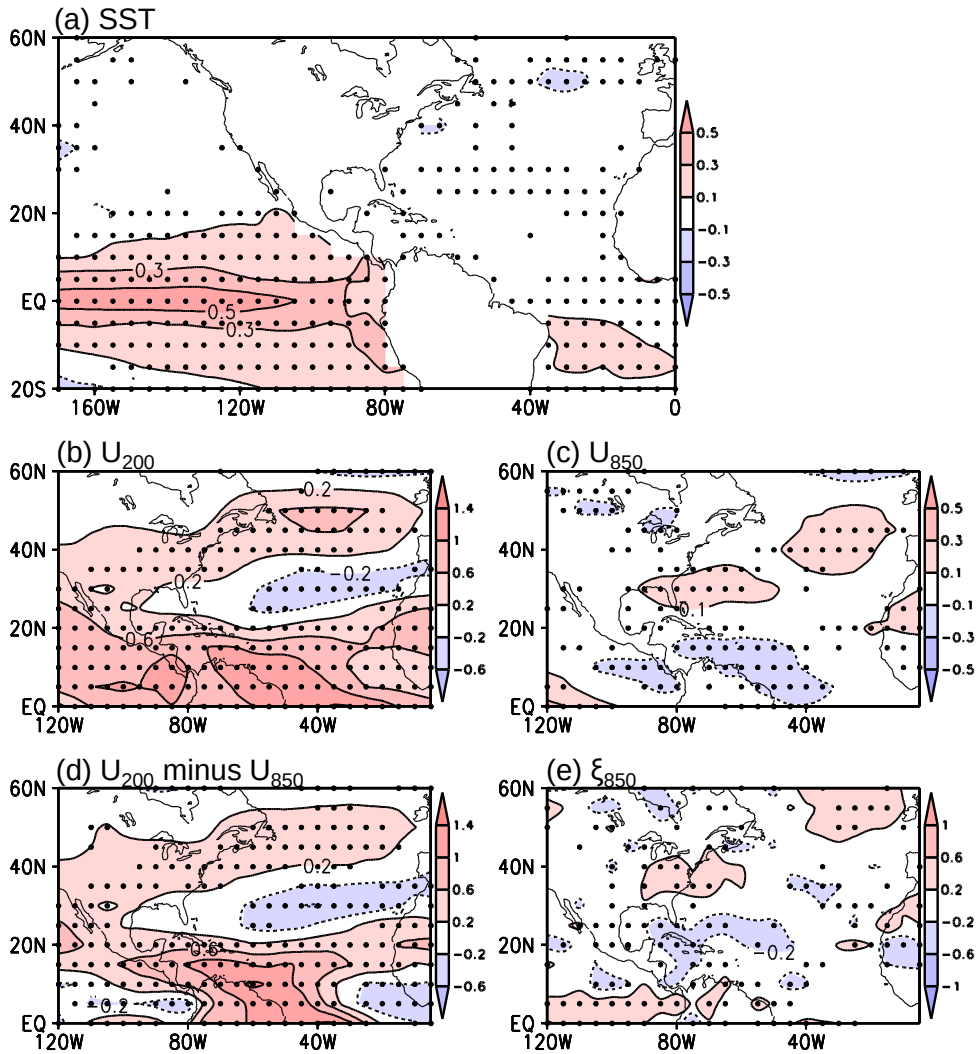

Figure 4.6. Same as Fig. 4.4 except for Niño 3.4-regressed fields.

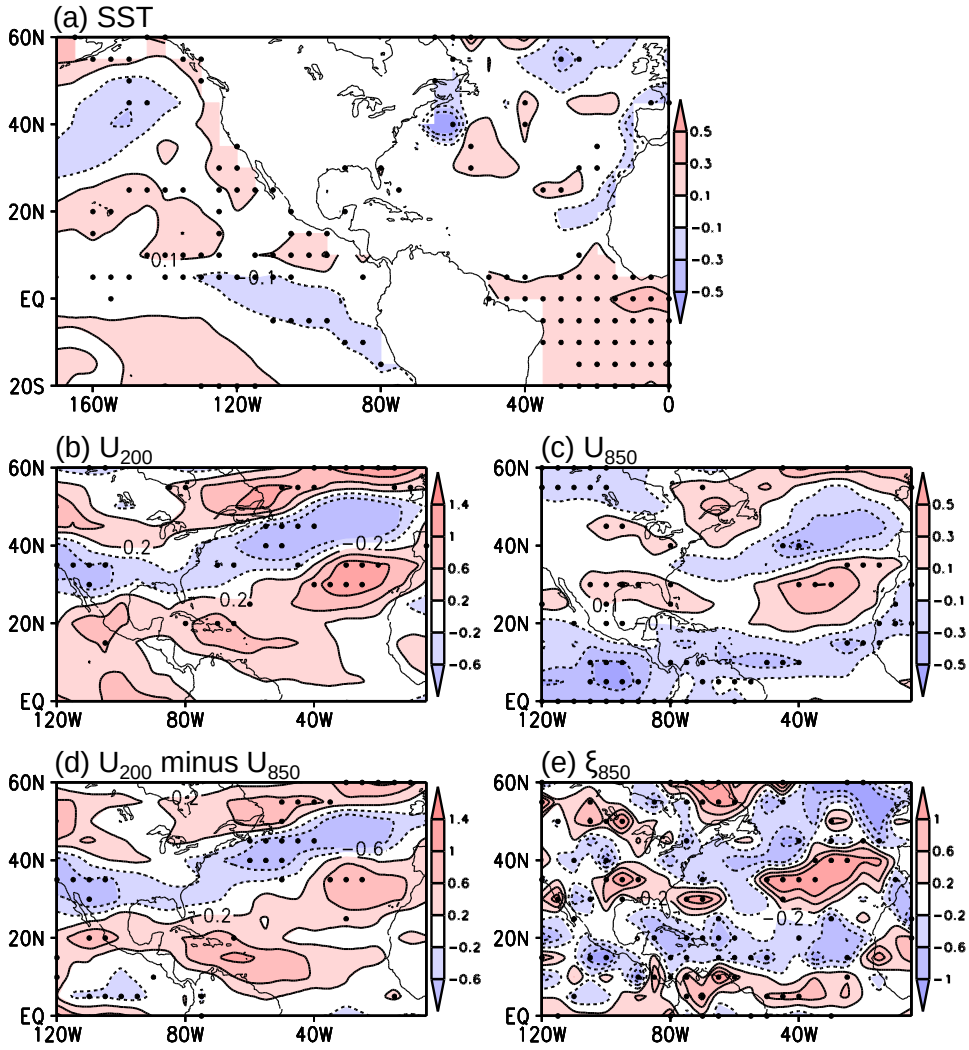

Figure 4.7. Same as Fig. 4.4 except for residual fields.

As for residual effects, many types of climate factors other than NASST and ENSO can affect NA TC activities. Considering the predictor variables and their critical domains of the model (see Fig. 4.1), we can infer these other factors. The change in VWS owing mainly to U200 over the subtropical NA could be a reason for the weakening of TC activities in the near-future period because this will have a significant impact by destroying the TC vertical structure (Figs. 4.7b–4.7d). In addition, strengthening of low-level easterlies (i.e., U850) in the tropical NA appear to suppressing factors for TC development because it can lead to the decrease in the relative vorticity (VOR850) over the main TC development region (Fig. 4.7e). These changes are not captured in our statistical decomposition and do not appear to be directly related to the NASST and ENSO variabilities (see Fig. 4.7a). However, the effects of these residual factors cancel out each other to result in small net effects (Fig. 4.3d).

As one of the candidates for other influences, long-term external forcing effects such as greenhouse effect may be considered as residual effects. However, greenhouse effects are not expected to have a significant impact in the near-future decades. Moreover, significant differences in NA TC activity are not detected even in the prediction using environmental fields regressed onto global warming (not shown). Therefore, if we want to accurately characterize the residual effects, further investigations of various time scales and spatial scales are needed.

4.2.3. Roles of the natural variability and external forcing

The cooling of NASST in the near-future period is an interesting issue when we consider recent global warming trend induced by the anthropogenic greenhouse gas emissions. As an attempt to understand this discrepancy, we analyzed the near-future SST predictions in other CMIP5 models to discuss the main driver of NASST variability and ultimately of TC activity changes in the near future. Figure 4.8 shows the ensemble-mean seasonal SST differences from 24 CMIP5 models following the historical and RCP4.5 scenarios between P2 and P1. The RCP4.5 scenario data are calculated from pre-industrial initial conditions and forced by anthropogenic influences. We can assess that difference in seasonal SST from the CMIP5 multi-model ensemble average is mainly attributable to the anthropogenic forcing rather than internal variability for each model. As expected, the ensemble-mean prediction shows prevailing SST warmings over the Atlantic and Pacific basins in the near-future period. For the ENSO, the CMIP5 models generally predict greater SST warmings in the eastern Pacific, which implies the models simulate more frequent occurrences of El Niño events. For the SST in the NA, the warming amplitude is relatively small in the NA subpolar gyre region because of the cooling from some models, but most of the models show warming SST in the tropical NA. Overall, anthropogenic forcing acts to increase the SST over both the NA and the eastern Pacific basins in the near

future. Considering that NASST warmings (more frequent El Niño events) can lead to enhancement (decline) in the NA TC activity, the near-future decrease in the NA TC activity may be small or almost unchanged if only anthropogenic impact affects to the NA TC change.

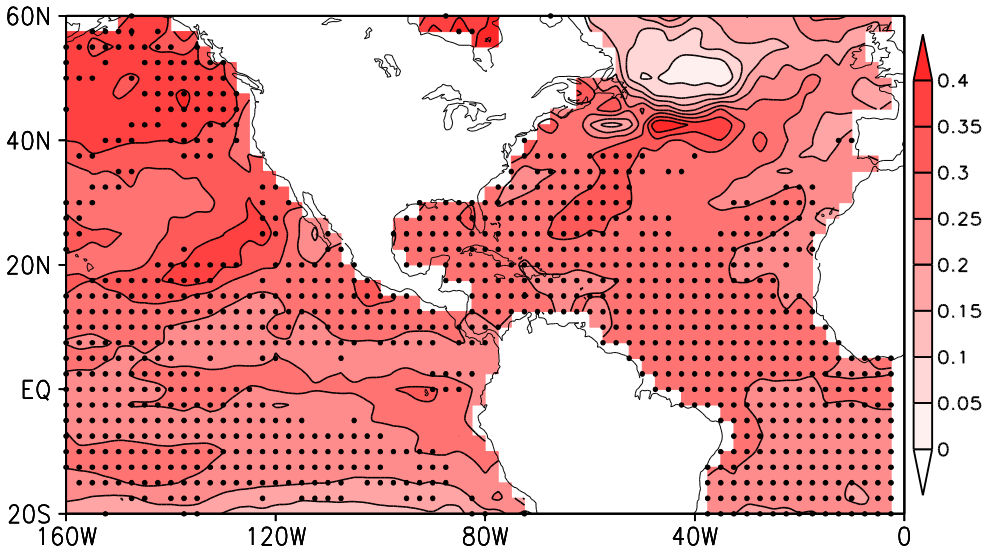

Figure 4.8. Ensemble-averaged seasonal difference in SST from 24 CMIP5 models for historical and RCP4.5 scenarios between the two periods (2016–2030 minus 2002–2015). Black dots indicate regions in which 18 of 24 CMIP5 models showing the same signs of averages in SST differences.

Our results based on the CFSv2 CMIP climate forecasts show clear decreases in the NA TC activity via the changes in both NASST and ENSO. Because the CFSv2 CMIP runs are initiated with the reanalysis data and forced by increased CO_2 concentration, the internal variability and external forcing are considered simultaneously in the near-future prediction (see Data). We can estimate the impact of natural variability to SST increases in the near future by comparing the CFSv2 CMIP runs and the CMIP5 multi-model products. The number of El Niño events is expected to increase due to natural variability or anthropogenic forcing. The difference between the CFSv2 and CMIP5 multi-model ensemble-mean SST predictions implies that the cooling effects of natural variability dominates the warming effects of anthropogenic forcing in determining the future NASST. Thus, this result suggests that the cooling phase of NASST in conjunction with increasing El Nino events will significantly decrease the NA TC activities in the near future.

Near-future prediction should be handled differently from long-term climate projection (e.g., late 21st century prediction) that is dominated by external forcing. Our study investigates the role of natural variability and anthropogenic forcing on the near-future climate and TC activity changes. We hope that this study can address the scientific challenges and the *predictability desert* fairly to satisfy the social needs in preparing for TC-induced disasters with long-range plans.

4.3 Near-future prediction of the WNP TC activity

4.3.1. Prediction results and ENSO contribution

As the NA basin, we attempted to predict the TC activity changes over the WNP basin. In the above section, we showed that more frequent El Niño events are expected in near future (Table 4.3). Because the ENSO is major natural variability to modulating the WNP TC activity, we developed linear regression model using the Niño 3.4 index. For the WNP basin, we excluded the NASST variability because its effect has been not revealed in any previous studies and the predictors of TC prediction model do not reflect the NASST variability. Prior to prediction of the near-future WNP TC changes, we extended training period of the track-pattern-based model developed in Ho et al. (2013) to include recent TC variability. The modified training period is 1982–2015 consistent with the NA TC prediction model.

Figure 4.9a shows observed composite differences between El Niño years minus La Niña years during the period of 1982–2015. As previous studies reported (Kim et al. 2013), the TC activity is enhanced over the southern-eastern part of the TC main develop region and significant high TC activity ridge leads to the southern Japan. The TC activity over the South China Sea is relatively weakened in El Niño years than La Niña years.

Figure 4.9b presents the prediction of near-future TC changes over the WNP. Except for tropical offshore sea where maximum core region in ENSO

composite map (Fig. 4.9a), the WNP TC activity is expected to be weakened in overall basin including Philippines Sea, Taiwan, and southeastern sea of the Japan. If we investigate the near-future TC change associated with ENSO variability, it is expected to increase from offshore tropical seas through the Japan and Korea, and decrease in the South China Sea (Fig. 4.9c). Considering the ENSO-related TC activity characteristics and near-future large-scale circulation fields changes related ENSO (Table 4.3 and Fig. 4.6a), more active TCs from offshore sea through the Korea and Japan would be reasonable prediction result. Residual changes unrelated to ENSO variability are expected to reduce TC activity in the East China Sea (Fig. 4.9d). However, it is necessary to further analyze other possible climate variability effects to the WNP TC changes because the summation of these two effects does not account for the near-future TC changes (Fig. 4.9b).

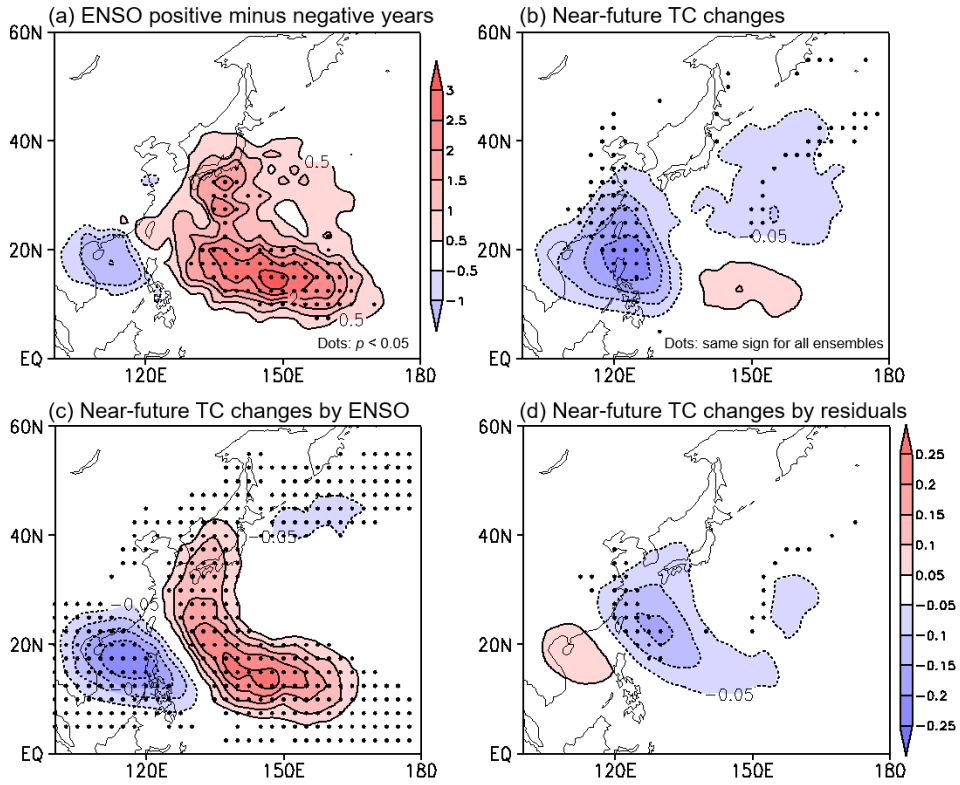

Figure 4.9. (a) Composite differences in seasonal TC occurrence for positive minus negative phase years of the El Niño–Southern Oscillation (ENSO) during the period 1982–2015. Black dots indicate that the differences are statistically significant at the 95% confidence level in each 2.5° × 2.5° latitude–longitude grid area. Ensemble-averaged differences for seasonal TC occurrence between the two periods (2016–2030 minus 2002–2015) by using the (b) total fields, (c) Niño 3.4-regressed fields, and (d) residual fields. Black dots indicate regions in which all three ensembles of reconstruction show the same sign in each 2.5° × 2.5° latitude–longitude grid area.

4.3.2. Possible influences from other variabilities

As we have seen, the ENSO-induced TC changes did not explain the near-future prediction of the WNP TC activity changes. There would be many climate variabilities for affecting the WNP TC activity other than ENSO. Thus, we should investigate various climatic influences to the near-future TC activity.

First of all, it is well known that the MJO may have an impact to the WNP TC activity on subseasonal time scale. If the MJO variability would be changed in climamtological perspective, therefore, we can expect the changes in the near-future TC activity. If there are changes in the mean state of the near-future WNP and associated wave propagation, the development and movement of MJO may change. In addition, variabilities of the stratospheric influences (e.g., QBO) and Pacific Decadal Oscillation (PDO) can affect the WNP TC activity. Previous study reported that the easterly phase of the stratospheric QBO can induce more TC occurrence in the offshore of Japan whereas more TCs approach over the East China Sea during the westerly phase (Ho et al. 2009). Regarding the PDO, Liu and Chan (2008) suggested the possible influence of PDO to the interdecadal WNP TC activity by changes in the strength and westward extension of the subtropical high. If climatic changes of the QBO and PDO occur in the near future, they can affect the WNP TC activity.

5. Future study

Long-term prediction of TC activity is a necessary process to reduce the damage caused by TCs and to utilize the positive side of TC including water resource supply and elimination of the red tide. This thesis shows the long-term prediction of TC track occurrences and intensity based on the understandings of variability of the WNP and NA TCs. Because the unskillful performance of seasonal TC simulations by the numerical modeling suggests that there are still several challenges to apply operational forecasts, this thesis explores the statistical relationships between the seasonal forecasts from the GCM (i.e., CFSv2 in this thesis) and the summertime TC activity, which is called as hybrid statistical-dynamical method, to predict TC activity as transition stage to the numerical TC prediction.

Nevertheless, the TC prediction using the high-resolution dynamic model should be continued for next generation. Statistical approach has fundamental limitations regarding TC intensity, which can be overcome by the high-resolution dynamics model. However, climate modeling of several-km resolution has not been attempted until now because of inappropriate dynamic core and model parameterization, limitation of computing source (i.e., promptness), and overall performance. We should overcome these limitations, so the numerical model should be used for long-term TC prediction in the

next generation.

For a disaster prevention perspective, the accurate prediction of TC-induced extreme weather is essential. At this generation, we anticipate that state-of-the-art numerical model with the order of few kilometers can reasonably predict the TC-induced precipitation and surface wind speed. Even though there are limitations for applying climate model to seasonal prediction at this moment, we have explored the possibility by investigating recent Korea-landfall TCs.

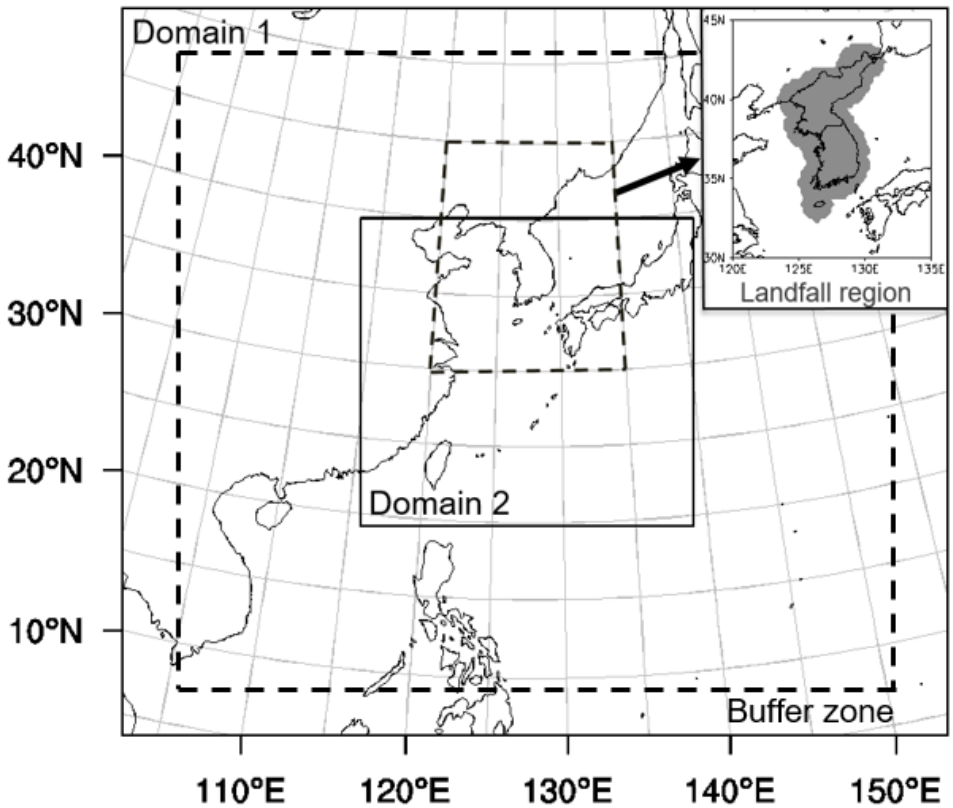

Figure 5.1. Model domains and Korea landfall region indicated by the shades.

In order to simulate TC structure and related environmental fields including precipitation and wind, we used the Weather Research and Forecasting (WRF, Skamarock et al. 2008) model, version 3.4. Many previous studies have been widely used in short-term TC simulation by using the WRF model (Davis et al. 2008; Fierro et al. 2009; Gentry and Lackmann 2010; Cha et al. 2011; Potty et al. 2012; Jin et al. 2013). The initial and lateral boundary conditions are acquired from the NCEP CFSv2 6-hourly forecasts. The two-way nested experiments containing fixed grid systems with horizontal resolution of 30 and 10 km (Fig. 5.1), respectively, and 30 vertical levels (1000–50 hPa). The domains are centered at 30°N, 128°E with 202 × 178 (domain 1) and 244 × 226 (domain 2) grid points. WRF single-moment 3-class microphysics (WSM3) scheme was used for microphysics scheme (Hong et al. 2004). The Kain–Fritsch scheme (Kain, 2004) was applied as the cumulus parameterization. The Yonsei University scheme (Hong et al. 2006) was chosen for the planetary boundary layer parameterization. The model also includes the radiative scheme for the NCAR Community Atmosphere Model (CAM 3.0) radiation scheme (Collins et al. 2004) and Noah land surface model (Chen and Dudhia 2001).

As target cases, the recent ten landfall TCs to the Korean Peninsula during the 2011–2016 are simulated. A TC makes landfall in Korea when its center is at a distance of 1° from the coastal lines of the Korea (Fig. 5.1). For each TC case, three experiments initialized in 1-day, 2-day, and 3-day leads to the

landfall date are conducted (Fig. 5.2). Although unrealistic TC tracks are simulated in far-lead cases (mostly 3-day leads simulation), it is found that most of the 1-day lead simulations can reasonably predict TC tracks. Therefore, all the following analyses are based on the 1-day simulations.

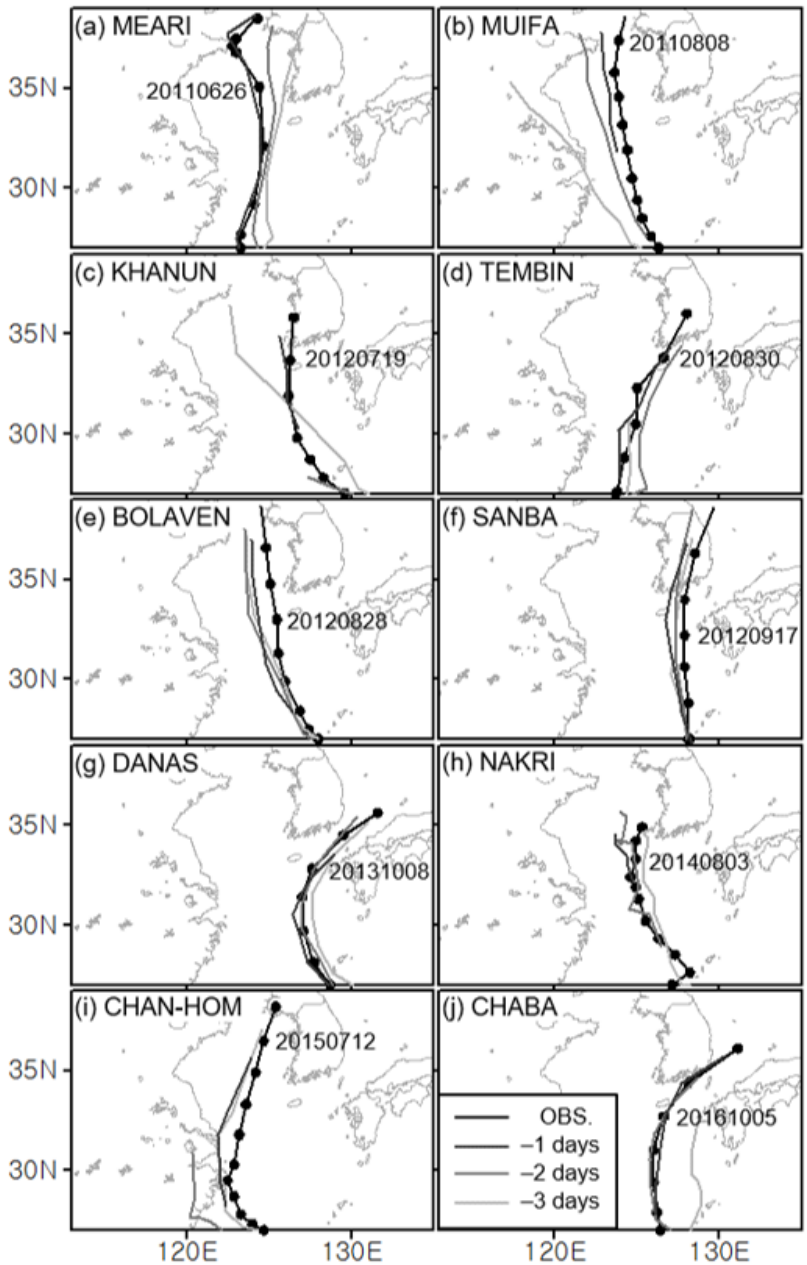

Figure 5.2. Observed and simulated tracks of 10 landfall TCs during the 2011–2016. The black line with closed circles plotted every 6 h denote the best-track observation. Simulated TC tracks by three experiments with initialized in 1-day, 2-day, and 3-day lead time to affecting day are presented in different gray colors.

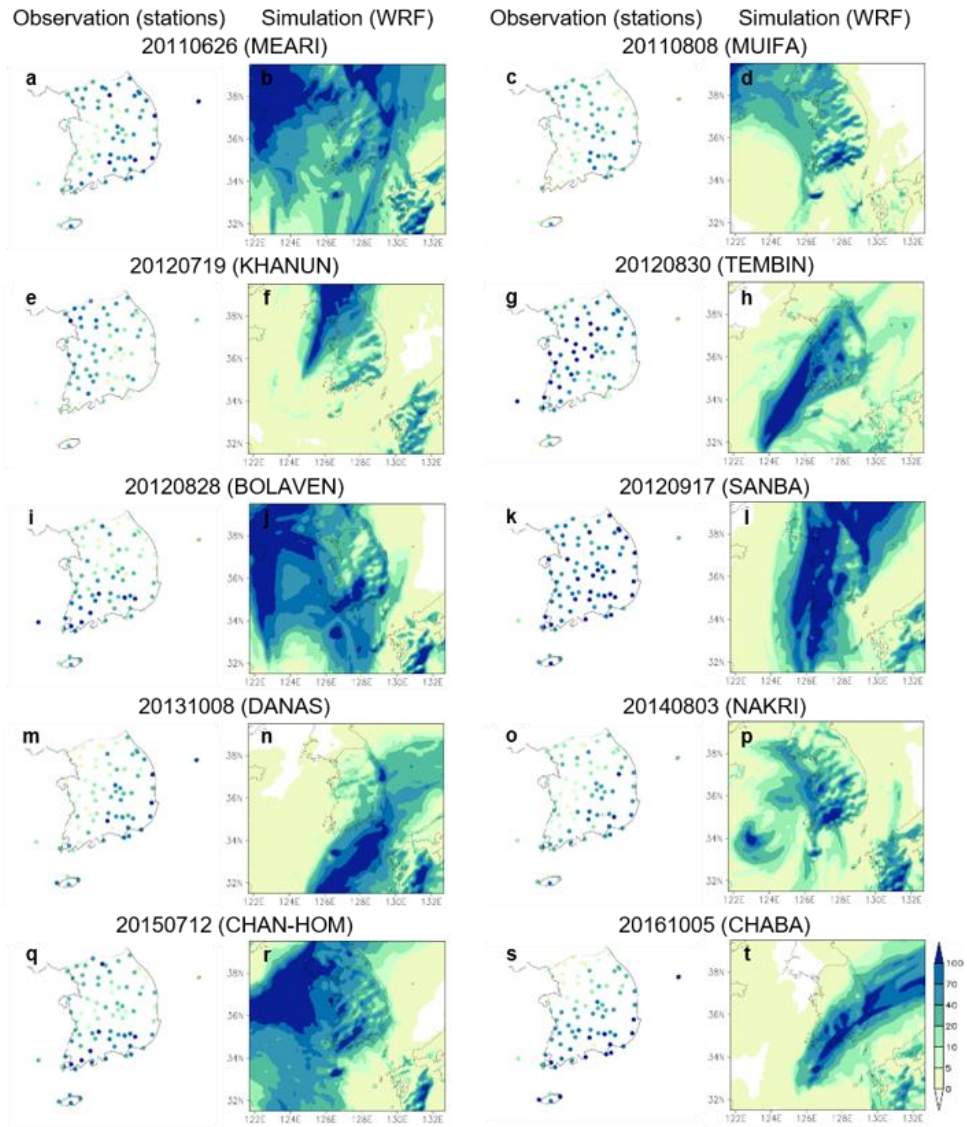

Figure 5.3. Observed and simulated daily accumulated precipitation (mm) in Korea from the experiment initialized in first affecting day. The most destructive day of 10 landfall TCs are plotted, respectively. All dates are based on the KST.

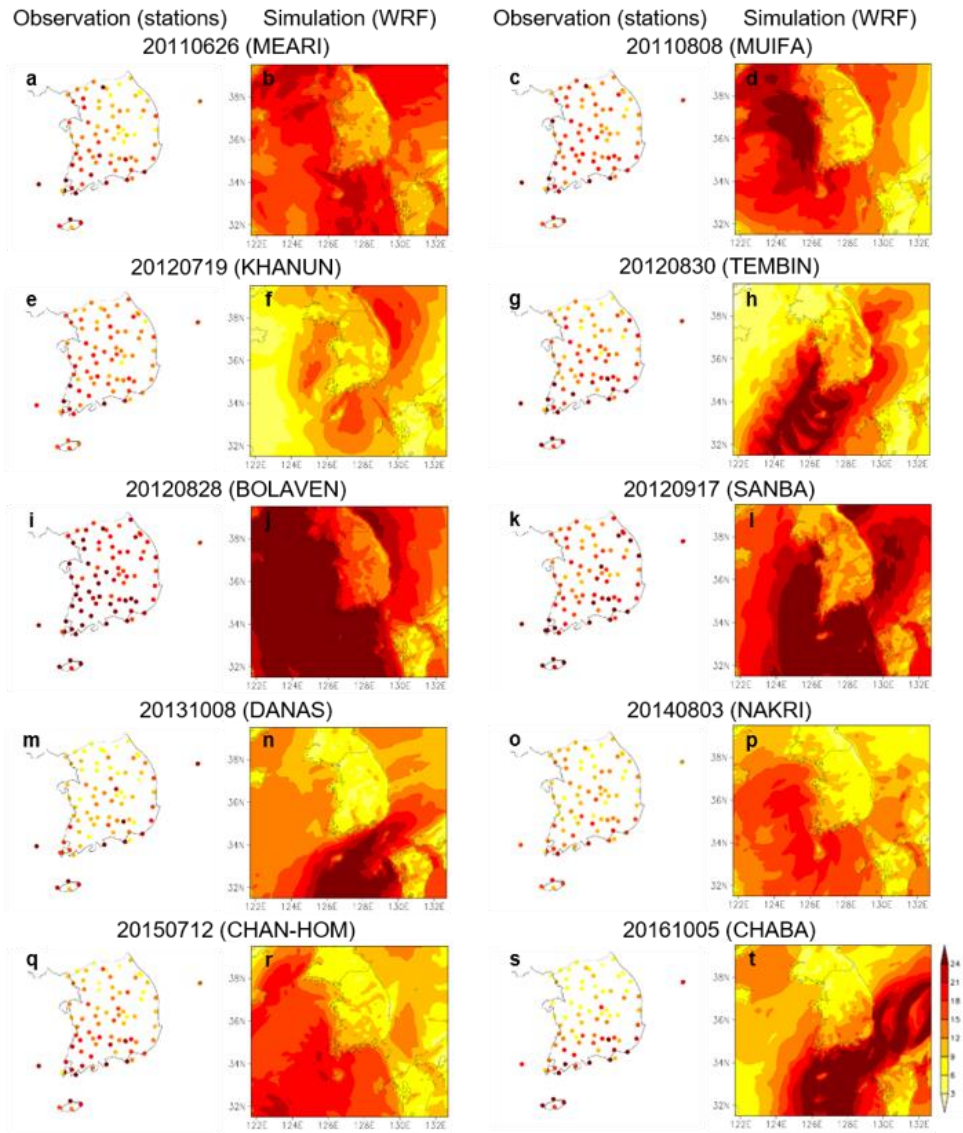

Figure 5.4. Same as Fig. 5.3 except for daily maximum surface wind speed (m s^{-1}).

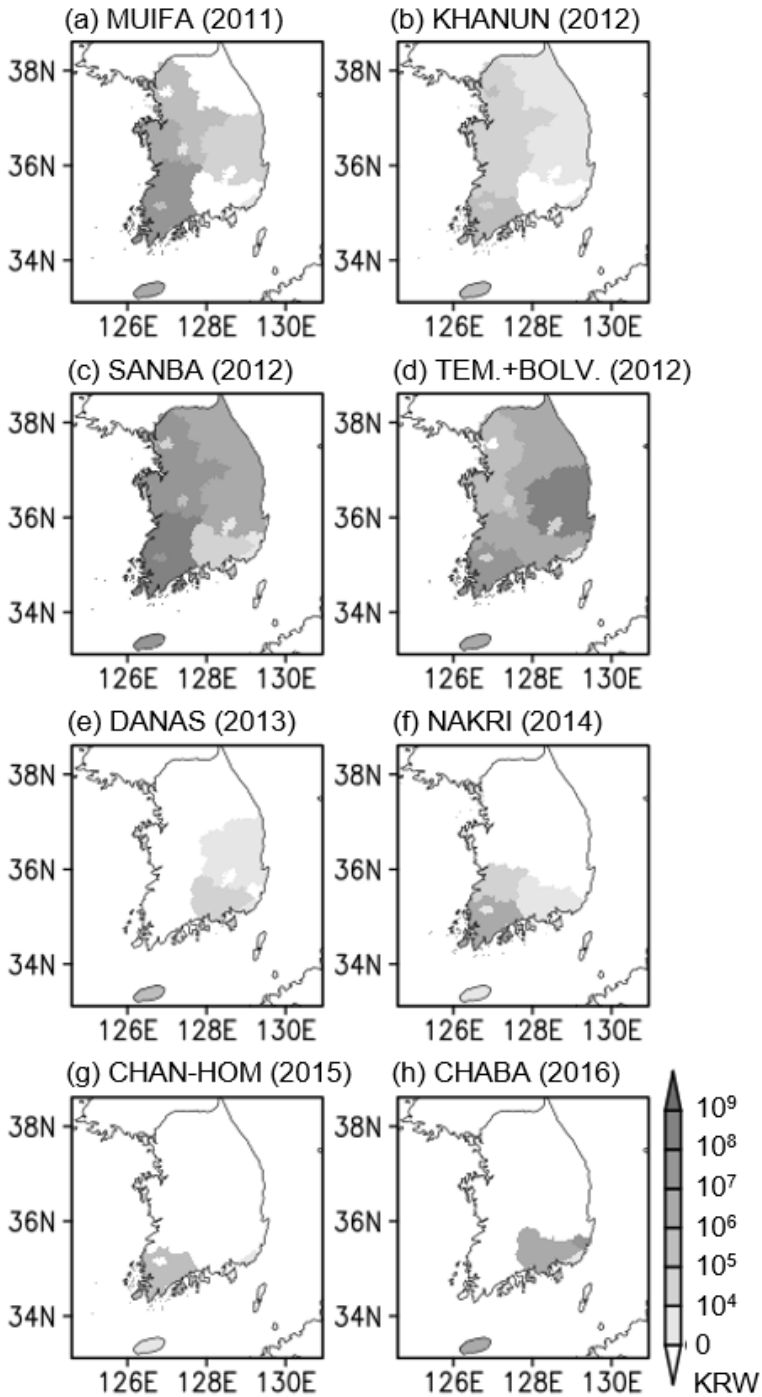

Figure 5.5. Property losses caused by recent 9 Korean landfall TCs for 16 metropolitan cities and provinces. The color scales are based on KRW.

The TC-induced precipitation and surface maximum wind speed are well simulated for all ten TC cases (Figs. 5.3 and 5.4). Among the ten landfall cases since 2011, there were several patterns of TC-induced precipitation: interaction with rain band called as Changma case (MEARI, 2011), intense precipitation near the Mt. Jiri by the topography effect case (MUIFA, 2011), more precipitation to the western and eastern part of Korean Peninsula case respectively (KHANUN, 2012; TEMBIN, 2012; DANAS, 2013; NAKRI, 2014; CHABA, 2016), and nation-wide rainfall (SANBA, 2012; CHAN-HOM, 2015). Compared to the station-based observation, the spatial distribution of daily accumulated precipitation during the most destructive landfall date are realistically predicted. Moreover, the predictions of the precipitation amounts for 79 stations are reliable enough to make use of operational forecasts. Although there are underestimations on the land by the land surface friction, overall spatial distributions of surface maximum wind speed are also reasonable to operational work. Before the TC landfall, therefore, we can estimate TC-induced extreme weather (heavy precipitation and surface wind gust) by the WRF-CFSv2 experiment.

On the basis of the annual report on disasters published by the Korean government, the damages caused by the recent nine TCs are analyzed for province level (Fig. 5.5). The annual reports on disasters aggregate the property loss by the meteorological extreme event on a case-by-case. Using the property loss datasets, we diagnose the effects of TC-induced extreme

weather (i.e., heavy precipitation and strong wind gust) to the economic damage. Based on this understanding, we hope to develop the prediction model for TC-induced property loss to raise public awareness of TC activity. If the development of TC simulation by the numerical model continues, in-depth understanding of the interaction between the TC and the surrounding environment field causing the TC-related extremes. This will enable predicting damages caused by TCs soon and will be a way for our academia to contribute to society.

6. Concluding remarks

The seasonal to near-future prediction of summertime TC activity over the WNP and NA is very important for both scientific and social-economical aspect. Understanding relationship between TC activity and climate variability of seasonal time range have been studied and development of TC activity prediction model with high predictability has long been required. As one of these efforts, we have launched the track-pattern-based model which predicts seasonal TC density over the WNP and NA. On the basis of high performance for the seasonal prediction model, we have tried to pioneer decadal prediction (up to 2030 in this thesis) of TC activity.

This model is characterized by the hybrid statistical-dynamical type model. It is based on the statistical relationship between the clustered TC number and the seasonal averaged predictors from the dynamically forecasted in NCEP CFS. The advantage of our model is that it can predict spatial patterns of the TC activity in the entire basin with minimal computational costs than using fine-resolution dynamical models, either regional or global. The prediction skills of the WNP TC prediction model for each track pattern show good performance by the leave-one-out cross validation process for hindcast with the correlation coefficient 0.71 to 0.81 (Kim et al. 2012). In particular, we examined predictability for the case of 13 named TCs formed

over the WNP in the 2010 typhoon season, representing the lowest number since 1951. The model reasonably predicts 16.4 TCs which are well below one standard deviation from the climatological mean. The model, using the NCEP CFSv1 operational ensemble forecasts, is thus considered feasible for forecasting the seasonal-total TC genesis frequency.

Regarding the end of CFSv1 operational data release, a new necessity is arisen to change the dynamic input data to new version of CFS. Ho et al. (2013) presents the procedure of the track-pattern-based model with brief technical background and rebuilding based on the CFSv2 data. After the modification, the performance of this model still good for climatological aspect (Table 2.1). Recently, in the light of this advantage, a track-pattern-based model for the WNP basin has been employed for quasi-real-time operational forecasting by the NTC of the Korea Meteorological Administration (Kim et al. 2012; Ho et al. 2013). This implementation of WNP TC prediction model to meteorological agency and satisfactory operation until now could partly dispel worries about artificial skill, argued in DelSole and Shukla (2009), of our methodology for application to real-time forecast.

Using this methodology, we also have developed a seasonal prediction model based on four TC track patterns of ASO TC activities over the NA basin and evaluated its forecasting skill for various lead months from February to July. Unlike previous studies focused on the seasonal forecast of the total

number of TCs in the NA basin, our model can also predict the basin-wide spatial distributions of TC activities in addition to the total number of TCs. Because TC-related damages are more closely related to its approach toward coastal areas or landfall rather than the total TC genesis number in the entire NA basin, this study can contribute directly to TC-impact preparedness which can significantly reduce the damages to life and property in TC-prone coastal areas.

TCs in the NA basin are objectively classified into four TC track patterns by using the FCM in which each pattern has its own unique track characteristics. The C1-pattern TCs pass along the East Coast of the US, and C2-pattern TCs develop over the Gulf of Mexico and the Caribbean Sea and remain in these areas for their entire lifetimes. C3-pattern TCs are generated in the subtropical NA, and C4-pattern TCs develop in open ocean of the equatorial–central NA. C3 TCs move to the mid-latitude NA with recurving pathways, whereas C4 TCs are confined to low-latitude regions and mainly move northwestward toward the islands in the Caribbean. After classifying the four track patterns, the prediction model for an individual pattern is constructed. Identifying the simultaneous relationships between each TC pattern and climate variables enables us to select appropriate predictors of model for each pattern. Combinations of candidate predictors (e.g., SST, VWS, VOR850, and U850) well known for affecting TC activities are determined by conducting several cross-validation tests with various sets of

candidate predictors to yield the best predictability for each pattern. A hybrid dynamical–statistical model is developed by using CFSv2 retrospective forecasts and TC frequencies in each cluster based on the Poisson regression.

To verify the performances of the forecasts initialized in six consecutive months from early February to early July, we conducted leave-one-out cross-validation for all forecasts. Validation of the TC frequency of individual clusters and the total counts in the NA basin suggests high prediction skill at the 99% confidence level regardless of forecast lead time. Our model also shows better predictability than the reforecast based on the NCEP R-2 predictors. In addition, the spatial distributions of rank-correlation for different forecast lead times are calculated to investigate predictability by regional groups. Because substantially high values of rank-correlation occur in a wide region, we can anticipate reliable regional TC activity prediction. To investigate regional TC activity more concretely, the model performance is evaluated for the three TC-vulnerable regions (i.e. R1, R2, and R3 in Fig. 3.8). Temporal variations of observed TC activities and the ensemble mean hindcasts for the three vulnerable regions confirm that the model is skillful in predicting regional TC activities. High forecast skill of our model shown in this study also supports the applicability of the hybrid model to operational seasonal TCs prediction for the NA basin in conjunction with seasonal forecast dataset from the CFSv2 as predictors.

Among the typical TCs, intense TCs are extremely dangerous weather

events than weak TCs in waterfront regions in summer and autumn. The powerful energy of intense TCs allow them make landfall on continents more often than weak TCs (Table 3.5 and 3.6). Therefore, track density predictions which are closely related to actual hazards of intense TCs, are of a special importance for disaster prevention. After checking the TC intensity distribution for various intensity intervals with respect to Saffir–Simpson hurricane wind scale, we adopted intensity criteria as category 3 for WNP and category 1 for NA for defining intense TCs.

To attempt seasonal forecasts of the tracks of intense TCs, first of all, all intense TC tracks were grouped into several representative patterns by using the fuzzy clustering method. For the WNP basin, three main clusters were identified (Fig. 3.11). These included TCs that developed over the southeastern part of the main TC genesis region that moved toward mid-latitudes through the East China Sea, those that tracked with a recurving pattern offshore Japan, and those that were active over the South China Sea and moved westward to a continent. For the NA basin, all tracks were clustered into two patterns including TCs entering the Gulf of Mexico and those moving into the mid-latitude region with recurving tracks (Fig. 3.14). Each pattern in the two basins showed statistically significant empirical relationships with large-scale environmental fields that are pertinent to the effects of climate on TC activity. Several variables such as SST distribution associated with periodic variabilities such as the ENSO and AMO; upper and

low-level zonal wind; the strength of the subtropical high; and low-level relative vorticity were analyzed by interannual correlation analysis. By inspecting the similarity between two COR distributions at the same time, seasonal averages of statistically significant grid point values in the critical regions were selected as potential predictors (Figs. 3.12 and 3.15). Second, the hybrid statistical–dynamical approach was used to develop the seasonal forecast model for each pattern based on simultaneous relationships between the intense TC activity and selected key predictors. In this step, we conducted a predictor sensitivity test iteratively to show the best performance of our model for each track pattern. Third, after model construction, the skill was objectively assessed by using the cross-validation technique for the training period of 1982–2013 and was applied for the 2014 prediction. Although the model showed limitations in simulating extreme cases such as 2005 for NA C1, 2010 for NA C2, and 2012 for WNP C1 (Figs. 3.13 and 3.16), the observational variabilities were effectively reproduced to show good statistical measurements regardless of the forecast date (Tables 3.7 and 3.8). In addition, our model was successfully applied to real-time prediction during the 2014 TC season for the total number of intense TCs for the WNP and NA basins and for track density behavior for the WNP basin (Fig. 3.17 and 3.18). Skillful predictions for the 2014 seasonal forecast experiment suggests that our model has a potential as an operational system for meteorological agencies, particularly for intense TC track density forecasts.

A number of studies focusing on typical TC track classifications for the two basins have shown that the optimal number of the patterns for WNP and NA TC tracks are seven and four, respectively (Camargo et al. 2007b, Kossin et al. 2010, Kim et al. 2012, Choi et al. 2016a). In this thesis, however, the classifications of intense TC tracks were three clusters for the WNP and two for the NA due to the strengthening intensity criteria. If we assume that the representative patterns of TC tracks from clustering analysis are static despite various clustering analysis methods and target periods, as discussed in previous studies, we can conclude that intense TC activities have their own characteristics that differ from those of general TCs. Therefore, a comparison of intense TC activity against the all TC track patterns is worthy of discussion. The intense TCs of WNP C1 were combined with C2 and C3 in Kim et al. (2012). It is estimated that the WNP C2 and C3 in this study are assembled by C4–C5 and C6–C7 of Kim et al. (2012), respectively. Similarly, the intense TC pattern of NA C1 is combination of C2 and C4 for total TC clustering results shown in previous work (Choi et al. 2016a). Moreover, the NA intense C2 TCs include C1 and C3 of the total TC groups. Because intense TCs generally have extended lifespans over ordinary TCs because their huge amounts of energy allow them to maintain their structures longer, it appears that the established two TC tracks were combined into one pattern in this study. The mixed effects of climate variabilities on intense TC activities can be more clearly divided than typical TCs because of strengthening criteria of

statistical sampling. Therefore, intense TC activity shows stronger empirical relationships with large-scale environments than typical TCs. This aspect contributes to the possibility of faithful model development.

This thesis provides bridgehead of an attempt at intense TC activity prediction by using our model for the two major basins in the Northern Hemisphere. We hope that our model widens new point of view and possibility for TC intensity prediction. From our model operation, the coastal nations will be provided a specified service for forecasting intense TC activities as well as whole TCs, which is important information for disaster prevention. It is expected that further researches will be performed continuously to provide even better insight into TC intensity prediction.

Prediction using a track-pattern-based model suggests that TC activities over the NA will decrease in the near future. As we mentioned above, this model is known to effectively simulate TC activities in the current climate (Choi et al. 2016a) and thus is expected to be useful for near-future TC prediction in conjunction with climate-model-projected atmospheric and oceanic fields. Changes in two dominant climate variabilities, the NASST and ENSO, in the upcoming decade are mainly related to the suppression of NA TC activities. The phase transition of NASST from positive to neutral and the greater frequency of El Niño events will work together to decrease SST for the overall NA basin and to strengthen VWS in the tropical NA. The impacts of changes for NASST and ENSO will make unfavorable environments for

TC developments for tropical regions in the near future. Considering the CMIP5 multi-model SST predictions, anthropogenic forcing causes SST warming over both the NA and eastern Pacific. This discrepancy suggests that strong natural variability is a key factor to the NASST cooling and to suppress the NA TC activities in the near future in combination with more frequent El Niño events.

The long-term prediction of TC activity should be more developed to reduce the socio-economic TC-induced damages. Only skillful long-term TC prediction can guarantee the safety of us during the summertime natural disasters. In addition to the hybrid statistical–dynamical prediction method presented in this thesis, we expect the improve the performance of high-resolution dynamic model through development of parametrization and many kind of TC simulating technique in the future. We should continue to study until we can predict all kinds of the future TC activity.

References

Bell, G. D., S. Goldenberg, E. Blake, C. Landsea, J. Schemm, R. Pasch, and T. Kimberlain, 2012: The 2011 North Atlantic hurricane season: A climate perspective. *State of the Climate in 2011*. Blunden J, Arndt DS, Eds. *Bulletin of the American Meteorological Society*, **93**, S99–S105.

Bengtsson, L., K. I. Hodges, M. Esch, N. Keenlyside, L. Kornblueh, J. –J. Luo, and T. Yamagata, 2007: How may tropical cyclones change in a warmer climate? *Tellus*, **59A**, 539–561.

Bensaid, A. M., L. O. Hall, J. C. Bezdek, L. P. Clarke, M. L. Silbiger, J. A. Arrington, and R. F. Murtagh, 1996: Validity-guided (re)clustering with applications to image segmentation. *IEEE Transactions on Fuzzy Systems*, **4**, 112–123.

Bezdek, J. C., 1981: *Pattern recognition with fuzzy objective function algorithms*. Kluwer Academic, 256 pp.

Blake, E. S., and W. M. Gray, 2004: Prediction of August Atlantic basin hurricane activity. *Weather and Forecasting*, **19**, 1044–1060.

Camargo, S. J., M. Ballester, A. G. Barnston, P. Koltzbach, P. Roundy, M. A. Saunders, F. Vitart, and M. C. Wheeler, 2006: Short-term climate (seasonal and intra-seasonal) prediction of tropical cyclone activity and intensity. Proc. Sixth Int., Workshop on Tropical Cyclones (IWTC-VI), San José, Costa Rica, WMO, TMRP 72, 493–499.

Camargo, S. J., A. G. Barnston, P. Klotzbach, and C. W. Landsea, 2007a: Seasonal tropical cyclone forecasts. *Bulletin of the World Meteorolocial Organization*, **56**, 297–309.

Camargo, S. J., A. W. Robertson, S. J. Gaffney, P. Smyth, and M. Ghil, 2007b: Cluster analysis of typhoon tracks. Part I: General properties. *Journal of Climate*, **20**, 3635–3653.

Camargo, S. J., and A. G. Barnston, 2009: Experimental Dynamical Seasonal Forecasts of Tropical Cyclone Activity at IRI. *Weather and Forecasting*, **24**, 472–491.

Camp, J., M. Roberts, C. MacLachlan, E. Wallace, L. Hermanson, A. Brookshaw, A. Arribas, and A. A. Scaife, 2015: Seasonal forecasting of tropical storms using the Met Office GloSea5 seasonal forecast system. *Quarterly Journal of the Royal Meteorological Society*, **141**, 2206–2219.

Cha, D.-H., C.-S. Jin, D.-K. Lee, and Y.-H. Kuo, 2011: Impact of intermittent spectral nudging on regional climate simulation using Weather Research and Forecasting model, *Journal of Geophysical Research*, **116**, D10103.

Chan, J. C. L., J.-E. Shi, and C.-M. Lam, 1998: Seasonal forecasting of tropical cyclone activity over the western North Pacific and the South China Sea. *Weather and Forecasting*, **13**, 997–1004.

Chan, J. C. L., J.-E. Shi, and K. S. Liu, 2001: Improvements in the seasonal forecasting of tropical cyclone activity over the western North Pacific. *Weather and Forecasting*, **16**, 491–498.

Chan, J. C. L., 2007: Interannual variations of intense typhoon activity. *Tellus*, **59A**, 455–460.

Chen, F., and J. Dudhia, 2001: Coupling an advanced land surface–hydrology model with the Penn State–NCAR MM5 modeling system. Part I: Model description and implementation. *Monthly Weather Review*, **129**, 569–585.

Chen, J.-H., and S.-J., Lin, 2011: The remarkable predictability of inter-annual variability of Atlantic hurricanes during the past decade. *Geophysical Research Letters*, **38**, L11804.

Choi, W., C.-H. Ho, J. Kim, H.-S. Kim, S. Feng, and K. Kang, 2016a: A track-pattern-based seasonal prediction of tropical cyclone activity over the North Atlantic. *Journal of Climate*, **29**, 481–494.

Choi, W., C.-H. Ho, C.-S. Jin, J. Kim, S. Feng, D.-S. R. Park, and J.-K. E. Schemm, 2016b: Seasonal forecasting of intense tropical cyclones over the North Atlantic and the western North Pacific basins. *Climate Dynamics*, **47**, 3063–3075.

Chu, P.-S., 2002: Large-scale circulation features associated with decadal variations of tropical cyclone activity over the central North Pacific. *Journal of Climate*, **15**, 2678–2689.

Chu, P.-S., and X. Zhao, 2007: A Bayesian regression approach for predicting seasonal tropical cyclone activity over the central North Pacific. *Journal of Climate*, **20**, 4002–4013.

Chu, P.-S., X. Zhao, C.-T. Lee, and M.-M. Lu, 2007: Climate prediction of tropical cyclone activity in the vicinity of Taiwan using the multivariate least absolute deviation regression method. *Terrestrial, Atmospheric and Oceanic Sciences*, **18**, 805–825.

Chu, P.-S., X. Zhao, C. Ho, H.-S. Kim, M.-M. Lu, and J.-H. Kim, 2010: Bayesian forecasting of seasonal typhoon activity: A track-oriented-pattern categorization approach. *Journal of Climate*, **23**, 6654–6668.

Chu, P.-S., and X. Zhao, 2011: Bayesian analysis for extreme climatic events: A review. *Atmospheric Research*, **102**, 243–262.

Chung, P.-H., C.-H. Sui, and T. Li, 2011: Interannual relationships between the tropical sea surface temperature and summertime subtropical anticyclone over the western North Pacific. *Journal of Geophysical Research*, **116**, D13111.

Colbert, A. J., and B. J. Soden, 2012: Climatological variations in North Atlantic tropical cyclone tracks. *Journal of Climate*, **25**, 657–673.

Collins, W. D., P. J. Rasch, B. A. Boville, J. J. Hack, J. R. McCaa, D. L. Williamson, J. T. Kiehl, B. Briegleb, C. Bitz, S.-J. Lin, M. Zhang, and Y. Dai, 2004: Description of the NCAR Community Atmosphere Model (CAM 3.0), *NCAR Tech. Note. NCAR Tech*, 226 pp.

Davis, C. E., J. E. Hyde, S. I. Bangdiwala, and J. J. Nelson, 1986: An example of dependencies among variables in a conditional logistic regression. *Modern Statistical Methods in Chronic Disease Epidemiology*, Eds. S. H.

Moolgavkar and R. L. Prentice, pp. 140–147, Wiley, New York.

Davis, C., W. Wang, S. S. Chen, Y. Chen, K. Corbosiero, M. DeMaria, J. Dudhia, G. Holland, J. Klemp, J. Michalakes, H. Reeves, R. Rotunno, C. Snyder, and Q. Xiao, 2008: Prediction of landfalling hurricanes with the advanced hurricane WRF Model. *Monthly Weather Review*, **136**, 1990–2005.

Davis, K., X. Zeng, and E. A. Ritchie, 2015: A new statistical model for predicting seasonal North Atlantic hurricane activity. *Weather and Forecasting*, **30**, 730–741.

DelSole T., and J. Shukla, 2009: Artificial skill due to predictor screening. *Journal of Climate*, **22**, 331–345.

Du, Y., L. Yang, and S.-P. Xie, 2011: Tropical Indian Ocean influence on northwest Pacific tropical cyclones in summer following strong El Niño. *Journal of Climate*, **24**, 315–322.

Dunn, J. C., 1973: A fuzzy relative of the ISODATA process and its use in detecting compact well-separated clusters. *Cybernetics and Systems*, **3**, 32–57.

Elsner, J. B., and C. P. Schmertmann, 1993: Improving extended-range seasonal predictions of intense Atlantic hurricane activity. *Weather and Forecasting*, **8**, 345–351.

Elsner, J. B., and C. P. Schmertmann, 1994: Assessing forecast skill through cross validation. *Weather and Forecasting*, **9**, 619–624.

Elsner, J. B., 2003: Tracking hurricanes. *Bulletin of the American Meteorological Society*, **84**, 353–356.

Elsner, J. B., and T. H. Jagger, 2006: Prediction models for annual U.S. hurricane counts. *Journal of Climate*, **19**, 2935–2952.

Emanuel, K., R. Sundararajan, and J. Williams, 2008: Hurricanes and global warming: results from downscaling IPCC AR4 simulations. *Bulletin of the American Meteorological Society*, **89**, 347–367.

Emanuel, K. A., 2013: Downscaling CMIP5 climate models shows increased tropical cyclone activity over the 21st century. *Proceedings of the National Academy of Sciences*, **110**, 12219–12224.

Fengjin, X., and X. Ziniu, 2010: Characteristics of tropical cyclones in China and their impacts analysis. *Nature Hazards*, **54**, 827–837.

Fierro, A. O., R. F. Rogers, and F. D. Marks, 2009: The impact of horizontal grid spacing on the microphysical and kinematic structures of strong tropical cyclones simulated with the WRF-ARW Model. *Monthly Weather Review*, **137**, 3717–3743.

Frank W. M., and G. S. Young, 2007: The interannual variability of tropical cyclones. *Monthly Weather Review*, **135**, 3587–3598.

Gentry, M. S., and G. M. Lackmann, 2010: Sensitivity of simulated tropical cyclone structure and intensity to horizontal resolution. *Monthly Weather Review*, **138**, 688–704.

Goldenberg S. B., C. W. Landsea, A. M. Mestas-Nunez, and W. M. Gray, 2001:

The recent increase in Atlantic hurricane activity: Causes and implications. *Science*, **293**, 474–479.

Goldenberg, S. B., and L. J. Shapiro, 1996: Physical mechanisms for the association of El Niño and West African rainfall with Atlantic major hurricane activity, *Journal of Climate*, **9**, 1169–1187.

Gerrity, J. P. Jr., 1992: A note on Gandin and Murphy's equitable skill score. *Monthly Weather Review*, **120**, 2709–2712.

Gray, W. M., 1968: Global view of the origin of tropical disturbances and storms. *Monthly Weather Review*, **96**, 669–700.

Gray, W.M., 1984a: Atlantic seasonal hurricane frequency. Part I: El Niño and 30 mb quasi-biennial oscillation influences. *Monthly Weather Review*, **112**, 1649–1668.

Gray, W.M., 1984b: Atlantic seasonal hurricane frequency. Part II: Forecasting its variability. *Monthly Weather Review,* **112**, 1669–1683.

Gray, W. M., C. W. Landsea, P. W. Mielke, and K. J. Berry, 1992: Predicting Atlantic seasonal hurricane activity 6–11 months in advance. *Weather and Forecasting*, **7**, 440–455.

Gray, W. M., 1998: The formation of tropical cyclones, *Meteorology and Atmospheric Physics*, **67**, 37–69.

Hall, T. M., and S. Jewson, 2007: Statistical modeling of North Atlantic tropical cyclone tracks. *Tellus*, **59A**, 486–498.

Hall, T. M., and S. Jewson, 2008: Comparison of local and basinwide methods

for risk assessment of cyclone landfall. *Journal of Applied Meteorology and Climatology*, **47**, 361–367.

Hermanson, L., R. Eade, N. H. Robinson, N. J. Dunstone, M. B. Andrews, J. R. Knight, A. A. Scaife, and D. M. Smith, 2014: Forecast cooling of the Atlantic subpolar gyre and associated impacts. *Geophysical Research Letter,* **41**, 5167–5174.

Hess, J. C., J. B. Elsner, and N. E. LaSeur, 1995: Improving seasonal hurricane predictions for the Atlantic basin. *Weather and Forecasting*, **10**, 425–432.

Ho, C.-H., H.-S. Kim, J.-H. Jeong, and S.-W. Son, 2009: Influence of stratospheric quasi-biennial oscillation on tropical cyclone tracks in the western North Pacific. *Geophysical Research Letter,* **36**, L06702.

Ho, C.-H., J.-H. Kim, H.-S. Kim, W. Choi, M.-H. Lee, H.-D. Yoo, T.-R. Kim, and S. Park, 2013: Technical note on a track-pattern-based model for predicting seasonal tropical activity over the western North Pacific. *Advances in Atmospheric Sciences*, **30**, 1260–1274.

Holland, G. J., and R. T. Merrill, 1984: On the dynamics of tropical cyclone structural changes, *Quarterly Journal of the Royal Meteorological Society*, **110**, 723–745.

Holland, G. J., and P. J. Webster, 2007: Heightened tropical cyclone activity in the North Atlantic: Natural variability or climate trend? *Philosophical Transactions of the Royal Society of London*, **365A**, 2695–2716.

Hong, S.-Y., J. Dudhia, and S.-H. Chen, 2004: A revised approach to ice microphysical processes for bulk parameterization of cloud and precipitation. *Monthly Weather Review*, **132**, 103–120.

Hong, S.-Y., Y. Noh, and J. Dudhia, 2006: A New Vertical Diffusion Package with an Explicit Treatment of Entrainment Processes, *Monthly Weather Review*, **134**, 2318–2341.

Jin, C.-S., C.-H. Ho, J.-H. Kim, D.-K. Lee, D.-H. Cha, and S.-W. Yeh, 2013: Critical role of northern off-equatorial sea surface temperature forcing associated with central Pacific El Niño in more frequent tropical cyclone movements toward East Asia. *Journal of Climate*, **26**, 2534–2545.

John, V. O., and B. J. Soden, 2007: Temperature and humidity biases in global climate models and their impact on climate feedbacks, *Geophysical Research Letters*, **34**, L18704.

Kain, J. S., 2004: The Kain-Fritsch convective parameterization: An update, *Journal of Applied Meteorology and Climatology*, **43**, 170–181.

Kanamitsu, M., W. Ebisuzaki, J. Woollen, S-K Yang, J.J. Hnilo, M. Fiorino, and G. L. Potter, 2002: NCEP–DOE AMIP-II Reanalysis (R-2). *Bulletin of the American Meteorological Society*, **83**, 1631−1643.

Kim, D., C.-S. Jin, C.-H. Ho, J. Kim, and J.-H. Kim, 2015: Climatological features of WRF-simulated tropical cyclones over the western North Pacific. *Climate Dynamics*, **44**, 3223–3235.

Kim, H.-M., and P. J. Webster, 2010: Extended-range seasonal hurricane

forecasts for the North Atlantic with a hybrid dynamical-statistical model. *Geophysical Research Letter*, **37**, L21705.

Kim, H.-M, M.-I. Lee, P. J. Webster, D. Kim, and J. H. Yoo, 2013: A Physical Basis for the Probabilistic Prediction of the Accumulated Tropical Cyclone Kinetic Energy in the Western North Pacific. *Journal of Climate*, **26**, 7981–7991.

Kim, H.-S., C.-H. Ho, P.-S. Chu, and J.-H. Kim, 2010: Seasonal prediction of summertime tropical cyclone activity over the East China Sea using the least absolute deviation regression and the Poisson regression. *International Journal of Climatology*, **30**, 210–219.

Kim, H.-S., J.-H. Kim, C.-H. Ho, and P.-S. Chu, 2011: Pattern classification of typhoon tracks using the fuzzy c-means clustering method. *Journal of Climate*, **24**, 488–508.

Kim, H.-S., C.-H. Ho, J.-H. Kim, and P.-S. Chu, 2012: Track-pattern-based model for predicting seasonal tropical cyclone activity in the western North Pacific. *Journal of Climate*, **25**, 4660–4678.

Kim, J.-H., C.-H. Ho, and C.-H. Sui, 2005a: Circulation features associated with the record-breaking typhoon landfall on Japan in 2004. *Geophysical Research Letters*, **32**, L14713.

Kim, J.-H., C.-H. Ho, C.-H. Sui, and S. K. Park, 2005b: Dipole structure of interannual variations in summertime tropical cyclone activity over East Asia. *Journal of Climate*, **18**, 5344–5356.

Kim, J.-H., C.-H. Ho, M.-H. Lee, J.-H. Jeong, and D. Chen, 2006: Large increase in heavy rainfall associated with tropical cyclone landfalls in Korea after the late 1970s. *Geophysical Research Letters*, **33**, L18706.

Kim, J.-H., C.-H. Ho, H.-S. Kim, and W. Choi, 2012: 2010 Western North Pacific typhoon season: Seasonal overview and forecast using a track-pattern-based model. *Weather and Forecasting*, **27**, 730–743.

Klotzbach, P. J., 2007: Recent developments in statistical prediction of seasonal Atlantic basin tropical cyclone activity. *Tellus*, **59A**, 511–518.

Klotzbach, P. J., 2010: On the Madden–Julian Oscillation–Atlantic hurricane relationship. *Journal of Climate*, **23**, 282–293.

Knutson T. R., J. J. Sirutis, S. T. Garner, I. M. Held, and R. E. Tuleya, 2007: Simulation of the recent multidecadal increase of Atlantic hurricane activity using an 18-km-grid regional model. *Bulletin of the American Meteorological Society,* **88**, 1549–1565.

Knutson, T. R., J. L. McBride, J. Chan, K. Emanuel, G. Holland, C. Landsea, I. Held, J. P. Kossin, A. K. Srivastava, and M. Sugi, 2010: Tropical cyclones and climate change. *Nature Geoscience*, **3**, 157–163.

Knutson, T. R., J. J. Sirutis, M. Zhao, R.E. Tuleya, M.Bender, G.A. Vecchi, G. Villarini, and D. Chavas, 2015: Global projections of intense tropical cyclone activity for the late twenty-first century from dynamical downscaling of CMIP5/RCP4.5 scenarios. *Journal of Climate*, **28**, 7203–7224.

Kossin, J. P., K. R. Knapp, D. J. Vimont, R. J. Murnane, and B. A. Harper, 2007: A globally consistent reanalysis of hurricane variability and trends. *Geophysical Research Letters*, **34**, L04815.

Kossin, J. P., S. J. Camargo, and M. Sitkowski, 2010: Climate modulation of North Atlantic hurricane tracks. *Journal of Climate*, **23**, 3057–3076.

Kozar, M. E., M. E. Mann, S. J. Camargo, J. P. Kossin, and J. L. Evans, 2012: Stratified statistical models of North Atlantic basin-wide and regional tropical cyclone counts. *Journal of Geophysical Research*, **117**, D18103.

Krishnamurthy, L., G. A. Vecchi, R. Msadek, H. Murakami, A. Wittenberg, and F. Zeng, 2016: Impact of strong ENSO on regional tropical cyclone activity in a high-resolution climate model in the North Pacific and North Atlantic Oceans. *Journal of Climate*, **29**, 2375–2394.

Kwon, H. J., W.-J. Lee, S.-H. Won, and E.-J. Cha, 2007: Statistical ensemble prediction of the tropical cyclone activity over the western North Pacific. *Geophysical Research Letters*, **34**, L24805.

LaRow, T. E., L. Stefanova, D.-W. Shin, and S. Cocke, 2010: Seasonal Atlantic tropical cyclone hindcasting/forecasting using two sea surface temperature datasets, *Geophysical Research Letters*, **37**, L02804.

Lehmiller, G. S., T. B. Kimberlain, and J. B. Elsner, 1997: Seasonal prediction models for North Atlantic basin hurricane location. *Monthly Weather Review*, **125**, 1780–1791.

Li, X., S. Yang, H. Wang, X. Jia, and A. Kumar, 2013: A dynamical-statistical

forecast model for the annual frequency of western Pacific tropical cyclones based on the NCEP Climate Forecast System version 2. *Journal of Geophysical Research*, **118**, 12,061–12,074.

Liu, K. S., and J. C. L. Chan, 2008: Interdecadal Variability of Western North Pacific Tropical Cyclone Tracks. *Journal of Climate*, **21**, 4464–4476.

Manganello, J. V., K. I. hodges, J. L. Kinter, B. A. Cash, L. Marx, T. Jung, D. Achuthavarier, J. M. Adams, E. L. Altshuler, B. Huang, E. K. Jin, C. Stan, P. Towers, and N. Wedi, 2012: Tropical cyclone climatology in a 10-km global atmospheric GCM: Toward weather-resolving climate modeling. *Journal of Climate*, **25**, 3867–3893.

McAdie, C. J., C. W. Landsea, C. J. Neumann, J. E. David, E. Blake, and G. R. Hammer, 2009: *Tropical cyclones of the North Atlantic Ocean, 1851–2006*. National Climatic Data Center/TCP/National Hurricane Center. Historical Climatology Series 6-2, 238 pp.

Meehl, G. A., L. Goddard, J. Murphy, R. J. Stouffer, G. Boer, G. Danabasoglu, K. Dixon, M. A. Giorgetta, A. M. Greene, E. Hawkins, G. Hegerl, D. Karoly, N. Keenlyside, M. Kimoto, B. Kirtman, A. Navarra, R. Pulwarty, D. Smith, D. Stammer, and T. Stockdale, 2009: Decadal prediction: Can it be skillful? *Bulletin of the American Meteorological Society*, **90**, 1467–1485.

Meehl, G. A., L. Goddard, G. Bore, R. Burgman, G. Branstator, C. Cassou, S. Corti, G. Danabasoglu, F. Doblas-Reyes, E. Hawkins, A. Karspeck, M.

Kimoto, A. Kumar, D. Matei, J. Mignot, R. Msadek, A. Navarra, H. Pohlmann, M. Rienecker, T. Rosati, E. Schneider, D. Smith, R. Sutton, H. Teng, G. J. v. Oldenborgh, G. Vecchi, and S. Yeager, 2014: Decadal climate prediction: An update from the trenches. *Bulletin of the American Meteorological Society*, **95**, 243–267.

Murakami. H., R. Mizuta, and E. Shindo, 2012: Future changes in tropical cyclone activity projected by multi-physics and multi-SST ensemble experiments using the 60-km-mesh MRI-AGCM. *Climate Dynamics*, **39**, 2569–2584.

Murakami. H., B. Wang, T. Li, and A. Kitoh, 2013: Projected increase in tropical cyclones near Hawaii. *Nature Climate Change*, **3**, 749–754.

Nakamura, J., U. Lall, Y. Kushnir, and S. J. Camargo, 2009: Classifying North Atlantic tropical cyclone tracks by mass moments. *Journal of Climate*, **22**, 5481–5494.

Nicholls, N., 1979: A possible method for predicting seasonal tropical cyclone activity in the Australian region. *Monthly Weather Review*, **107**, 1221–1224.

O'Brien, R. M., 2007: A caution regarding rules of thumb for variance inflation factors. *Quality & Quantity*, **41**, 673–690.

Oouchi, K., J. Yoshimura, H. Yoshimura, R. Mizuta, S. Kusunoki, and A. Noda, 2006: Tropical cyclone climatology in a global warming climate as simulated in a 20 km-mesh global atmospheric model: Frequency and

wind intensity analyses. *Journal of the Meteorological Society of Japan*, **84**, 259–276.

Park, D.-S. R., C.-H. Ho, C. C. Nam, and H.-S. Kim, 2015: Evidence of reduced vulnerability to tropical cyclones in the Republic of Korea. *Environmental Research Letters*, **10**, 054003.

Park, D.-S. R., C.-H. Ho, J. C. L. Chan, K.-J. Ha, H.-S. Kim, J. Kim, and J.-H. Kim, 2017: Asymmetric response of tropical cyclone activity to global warming over the North Atlantic and the western North Pacific from CMIP5 model projections. *Scientific Reports*, **7**, 41354.

Pielke, R. A., Jr., and C. W. Landsea, 1998: Normalized hurricane damages in the United States: 1925–95. *Weather and Forecasting*, **13**, 621–631.

Pielke, R. A., Jr., J. Gratz, C. W. Landsea, D. Collins,M. A. Saunders, and R. Musulin, 2008: Normalized hurricane damage in the United States: 1900–2005. *Natural Hazards Review*, **9**, 29–42.

Potty J., S. M. Oo, P. V. S. Raju, and U. C. Mohanty, 2012: Performance of nested WRF model in typhoon simulations over West Pacific and South China Sea. *Natural Hazards*, **63**, 1451–1470.

Rodgers, E. B., S. W. Chang, J. Stout, J. Steranka, and J. J. Shi, 1991: Satellite observations of variations in tropical cyclone convection caused by upper-tropospheric troughs. *Journal of Applied Meteorology and Climatology,* **30**, 1163– 1184.

Saha S., S. Moorthi, H.-L. Pan, X. Wu, J. Wang, S. Nadiga, P. Tripp, R. Kistler,

J. Woollen, D. Behringer, H. Liu, D. Stokes, R. Grumbine, G. Gayno, J. Wang, Y.-T. Hou, H.-Y. Chuang, H.-M. H. Juang, J. Sela, M. Iredell, R. Treadon, D. Kleist, P. V. Delst, D. Keyser, J. Derber, M. Ek, J. Meng, H. Wei, R. Yang, S. Lord, H. V. D. Dool, A. Kumar, W. Wang, C. Long, M. Chelliah, Y. Xue, B. Huang, J.-K. Schemm, W. Ebisuzaki, R. Lin, P. Xie, M. Chen, S. Zhou, W. Higgins, C.-Z. Zou, Q. Liu, Y. Chen, Y. Han, L. Cucurull, R. W. Reynolds, G. Rutledge, and M. Goldberg, 2010: The NCEP climate forecast system reanalysis. *Bulletin of the American Meteorological Society*, **91**, 1015–1057.

Saha S, S. Moorthi, X. Wu, J. Wang, S. Nadiga, P. Tripp, D. Behringer, Y.-T. Hou, H.-Y. Chuang, M. Iredell, M. Ek, J. Meng, R. Yang, M. P. Mendez, H. van den Dool, Q. Zhang, W. Wang, M. Chen, and E. Becker, 2014: The NCEP climate forecast system version 2. *Journal of Climate*, **27**, 2185–2208.

Saha, S., S. Nadiga, C. Thiaw, J. Wang, W. Wang, Q. Zhang, H. M. Van den Dool, H.-L. Pan, S. Moorthi, D. Beheringer, D. Stokes, M. Peña, S. Lord, G. White, W. Ebisuzaki, P. Peng, and P. Xie, 2006: The NCEP Climate Forecast System. *Journal of Climate*, **19**, 3483–3517.

Saunders, M. A., and A. S. Lea, 2005: Seasonal prediction of hurricane activity reaching the coast of the United States. *Nature*, **434**, 1005–1008.

Shi, J. J., S. Chang, and S. Raman, 1997: Interaction between hurricane Florence (1988) and an upper-tropospheric westerly trough, *Journal of*

the Atmospheric Sciences, **54**, 1231– 1247.

Skamarock, W. C., J. B. Klemp, J. Dudhia, D. O. Gill, D. M. Barker, M. G Duda, X.-Y. Huang, W. Wang, and J. G. Powers, 2008: A Description of the Advanced Research WRF Version 3. *NCAR Tech. Note NCAR/TN-475+STR*, 113 pp.

Smith, A. B., and R. W. Katz, 2013: US billion-dollar weather and climate disasters: Data sources, trends, accuracy and biases, *Natural hazards*, **67**, 387–410.

Smith, T. M., R. W. Reynolds, T. C. Peterson, and J. Lawrimore, 2008: Improvements to NOAA's Historical Merged Land–Ocean Surface Temperature Analysis (1880–2006). *Journal of Climate*, **21**, 2283–2296.

Sobel, A. H., and C. S. Bretherton, 1999: Development of synoptic-scale disturbances over the summertime tropical northwest Pacific. *Journal of Atmospheric Sciences*, **56**, 3106–3127.

Stowasser M., Y. Wang, and K. Hamilton, 2007: Tropical cyclone changes in the western North Pacific in a global warming scenario. *Journal of Climate*, **20**, 2378–2396.

Sui, C.-H., P.-H. Chung, and T. Li, 2007: Interannual and interdecadal variability of the summertime western North Pacific subtropical high. *Geophysical Research Letter*, **34**, L11701.

Taylor, K. E., R. J. Stouffer, and G. A. Meehl, 2012: An overview of CMIP5 and the experiment design. *Bull. Amer. Meteor. Soc.* **93**, 485–498.

Teng, H., and B. Wang, 2003: Interannual variations of the boreal summer intraseasonal oscillation in the Asian–Pacific region. *Journal of Climate*, **16**, 3572–3584.

Tu, J.-Y., C. Chou, and P.-S. Chu, 2009: The abrupt shift of typhoon activity in the vicinity of Taiwan and its association with western North Pacific–East Asian climate change. *Journal of Climate*, **22**, 3617–3628.

Vecchi, G. A., and B. J. Soden, 2007: Global warming and the weakening of the tropical circulation. *Journal of Climate*, **20**, 4316–4340.

Vecchi, G.A., M. Zhao, H. Wang, G. Villarini, A. Rosati, A. Kumar, I. M. Held, and R. Gudgel, 2011: Statistical–dynamical predictions of seasonal North Atlantic hurricane activity. *Monthly Weather Review*, **139**, 1070–1082.

Vecchi, G. A., T. Delworth, R. Gudgel, S. Kapnick, A. Rosati, A. T. Wittenberg, F. Zeng, W. Anderson, V. Balaji, K. Dixon, L. Jia, H.-S. Kim, L. Krishnamurthy, R. Msadek, W. F. Stern, S. D. Underwood, G. Villarini, X. Yang, and S. Zhang, 2014: On the seasonal forecasting of regional tropical cyclone activity. *Journal of Climate*, **27**, 7994–8016.

Villarini, G., G. A. Vecchi, T. R. Knutson, and J. A. Smith, 2011: Is the recorded increase in short-duration North Atlantic tropical storms spurious? *Journal of Geophysical Research,* **116**, D10114.

Vimont, D. J., and J. P. Kossin, 2007: The Atlantic meridional mode and hurricane activity. *Geophysical Research Letters*, **34**, L07709,

doi:10.1029/2007GL029683.

Wang, B., and J. C. L. Chan, 2002: How strong ENSO events affect tropical storm activity over the Western North Pacific. *Journal of Climate*, **15**, 1643−1658.

Wang, H., J.-K. E. Schemm, A. Kumar, W. Wang, L. Long, M. Chelliah, G. D. Bell, and P. Peng, 2009: A statistical forecast model for Atlantic seasonal hurricane activity based on the NCEP dynamical seasonal forecast. *Journal of Climate,* **22**, 4481–4500.

Weinkle J., R. Maue, and R. A. Pielke Jr., 2012: Historical global tropical cyclone landfalls. *Journal of Climate*, **25**, 4729–4735.

Wilks, D.S., 2006: *Statistical methods in the atmospheric science.* 2nd Ed., Academic Press, 627 pp.

World Meteorological Organization, 2002: *Standardized verification system for long-range forecasts, New attachment II-9 to the manual on the GDPFS*. World Meteorological Organization Rep. WMO-No. 485, 22 pp.

Wu, B, T. Li, and T. Zhou, 2010: Relative contributions of the Indian Ocean and local SST anomalies to the maintenance of the western North Pacific anomalous anticyclone during the El Niño decaying summer. *Journal of Climate*, **23**, 2974–2986.

Wu, L., Z. Wen, R. Huang, and R. Wu, 2012: Possible Linkage between the Monsoon Trough Variability and the Tropical Cyclone Activity over the Western North Pacific. *Monthly Weather Review,* **140**, 140–150.

Xie, L., T. Yan, L. J. Pietrafesa, J. M. Morrison, and T. Karl, 2005: Climatology and interannual variability of North Atlantic hurricane tracks. *Journal of Climate*, **18**, 5370– 5381.

Xie, S.-P., K. Hu, J. Hafner, H. Tokinaga, Y. Du, G. Huang, and T. Sampe, 2009: Indian Ocean capacitor effect on Indo–Western Pacific climate during the summer following El Niño. *Journal of Climate*, **22**, 730–747.

Xie, X. L., and G. A. Beni, 1991: Validity measure for fuzzy clustering. *IEEE Transactions on Pattern Analysis and Machine Intelligence*, **3**, 841–846.

Zhao, M., I. M. Held, and G.A. Vecchi, 2010: Retrospective forecasts of the hurricane season using a global atmospheric model assuming persistence of SST anomalies. *Monthly Weather Review*, **138**, 3858–3868.

Zhan, R., Y. Wang, and X. Lei, 2011: Contributions of ENSO and east Indian Ocean SSTA to the interannual variability of tropical cyclone frequency. *Journal of Climate*, **24**, 509–521.

Zhang, Q., Q. Liu, and L. Wu, 2009: Tropical cyclone damages in China 1983–2006. *Bulletin of the American Meteorological Society*, **90**, 489–495.

Zhao, H. K., L. G. Wu, and W. C. Zhou, 2010: Assessing the influence of the ENSO on tropical cyclone prevailing tracks in the western North Pacific. *Advances in Atmospheric Sciences*, **27**, 1361–1371.

Zhou, B., and X. Cui, 2008: Hadley circulation signal in the tropical cyclone frequency over the western North Pacific. *Journal of Geophysical Research*, **113**, D16107.

국문 초록

여름철 태풍 활동은 인구와 산업이 밀집한 해안가 주변 지역에 막대한 피해를 야기할 수 있기 때문에 주목 받고 있다. 호우와 강풍을 동반하는 태풍의 접근이나 상륙으로 인한 잠재적인 피해를 줄이기 위해 지난 수십 년간 태풍 활동을 이해하고 신뢰도 높은 태풍 예측 모델을 개발하는 것은 세계 선진 기상 기관들의 가장 중요한 임무 중 하나였다. 이러한 노력의 일환으로 본 박사학위 논문에서는 태풍 활동과 여름철 대규모 순환장 사이의 물리적 관계를 상세하게 규명한다. 이러한 이해를 바탕으로, 북서태평양 및 북대서양 지역에서 활동하는 태풍 활동의 계절 및 가까운 미래 예측을 진로 유형 기반 태풍 예측 모델을 통해 수행한다. 이 모델은 하이브리드 통계-역학 방법을 사용하며 대양 전체 태풍 활동의 공간 분포를 예측하는 세계 최초의 모델이다. 본 모델은 수치 모델을 활용한 기후 모의를 수행하지 않으면서도 장기 태풍 진로 분포를 우수한 성능으로 예측할 수 있는 장점이 있다.

이러한 진로 유형 기반 태풍 예측 모델은 세 가지 주요 단계로 구성되어 있다. 첫 번째로, 태풍 주 활동 기간 동안의 태풍 진로들을 퍼지 군집 분류(Fuzzy clustering method) 방법을 사용하여 대양의 대표적인 여러 유형으로 구분한다. 두 번째 단계에서는 하이브리드 통계-역학 방법을 사용하여 앞서 조사된 각 태풍 진로 유형들 마다 독립적으로 태풍 발생 개수를 예측한다. 각 유형에 대한 하이브리드 예측은 군집 별 계절 태풍

빈도 수와 미국 환경청(National Center for Environmental Prediction)에서 제공하는 기후 예측 시스템 (Climate Forecast System version 2; CFSv2)자료의 계절 평균 예측 인자 사이 통계적 관계성을 활용하여 수행된다. 마지막으로 대양 전체의 태풍 진로 밀도를 나타내는 최종 예측 결과는 모든 진로 유형들의 예측 결과들을 병합하고, 필요할 경우 오차 보정 작업을 추가적으로 수행하여 생산된다.

개발된 북서태평양 태풍 계절 예측 모델의 예측성을 평가하기 위해 교차 검증방법(leave-one-out cross validation)을 활용하였다. 이 모델을 활용하여 과거 기간에 대해 재모의된 북서태평양 진로 유형 별 태풍 개수와 관측치 간의 상관 계수는 0.71–0.81로써 통계적으로 99 % 수준에서 유의미하게 우수한 예측 성능을 보이는 것으로 나타났다. 게다가 북서태평양의 계절 태풍 진로 밀도의 공간 분포를 과거 기간에 대해 재현해 보았을 때 관측된 태풍의 공간 분포를 현실적으로 모의하는 것을 확인할 수 있다. 실제 사례 예측에서도 이 모델은 1951 년 관측 이후 가장 적은 태풍 활동을 나타냈던 2010 년 북서태평양 태풍 진로 밀도에서 동중국해 부근의 평년보다 활발한 태풍 활동을 성공적으로 예측하였다. 총 7 가지 진로 유형 예측 결과에서 도출할 수 있는 총 계절 태풍 빈도수 예측에서는 관측치에 가까운 약 16.4 개가 예측되었으며 이 결과는 타 기관 예측 결과와 비교해 보았을 때 상대적으로 작은 오차이다. 이러한 2010 년의 성공적 예측은 NCEP CFSv2에서 모의한 현실적인 엘니뇨 남방진동의 위상 변화와 예측 모델 자체의 특성에서 기인하는 것으로 나타

났다.

본 박사학위 논문에서는 북서태평양 이외에도 북아메리카 대륙과 인접하고 태풍 활동이 활발한 북대서양 지역에 본 예측 방법을 적용하여 예측모델을 개발하였다. 북대서양 예측 모델은 8–10 월의 기간 동안 발생하는 태풍 활동의 계절 예측을 위해 개발되었으며 북서태평양과 마찬가지로 태풍의 진로 유형을 기반으로 개발되었다. 퍼지 군집 분류 방법을 활용하여 1965–2012 기간 동안 발생한 총 432 개의 태풍이 다음과 같은 4 가지 그룹으로 분류된다; 1) 미국 동부 연안의 태풍, 2) 멕시코만의 태풍, 3) 중앙 북대서양의 해양에서 주로 활동하며 전향하는 태풍, 그리고 4) 열대 북대서양에서 발생하며 서쪽으로 이동하는 태풍. 이 모델은 NCEP CFSv2의 전지구 기후 예측을 활용하여 4 개의 태풍 그룹을 독립적으로 예측하며, 개별적으로 예측된 각 진로 유형들의 태풍 빈도수를 각각의 기후적 공간 분포와 결합한 후 병합함으로써 전체 북대서양 지역의 태풍 활동 공간 분포를 제공한다. 2 월에서 7 월까지 다양한 초기 조건에 따른 예측 성능을 검증하여 본 모델의 현업 적용 가능성을 조사한 결과, 본 예측 모델이 통계적으로 99 % 신뢰 수준에서 북대서양의 관측 된 태풍 발생 수를 현실적으로 모의할 수 있다는 것을 확인할 수 있었다. 예측 시점 변화에 관계 없이 이 모델은 안정적인 공간 예측 성능을 나타내며 미국 동부 해안가, 멕시코만, 섬나라 등지의 지역적인 태풍 활동 까지도 신뢰할 수 있는 정보를 제시할 수 있다는 이점을 보여준다.

태풍 활동과 동반된 집중 호우 및 강한 바람은 주로 일반적인 태풍보

다 강도가 강한 태풍에서 그 위력이 더 강력하다. 따라서 일반적인 태풍보다 강한 태풍에 의한 사회 경제적 손실이 더 크다. 본 박사학위 논문에서는 북서태평양과 북대서양 지역에서 발생하는 강한 태풍의 지역적인 활동을 집중적으로 예측하는 모델을 개발한다. 기후적으로 북대서양에서의 태풍 및 강한 태풍 수가 북서태평양 보다 훨씬 적은 것을 고려하여 북서태평양의 경우 카테고리 3 이상, 북대서양의 경우 카테고리 1 이상의 강도를 가진 태풍을 강한 태풍으로 정의하여 예측 모델을 개발하였다. 퍼지 군집 분류 방법을 사용하여 기후적인 강한 태풍들의 진로를 분류한 결과 북서태평양 및 북대서양 지역의 강한 태풍 진로 유형은 각각 3 가지 및 2 가지의 대표적 유형으로 분류되는 것을 확인할 수 있다. 군집 분류 결과에 근거하여 진로 유형 기반 모델을 독립적으로 개발하고 두 지역에서 발생하는 강한 태풍의 계절적 활동을 예측한다. 일반적으로 북서태평양에서는 이미 태풍 발생에 충분한 열적 조건을 보이기 때문에 주로 역학적 요소(연직 바람 시어 또는 하층 상대 와도)를 북서태평양 태풍 예측 모델의 주 예측인자로 선정하는 반면, 북대서양에서는 열적으로 불충분한 환경 조건을 보이기 때문에 강한 태풍 활동은 주로 열역학적 요인(해수면 온도)에 의해 조절되며 이를 예측 인자로써 활용한다. 모델 개발에 활용된 분석 기간 동안 모델의 성능을 교차 검증하고 2014 태풍 시즌에 대한 예측을 확인해 보면 강한 태풍 예측 모델이 현업 운영에 적용될 수 있을 만큼 충분한 성능을 나타내는 것을 알 수 있다.

많은 연구들에서 앞서 언급한 계절 예측을 포함하여 다양한 시간 규모

의 태풍 활동을 예측하고자 시도했지만, 가까운 미래 예측에 초점을 맞춘 연구는 지금까지 거의 없었다. 본 박사학위 논문에서 진로 유형 기반 태풍 예측 모델을 이용하여 2016–2030 기간의 북대서양 계절 태풍 활동이 현재보다 감소할 것을 예측하였다. 예측 모델은 장기 결합 시뮬레이션, 즉 CFS 재분석 자료를 사용하여 초기화 된 CFSv2 장기 실험을 입력 자료로 활용하였다. 대규모 순환장 변화를 확인하였을 때 가까운 미래에는 연직 바람 시어의 증가와 강화된 고기압성 회전 흐름 및 북대서양 지역의 낮은 해수면 온도를 포함하는 태풍 발달의 악조건이 형성될 것으로 전망된다. 이러한 환경장 변화의 대부분은 북대서양 해수면 온도의 장주기 변동성에 기인한 해수면 온도 감소 및 가까운 미래에 더 잦은 엘니뇨 현상의 발달에 기인한다. Coupled Model Intercomparison Project phase 5에 참여한 다중 기후 모델들에서 일관적으로 나타난 북대서양 해수면 온도의 온난화와 비교해 보았을 때 북대서양 해수면 온도의 감소는 주로 자연적인 변동성에 의한 것이며, 이러한 자연 변동성이 가까운 미래에는 여전히 인위적인 강제력보다 지배적인 영향을 미칠 것 이라고 제안한다.

주요어: 태풍, 강한 태풍, 진로 유형 기반, 하이브리드 통계–역학, 기후 예측 시스템, 계절, 가까운 미래, 북서태평양, 북대서양, 공간 분포, 자연 변동성

학 번: 2010–20354